

**Fission-Track analyses in the area of the southern  
Upper Rhine Graben**

**Inauguraldissertation**

zur

Erlangung der Würde eines Doktors der Philosophie  
vorgelegt der  
Philosophisch-Naturwissenschaftlichen Fakultät  
der Universität Basel

von

**Horst Dresmann**

aus

Freiburg im Breisgau (Deutschland)

Basel, 2009

Genehmigt von der Philosophisch-Naturwissenschaftlichen Fakultät

auf Antrag von Prof. Dr. Andreas Wetzel  
Institut für  
Geologie und Paläontologie  
Departement Umweltwissenschaften  
Universität Basel

Prof. Dr. Bernhard Fügenschuh  
Institut für  
Geologie und Paläontologie  
Universität Innsbruck

PD Dr. Ullrich Glasmacher  
Institut  
für Geowissenschaften  
Universität Heidelberg

Basel, den 24.04.2007

Prof. Dr. Hans-Peter Hauri  
Dekan

## Danksagung

Zuerst und vor allen anderen danke ich Dir, Alexandra. Vielen Dank für alles auch wenn es manchmal schwer war! Johannes, Für mangelnden Schlaf und Dein Lachen, insbesondere im letzten Jahr, werde ich Dir immer dankbar sein!  
Für Unterstützung jeder Art bedanke ich mich herzlich bei meinen Eltern und der übrigen Familie. Verzeiht mir, wenn ich Euch hier einfach zusammenfasse.

Meinen Betreuern Prof. Andreas Wetzel und Prof. Bernhard Fügenschuh gehört ebenso mein Dank! Insbesondere in der Schlussphase haben Sie durch schnelles Korrekturlesen zum einhalten aller Fristen beigetragen. Des weiteren möchte ich mich bei Ihnen für die wissenschaftliche Unterstützung die mir zuteil wurde herzlich bedanken und ausserdem dafür, dass Sie die Zeichen der Zeit erkannt hatten, und neben der Doktorarbeit von Zoltan Timar-Geng (2004, 2006a,b) auch diese nun vorliegende Dissertation initiierten. Somit waren die nötigen finanziellen Mittel bereit gestellt wofür ich dem Schweizer National Fond ewig dankbar sein werde.

Ein riesiges Dankeschön für einfach alles, inklusive guter Laune, gehört meinen Kollegen in Basel, insbesondere Mathias Tischler, Nynke Keulen, Kamil Ustaszewski, Zoltan Timar-Geng, Achim Reisdorf, Erich Fäh, James Mac Kennzie, Pierre Dezes, Stephane Kock, Fred Gaidies, Katy Waite, Heike Gröger, Alexandre Kounov, Elmar Wosnitza, Yvonne Fazies, Tjerk Heijboer, Sebastian Hinsken, Markus Schumacher, Herfried.Madritsch, Marielle Fraefel, Markus Jank, Michi Wiederkehr, Senecio Schefer, Nathalie Dalcher, Marcio Giamboni, Niels Oesterling, Stefan Bucher und all den anderen die ich hier leider vergessen habe.

Nicht vergessen, habe ich meine lieben „Steinbeisser“ und „Dichtentrenner“, Richard Waite, Christian Seiler und Laurent Cartier, Euch sei herzlichst für Euren Einsatz im Dienste der Wissenschaft gedankt.

Ebenso herzlich möchte ich den guten Geistern dieses Instituts danken Ihr hattet immer ein offenes Ohr und sonstige Hilfe für mich auf Lager. Also, vielen Dank an Joelle Glanzmann, Hans-Ruedi Ruegg, Verena Scheuring, Willi Tschudin, Koni Leu, Claude Schneider und Heinz Hürlimann



## Table of Content

|   |           |
|---|-----------|
| <b>Introduction</b>   | <b>IX</b> |
| <b>Concept</b>  | <b>X</b>  |
| <br>  |           |
| <b>I. A palaeo-high-temperature event related to seismic activity at the Upper Rhine Graben Main Border Fault: constrained by fission-track and microstructural analysis.</b> | <b>1</b>  |
| Abstract  | 1         |
| <b>1. Introduction</b>  | 2         |
| <b>2. Geological framework and samples</b>  | 5         |
| <b>3. Methods and analytical procedure</b>  | 6         |
| <i>Fission Track method</i>   | 6         |
| Microstructural analysis  | 7         |
| <b>4. Results</b>   | 8         |
| <i>Burial depth estimate</i>  | 8         |
| <i>FT-Analysis</i>  | 9         |
| <i>Microstructural observations</i>   | 11        |
| <b>5. Discussion and interpretation</b>   | 14        |
| <i>Regional temperature history</i>   | 14        |
| <i>Local temperature history of the Kandern Fault Zone</i>  | 16        |
| <b>6. Conclusions</b>   | 27        |
| Appendix: Numerical modelling of heat conduction  | 28        |
| <br>  |           |
| <b>II. Upper Jurassic to Early Cretaceous thermal pulse in the later Upper Rhine Graben area</b>  | <b>31</b> |
| Abstract  | 31        |
| <b>1. Introduction</b>  | 31        |
| <b>2. Geological background</b>   | 34        |
| <b>3. Sample material</b>   | 37        |
| <b>4. Methods</b>   | 39        |

|             |   |           |
|-------------|---|-----------|
|             | <i>FT method</i>  | 39        |
|             | <i>Subsidence analysis</i>  | 41        |
|             | <i>Thermal history analysis</i>   | 43        |
| <b>5.</b>   | <b>Results</b>  | 44        |
|             | <i>FT data</i>  | 44        |
|             | <i>Subsidence curves</i>  | 48        |
|             | <i>Palaeo-geothermal gradients</i>  | 49        |
| <b>6.</b>   | <b>Discussion and interpretation</b>  | 51        |
|             | <i>Time vs. temperature paths</i>   | 51        |
|             | <i>Subsidence analysis and FT data</i>  | 55        |
| <b>7.</b>   | <b>Conclusions</b>  | 58        |
|             | <b>Appendix</b>   | 60        |
| <br>        |   |           |
| <b>III.</b> | <b><i>Thermal evolution and provenance regions of Cenozoic sediments from the southern Upper Rhine Graben</i></b> | <b>61</b> |
|             | Abstract  | 63        |
| <b>1.</b>   | <b>Introduction</b>   | 63        |
| <b>2.</b>   | <b>Drainage systems attributed to the southern URG area</b>   | 66        |
| <b>3.</b>   | <b>Fission Track (FT) Method</b>  | 69        |
| <b>4.</b>   | <b>Sample Material</b>  | 70        |
| <b>5.</b>   | <b>Potential provenance regions</b>   | 71        |
| <b>6.</b>   | <b>Results</b>  | 74        |
| <b>7.</b>   | <b>Discussion and interpretation</b>  | 79        |
|             | <i>Salt Formation</i>   | 83        |
|             | <i>Grey Marl Formation</i>  | 85        |
|             | <i>Bois de Raube Formation</i>  | 86        |
|             | <i>Juranagelfluh</i>  | 87        |
|             | <i>Karst pocket of Glovelier</i>  | 88        |
|             | <i>Sundgau gravels</i>  | 88        |
| <b>8.</b>   | <b>Conclusions</b>  | 91        |
|             | Appendix  | 92        |

|             |                                      |            |
|-------------|--------------------------------------|------------|
| <b>IV.</b>  | <b>Key conclusions of the Thesis</b> | <b>94</b>  |
| <b>V.</b>   | <b>References (Bibliography)</b>     | <b>95</b>  |
| <b>VI.</b>  | <b>Appendix (data)</b>               | <b>108</b> |
| <b>VII.</b> | <b>Curriculum Vitae</b>              | <b>119</b> |





## Introduction

Fission-Track (FT) analysis of the Palaeozoic crystalline bedrock in the area of the southern Upper Rhine Graben (URG) showed complex and rapid changing upper crustal thermal conditions during the Mesozoic and the Cenozoic (Timar-Geng et al. 2004, 2006a). While an Eo-Oligocene thermal pulse accompanying the rifting of the URG is well documented by apatite FT modelling results (Timar-Geng et al. 2006a,b), the Jurassic hydrothermal period leading to a broad scatter of zircon FT data (Timar-Geng et al. 2004) are only weakly constrained. Additionally, due to a large sedimentary hiatus between the Upper Jurassic and the Late Eocene the pre-rift evolution remains still unclear. Knowledge about the thermal evolution of the area is essential for development of crustal scale models, which evaluate the rift-evolution.

This study aims to clarify the timing of the Jurassic thermal pulse(s) and its potential to heat the Mesozoic sediments, which covers the Palaeozoic basement. Especially, the temperatures and geothermal-gradients that were reached are of mayor interest. During a hydrothermal period is convective heat transport the important mechanism, which influences the reached temperatures in the upper crust. Therefore, addresses a localised detail study at the URG main border fault the potential of fault-bounded thermal anomalies caused by ascending hot fluids to heat the surrounding rocks.

The FT method, which is the base method used here, is a low-temperature thermochronological method widely used to quantify the thermal history of igneous, metamorphic and clastic sedimentary rocks. In particular, the FT analyses of detrital samples provide the advantage to discriminate between a pre-depositional thermal history of the provenance regions and a post-depositional basin related thermal history (e.g. Brandon 1998, Carter 1999, Bernet & Garver 2005, Armstrong 2005).

The FT analyses of the Permian and Mesozoic sediment column in the URG area, this study, compared with previous FT studies from the Black Forest and the Vosges (Michalski 1988, Wyss 2000, Timar-Geng et al. 2004, 2006a, b) led to a complete overview of the FT age signatures of URG pre-rift units. This is a requirement for the interpretation of Cenozoic detrital syn-rift deposits of the region by the FT method. New FT analyses on Cenozoic samples from the southern URG area led to basal insights in the syn-rift river drainage patterns.

## Concept

### Chapter I

#### **A palaeo-high-temperature event related to seismic activity at the Upper Rhine Graben Main Border Fault: constrained by fission-track and microstructural analysis.**

*Dresmann H., Keulen N., Gaidies F., Timar-Geng Z., Fügenschuh B.,  
Wetzel A. & Stünitz H.*

*(in parts published: Dresmann H., Keulen N., Timar-Geng Z., Fügenschuh B.,  
Wetzel A., & Stünitz H. 2009. The south-western Black Forest and the Upper Rhine  
Graben Main Border Fault: thermal history and hydrothermal fluid flow. International  
Journal of Earth Science. DOI 10.1007/s00531-008-0391-3*

Convective heat transport along structural discontinuities is the main factor influencing the regional thermal pattern. This chapter is a combined study of microstructural and FT analyses regarding the temperature evolution of an intensely deformed fault zone at the border of the Upper Rhine Graben. The importance and the influence of hot hydrothermal fluid flow on FT data at an active fault zone are shown.

N. Keulen and H. Dresmann have performed the fieldwork. N. Keulen performed also the microstructural studies and wrote the corresponding parts of the manuscript. F. Gaidies performed in collaboration with H. Dresmann the numerical model and wrote the Appendix. The first author performed the fission-track analyses, compiled and interpreted the data and wrote the first draft of this manuscript. Z. Timar-Geng, B. Fügenschuh, A. Wetzel and H. Stünitz helped to shape ideas and improved significantly the quality of the resulting text manuscript.

### Chapter II

#### **Upper Jurassic to Early Cretaceous thermal pulse in the later Upper Rhine Graben area**

This chapter addresses the Permian to Cenozoic thermal history, which can be recognised within the Mesozoic sediments of the southern URG area. In this

integrated study of fission-track and subsidence analyses on the Mesozoic deposits of the area, the relation between heating of sediments by burial and by hydrothermal activity is shown.

The author performed the fieldwork, the fission-track analyses, compiled and interpreted the data and wrote the manuscript. Z. Timar-Geng, B. Fügenschuh, A. Wetzel and A. Kounov discussed ideas and improved the resulting text manuscript.

### **Chapter III**

#### **Thermal evolution and provenance regions of Cenozoic sediments from the southern Upper Rhine Graben**

During the rifting of the Upper Rhine Graben (URG) various fluvial drainage systems developed, were changed and later disappeared. FT analyses of these drainage system deposits was performed and provided information on the thermal history of their source areas. In addition, this type of analysis also allowed the determination of the post-depositional basin related thermal history.

The author performed the fieldwork, the fission-track analyses, compiled and interpreted the data and wrote the manuscript. Z. Timar-Geng, B. Fügenschuh, A. Wetzel and A. Kounov discussed ideas and improved the resulting text manuscript.



# I. A palaeo-high-temperature event related to seismic activity at the Upper Rhine Graben Main Border Fault: constrained by fission-track and microstructural analysis

*Dresmann H.<sup>1</sup>, Keulen N.<sup>1\*</sup>, Gaidies F.<sup>2</sup>, Timar-Geng Z.<sup>3\*\*</sup>,  
Fügenschuh B.<sup>4</sup>, Wetzel A.<sup>1</sup> & Stünitz H.<sup>1\*\*\*</sup>*

<sup>1</sup>Geologisch-Paläontologisches Institut, Universität Basel, Bernoullistrasse 32, CH-4056 Basel, Switzerland; \*) now at: GEUS, Øster Voldgade 10, DK-1350 København K, Denmark; \*\*\*) now at: Institutt for geologi, Universitetet i Tromsø, Dramsveien 210, 9037 Tromsø, Norge

<sup>2</sup>Mineralogisch-Petrographisches Institut, Universität Basel, Bernoullistrasse 30, CH-4056 Basel, Switzerland

<sup>3</sup>Geologisches Institut, Albert-Ludwigs-Universität Freiburg, Albertstr. 23b, D-79104 Freiburg, Germany; \*\*) now at: Geoenergie Bayern GmbH, Schwandorfer-Str. 12, 93059 Regensburg, Germany

<sup>4</sup>Institut für Geologie und Paläontologie, Universität Innsbruck, Innrain 52, A-6020 Innsbruck, Austria

(in parts published: Dresmann H., Keulen N., Timar-Geng Z., Fügenschuh B., Wetzel A., & Stünitz H. 2009. The south-western Black Forest and the Upper Rhine Graben Main Border Fault: thermal history and hydrothermal fluid flow. *International Journal of Earth Science*. DOI 10.1007/s00531-008-0391-3)

## Abstract

Apatite and zircon fission-track (FT) analyses on fault rocks, combined with detailed microstructural observations, have been carried out to constrain the influence of highly localized thermal anomalies on FT data. The differentiation between a regional thermal evolution and local fault-related formation of thermal anomalies provides a model to explain for a wide overlap in apatite and zircon FT ages.

Near the village of Kandern (Upper Rhine Graben, Germany) the eastern Main Border Fault intersects a Palaeozoic structure. FT analysis of fault-affected material yields zircon FT central ages that are distinctly younger ( $109 \pm 17$  Ma and  $120 \pm 20$  Ma) than those documented in the adjacent area (Black Forest and Vosges) in general ( $136 \pm 16$  Ma -  $312 \pm 29$  Ma). The spread in zircon single grain ages ( $44 \pm 32$  Ma –  $284 \pm 99$  Ma) broadly overlaps with the apatite FT single grain age distributions ( $13 \pm 8$  Ma -  $176 \pm 134$  Ma). Microstructural analyses indicate repeated tectonic activity since the Variscan orogeny, in which the youngest cataclasite generation has been formed during a seismic or fast a-seismic event associated with an enhanced fluid flow. Numerical modelling compared to FT annealing experiments suggests that a short-lived heat pulse (about 30-45 h) with a temperature of 350 °C to 400 °C is able to produce the observed FT age record. Therefore, a local, fault-related thermal event is proposed, hot fluids flowed along short-lived, high permeable pathways that formed during earthquakes. The most probable

timing of such an anomalous heating event is the Late Eocene, which is evidenced by interpretation of apatite and zircon FT data in the light of the Upper Rhine Graben evolution.

## **1. Introduction**

Thermal anomalies within active rift systems are very common features. In the Upper Rhine Graben (URG), several of these thermal anomalies have been identified (e.g. Haas and Hoffmann 1929, Werner and Doebel 1974, Teichmüller 1979, Person and Garven 1992, Schellschmidt and Clauser 1996, Lampe and Person 2002). Today thermal springs document such anomalies for instance the springs of Baden-Baden (Wohnlich 1996). Recently, areas with high geothermal gradients are investigated and explored for their potential of geothermal energy.

Faults play a major role as pathways for thermal fluids and may lead to locally elevated temperatures within their vicinity. Thermal springs and hydrothermal ore deposits are often related to such structural discontinuities (e.g. Sibson 1990).

East of the village Kandern at the south-eastern side of the URG, a road cut expresses the junction of the eastern URG Main Border Fault with a Palaeozoic fault (Fig. 1). The outcropping granite is intensely deformed and displays substantial cataclasis, joints and discrete fault planes (Fig. 2). Consolidated cataclasites and silicate veins indicate that pathways were formed allowing for the ascent of fluids.

Only rarely, fission-track (FT) analysis, which is a low-temperature thermochronological method (e.g. Tagami and O'Sullivan 2005), has been applied to study such locally occurring anomalies (e.g. Seward and Sibson 1985, Jelinek et al. 1999, Parry et al. 2001, Murakami and Tagami 2004). For a more detailed understanding of the thermal history of such a fault zone we analysed the deformation microstructures and integrated these observations with new and published FT data. The purpose of this paper is to distinguish between the regional thermal evolution and the local fault-related formation of thermal anomalies.

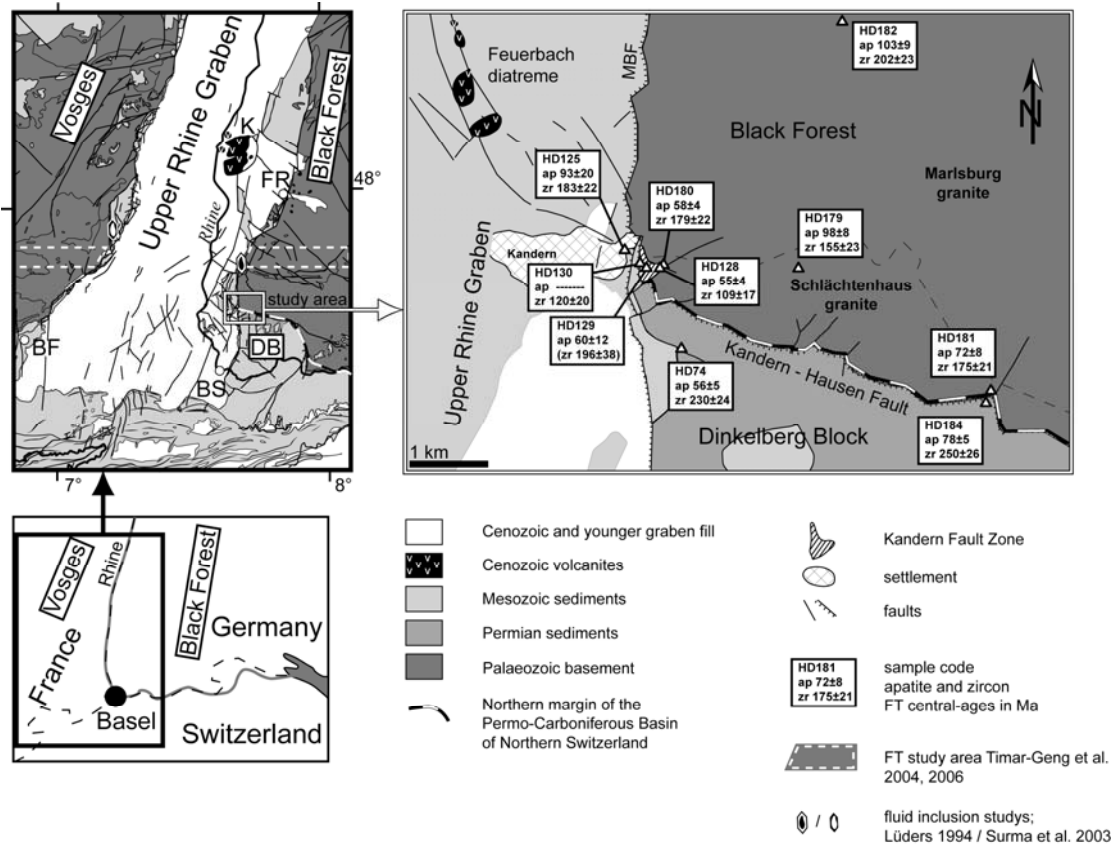


Fig. 1  
 Geological map of the study area (modified after Metz and Rein 1957, Scharrenberger 1985, Chantraine et al. 1996, Ernst and Herrgesell 1996, Ustaszewski et al. 2005) DB Dinkelberg Block, BF Belfort, BS Basel, FR Freiburg, MBF main border fault, K Kaiserstuhl volcano.

## 2. Geological framework and samples

The studied area is situated in SW Germany between the Black Forest, the URG and the associated Dinkelberg Block (Fig. 1). Regional metamorphism, large-scale thrust tectonics and extensive magmatic activity affected the pre-Variscan rocks during the Variscan orogeny (e.g. Eisbacher et al. 1989, Echtler and Chauvet 1992, Hann and Sawatzki 2000, Ziegler and Dèzes 2005). At the end of the Variscan orogeny numerous intramontane basins formed, among them the so-called Permo-Carboniferous Basin of Northern Switzerland (e.g. Thury et al. 1994). The Dinkelberg Block is located in the SE of the Black Forest; its northern border spatially coincides with the northern border of the Permo-Carboniferous Basin of Northern Switzerland (Fig. 1). During the Mesozoic, thermal subsidence and subordinate extensional crustal movements led to the deposition of several hundreds of meters of continental

or shallow marine sediments (e.g. Geyer and Gwinner 1991, Ziegler and Dèzes 2005). During the Cenozoic, the URG evolved in response to a changing stress field and reactivation of pre-existent Palaeozoic structures (e.g. Schumacher 2002, Hinsken et al. 2007). Middle Eocene fresh-water limestones are the first indicator of the onset of subsidence in the URG area (e.g. Berger et al. 2005a,b); in addition, the Eocene-Oligocene alluvial fan deposits along the basin margins indicate an increasing relief and erosion of the rift flanks (Düringer 1988, Hinsken et al. 2007). In the southern URG, Upper Oligocene to Miocene strata were largely eroded due to Miocene regional uplift (e.g. Laubscher 1987, Ziegler 1994, Sissingh 1998, Berger et al. 2005a and b). At that time the uplift of the graben flanks (Vosges and Black Forest) started. In the study area, the NNE-trending and nearly vertical URG Main Border Fault cuts the WNW-ESE striking Kandern-Hausen Fault east of the village Kandern (Figs. 1, 2). In the following, this junction will be called “Kandern Fault Zone”. The Kandern-Hausen Fault separates the Black Forest from the Dinkelberg Block, which takes an intermediate tectonic position between the Black Forest and the URG in the west. Here, Triassic and Jurassic strata are still preserved on top of thick Upper Permian sediments. The Kandern-Hausen Fault formed during the Palaeozoic as a dextral transtensive normal fault (Wirth 1984) and has been reactivated during the formation of the URG. Near Kandern along a steeply SSW-dipping fault plane (Fig. 2) a post-Mesozoic vertical displacement of about 450 m has been estimated (Wilser 1914). However, since no marker horizon is available on the hanging wall, this value bears some uncertainty. A vertical displacement of ca. 1500 m was estimated along the Main Border Fault between the Dinkelberg Block and the URG (Gürler et al. 1987). Towards the Graben interior the Main Border Fault was accompanied by a complex set of structures, which form a step-like escarpment and accommodate further graben subsidence.



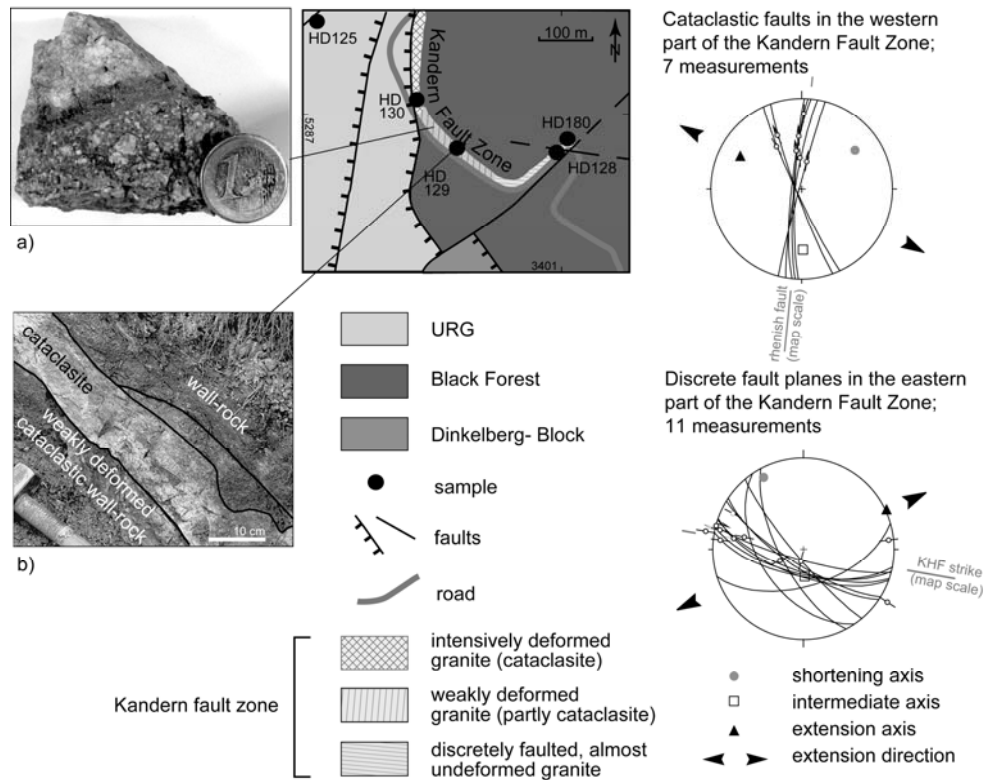


Fig. 2  
Detailed geological map of the Kandern Fault Zone (modified after Hinsken 2003) with structural measurements; lower hemisphere, equal area projections (K. Ustaszewski in Dresmann et al. 2004)

a) Rhenish-trending cataclasite (diameter of coin = 2.3 cm)

b) sampled Rhenish-trending cataclasite with adjacent wall-rock (HD129)

About 2.5 km NW of Kandern the Feuerbach diatreme forms the southernmost evidence of Cenozoic volcanic activity in the URG. Although the Feuerbach diatreme has never been dated directly, its mineralogical and petrographical similarities with the Kaiserstuhl volcanism suggest a Cenozoic age (Schreiner et al. 1957). Yet, the relevance of the Feuerbach diatreme with respect to rifting is still unknown.

### Sample material

Two groups of samples have been collected. A first set of samples covers a wide area and serves to evaluate the regional thermal history (Fig. 1). The second set was taken from the Kandern Fault Zone (Fig. 2) to decipher the fault-related local thermal history. The regional sample set consists of four samples from the uplifted Black Forest crystalline basement (HD179, HD180, HD181, HD182), two samples from the Upper Permian sedimentary rocks of the Dinkelberg Block (HD74, HD184) and one sample from the Lower Jurassic

sedimentary rocks (HD125) within the stepwise faulted graben margin at Kandern (Figs. 1, 2).

The samples from the Kandern Fault Zone were collected from a ca. 400 m long road cut (Fig. 2). The granite at the western end of the road cut is intensely deformed by cataclasis. The individual cataclasites are approximately 5 to 30 cm wide and follow the Rhenish NNE-SSW trend. Towards the east the degree of cataclastic deformation decreases. The orientation of the fault zones changes as they merge into the strike of the Kandern-Hausen Fault (WNW-ESE) in the eastern part of the road cut.

Two consolidated cataclasites and their adjacent wall-rock (HD129, HD130; ca. 10x10x20 cm in size) have been sampled (Fig. 2). The cataclasites are associated with a Rhenish NNE-SSW striking fault set, which forms part of the several meter thick URG Main Border Fault. Additionally, a nearly undeformed granite (HD128) has been collected some 100 m east of the cataclasite sample location. It originates directly from a subordinate fault plane, which strikes parallel to the Kandern-Hausen Fault. Sample HD180, an undisturbed granite, has been collected about 10 m NE from sample HD128. This sample has been used as a reference of undeformed rock close to the fault.

### **3. Methods and analytical procedure**

#### ***Fission-Track method***

The thermochronological interpretation of fission-track (FT) data is based on FT densities resulting mainly from the spontaneous fission of the unstable isotope  $^{238}\text{U}$  and the annealing behaviour of previously produced FTs, at elevated temperatures. The temperature interval within annealing rates increase is the so-called partial annealing zone (Wagner and van de Haute 1992), which is well established for apatite (APAZ) ranging from 60 °C to 120 °C with respect to a geological time span of 10 Myr (e.g. Green 1989). Nevertheless, due to the chemical composition of apatite, variations of the total annealing temperature are known (e.g. Gleadow and Duddy 1981). For zircon the estimated partial annealing zone (ZPAZ) ranges between 180 °C and 380 °C (Tagami 2005). With respect to a geological time span of about

1 Myr to 10 Myr, FTs above this temperature interval disappear fast whereas below they are stable (for detailed overview see Reiners and Ehlers 2005).

In this study, FTs in apatite and zircon were analysed by the external detector method after Naeser (1976) and Gleadow (1981). The analytical procedure was identical for all samples. Apatite and zircon grains were separated from each sample (4 to 6 kg rock material) using standard crushing, magnetic and heavy liquid methods. The zircon samples were mounted in Teflon PFA<sup>®</sup>, while the apatite samples were embedded in epoxy resin. After polishing, the apatites were etched for 40 s in 6.5 % HNO<sub>3</sub> at ~18 °C and the zircons for 6 to 12 h in a eutectic-melt of KOH-NaOH (220 °C). Mica was used as an external detector and CN-5 (apatite) and CN-1 (zircon) standards as dosimeter glasses. Irradiation with thermal neutrons was carried out at the Australian Nuclear Science and Technology Organisation facility (ANSTO).

Mica detectors were etched in 40 % HF for 40 min at ~18 °C. Tracks were counted at a magnification of 1600x (dry) on a Zeiss Axioplan2 optical microscope with a computer-controlled motorised scanning stage, run by the program "FT-STAGE 3.11" (Dumitru, 1993).

The FT age determination followed the zeta calibration method (Hurford and Green 1983) with a zeta value of  $380.67 \pm 10.58$  (Durango, CN-5) for apatite and  $145 \pm 6.88$  (Fish Canyon Tuff, CN-1) for zircon. The FT ages and errors were calculated using the software Trackkey V.4.1 (Dunkl 2002). Unless mentioned all reported ages are central ages (Galbraith and Laslett, 1993).

### ***Microstructural analysis***

#### *Microscopy*

Thin sections of selected granitoid cataclasites were made for optical and scanning electron microscope (LM and SEM) studies. The samples originate from the same localities as the FT samples HD129 and HD130. Additionally, cathodoluminescence (CL) was studied on a light microscope connected to a CL-camera using 25kV acceleration voltage and 0.025 mA sample current (Ramseyer et al. 1989).

#### *Grain size analyses*

Several sets of back-scattered electron contrast SEM micrographs with a range of magnifications from 50x to 5000x were used to obtain the grain size

distribution of the cataclasites. After manually tracing the grain boundaries in each of the individual images the grain areas were measured automatically with help of the public domain software ImageSXM (<http://www.liv.ac.uk/~sdb/ImageSXM/>) and recalculated to radii of their equivalent circles. By combining the analyses of the individual images a composite grain-size distribution over several orders of magnitude can be obtained, described as a log (frequency) - log (size) histogram (Keulen et al. 2007). The slope, D, of the best-fit power-law curve through the points in this histogram represents the grain-size distribution of the fault gouge (Sammis et al. 1987). Post-fracture healing of cataclasites reduces the relative amount of small grains with respect to large grains and causes a decrease in the D-value. The decrease in D-value may provide a measure for the consolidation of cataclasite (Keulen et al. 2008).

#### **4. Results**

##### ***Burial depth estimate***

For reconstruction of the thermal history knowledge of the burial depth of the samples before the onset of Cenozoic rifting is crucial. Although a direct estimate is impossible due to the lack of reference horizons a minimum value can be given based on the extrapolated thickness of the eroded Mesozoic sediments plus the approximate amount of eroded Black Forest crystalline basement. The Otterbach II borehole near Basel/Switzerland comprises a fairly complete section close to the study area. About 1350 m of Triassic to Upper Jurassic sediments were deposited on top of the Palaeozoic units (Häring 2002). The thickness of eroded crystalline basement at the sampled outcrops has been estimated to be at least ca. 300 m to 600 m, based on the present altitude of the outcrops beneath the mapped base of the Triassic palaeo-surface in the Black Forest (e.g. Paul 1955, Zienert 1986, Wimmenauer and Schreiner 1990). This estimate, however, does not take into account vertical block tectonics in the Black Forest, which at present cannot be accurately quantified (Huber and Huber-Aleffi 1990). In this study, a pre-rifting minimum sample depth (Mesozoic cover plus eroded basement) of

1650 m to 1950 m has been used, depending on the topographic position of the sample.

### FT-Analysis

Ten samples yielded 9 apatite and 10 zircon ages. The results are displayed in Table 1 according to the I.U.G.S. recommendations (Hurford 1990) and as radial plots (Galbraith 1988, 1990) in Figure 3.

|                     | sample code           | sample description      | coordinates x, y                  | elev. [m]        | n   | $\rho_s$ (Ns) | $\rho_i$ (Ni) | $P(\chi^2)$ (%) | $\rho_d$ (Nd) | Disp.        | Central-age (Ma) $\pm 1\sigma$ |              |
|---------------------|-----------------------|-------------------------|-----------------------------------|------------------|-----|---------------|---------------|-----------------|---------------|--------------|--------------------------------|--------------|
| Kandern Fault Zone  | <b>Apatite</b>        |                         |                                   |                  |     |               |               |                 |               |              |                                |              |
|                     | HD 128                | undeformed wall-rock    | 3401000, 5286950                  | 425              | 28  | 13 (833)      | 58 (3629)     | 0.14            | 12.83 (2797)  | 0.2          | 55 $\pm$ 4                     |              |
|                     | HD 129                | cataclasite + wall-rock | 3400840, 5286920                  | 410              | 15  | 2 (47)        | 8 (205)       | 22.76           | 12.5 (2797)   | 0.34         | 60 $\pm$ 12                    |              |
| Regional sample set | detrital samples      | HD 074                  | Permian, Rotliegendes             | 3401245, 5285735 | 530 | 10            | 19 (504)      | 44 (1172)       | 0.42          | 6.9 (3641)   | 0.21                           | 56 $\pm$ 5   |
|                     |                       | HD 125                  | Jurassic, Posidoniensch.          | 3400520, 5287150 | 350 | 9             | 14 (209)      | 23 (331)        | 0.01          | 9.15 (2648)  | 0.52                           | 93 $\pm$ 20  |
|                     |                       | HD 184                  | Permian, Rotliegendes             | 3405170, 5285095 | 430 | 40            | 13 (869)      | 28 (1931)       | 6.27          | 9.17 (2797)  | 0.15                           | 78 $\pm$ 5   |
|                     | Black Forest basement | HD 179                  | Schlächtenhaus granite            | 3402725, 5286915 | 685 | 20            | 18 (1007)     | 35 (1978)       | 0             | 10.64 (2797) | 0.26                           | 98 $\pm$ 8   |
|                     |                       | HD 180                  | Schlächtenhaus granite            | 3401020, 5286960 | 430 | 28            | 16 (845)      | 46 (2455)       | 1.26          | 8.81 (2797)  | 0.16                           | 58 $\pm$ 4   |
|                     |                       | HD 181                  | Schlächtenhaus granite, mylonitic | 3405255, 5285340 | 430 | 20            | 8 (354)       | 22 (957)        | 0.01          | 10.27 (2797) | 0.35                           | 72 $\pm$ 8   |
|                     |                       | HD 182                  | Marisburg granite                 | 3403713, 5290143 | 590 | 34            | 13 (750)      | 22 (1331)       | 0             | 9.9 (2797)   | 0.32                           | 103 $\pm$ 9  |
|                     |                       | <b>Zircon</b>           |                                   |                  |     |               |               |                 |               |              |                                |              |
| Kandern Fault Zone  | HD 128                | undeformed wall-rock    | 3401000, 5286950                  | 425              | 14  | 178 (1054)    | 26 (155)      | 0.03            | 2.63 (1625)   | 0.39         | 109 $\pm$ 17                   |              |
|                     | HD 129                | cataclasite + wall-rock | 3400840, 5286920                  | 410              | 5   | 170 (247)     | 23 (33)       | 13.57           | 3.67 (936)    | 0            | 196 $\pm$ 38                   |              |
|                     | HD 130                | cataclasite + wall-rock | 3400735, 5286980                  | 410              | 12  | 222 (296)     | 35 (46)       | 57.51           | 2.6 (1625)    | 0.05         | 120 $\pm$ 20                   |              |
| Regional sample set | detrital samples      | HD 074                  | Permian, Rotliegendes             | 3401245, 5285735 | 530 | 12            | 310 (3335)    | 27 (290)        | 0.91          | 2.86 (1625)  | 0.22                           | 230 $\pm$ 24 |
|                     |                       | HD 125                  | Jurassic, Posidoniensch.          | 3400520, 5287150 | 350 | 8             | 232 (731)     | 34 (106)        | 85.39         | 3.71 (1338)  | 0.01                           | 183 $\pm$ 22 |
|                     |                       | HD 184                  | Permian, Rotliegendes             | 3405170, 5285095 | 430 | 14            | 268 (1639)    | 25 (153)        | 68.64         | 3.28 (936)   | 0.01                           | 250 $\pm$ 26 |
|                     | Black Forest basement | HD 179                  | Schlächtenhaus granite            | 3402725, 5286915 | 685 | 10            | 226 (519)     | 35 (81)         | 25.37         | 3.4 (936)    | 0.18                           | 155 $\pm$ 23 |
|                     |                       | HD 180                  | Schlächtenhaus granite            | 3401020, 5286960 | 430 | 13            | 313 (966)     | 41 (127)        | 14.81         | 3.38 (936)   | 0.18                           | 179 $\pm$ 22 |
|                     |                       | HD 181                  | Schlächtenhaus granite, mylonitic | 3405255, 5285340 | 430 | 16            | 264 (3110)    | 34 (397)        | 0             | 3.35 (936)   | 0.35                           | 175 $\pm$ 21 |
|                     |                       | HD 182                  | Marisburg granite                 | 3403713, 5290143 | 590 | 13            | 364 (1784)    | 43 (213)        | 2.98          | 3.33 (936)   | 0.24                           | 202 $\pm$ 23 |

Tab.1

Apatite and zircon FT data

Coordinates (x,y) of Gauss Krüger DHDN Zone 3, Elevation (elev.) in metres above sea level, Number of grains counted (n).  $\rho_s$ ,  $\rho_i$  and  $\rho_d$  are spontaneous, induced and dosimeter track densities in  $10^5$  tracks/cm<sup>2</sup>. N are number of tracks counted shown in brackets. Analyses by external detector method using 0.5 for the  $4\pi/2\pi$  geometry correction factor. Disp., Dispersion, according to Galbraith and Laslett (1993). Ages calculated as central ages according to Galbraith and Laslett (1993) using dosimeter glass CN5 for apatite with  $\zeta_{CN5} = 380.67 \pm 10.58$  (H. Dresmann) and CN1 for zircon with  $\zeta_{CN1} = 145 \pm 6.88$  (H. Dresmann).  $P(\chi^2)$  is the probability of obtaining  $\chi^2$  value for  $\nu$  degrees of freedom where  $\nu =$  number of crystals-1

### Zircon samples

Zircons in all samples exhibit a relatively strong zonation and metamictization. Therefore only a low number of grains could be analysed. The low number of

datable grains influences the statistics. Especially the  $\chi^2$ -test, a commonly used tool to detect multiple age populations within single samples, depends on the amount of counted tracks. For a low numbers of dated grains and, therefore, low numbers of counted tracks the overall significance of the  $\chi^2$ -test is low (Timar-Geng et al. 2004, Galbraith 2005).

In the regional sample set, which acts as the reference system for the fault-related samples, the zircon central ages range between  $155 \pm 23$  Ma (HD179) and  $250 \pm 26$  Ma (HD184) and the single grain ages between  $80 \pm 16$  Ma (HD181) and  $428 \pm 94$  Ma (HD74) (Tab. 1, Fig. 3). Central ages of the detrital samples HD125 and HD184 do not differ significantly from their deposition ages within errors. On the other hand, single grain ages from the Upper Permian sample HD74 show a tendency corresponding to Jurassic ages.

Zircons from the faultzone samples show central ages between  $109 \pm 17$  Ma (HD128) and  $196 \pm 38$  Ma (HD129) and a single grain age distribution between  $44 \pm 32$  Ma (HD129) and  $284 \pm 99$  Ma (HD128). Compared to the regional samples, a clear shift towards younger ages can be observed.

#### *Apatite samples*

The majority of the apatite grains were of good quality. Nevertheless, only in one sample (HD128) at least a low number (17) of confined horizontal tracks could be measured, yielding a mean track length of  $10.5 \mu\text{m}$ . Yet due to the low number of measurable tracks this sample is not used for thermal modelling. The regional samples yield central ages ranging from  $56 \pm 5$  Ma (HD74) to  $103 \pm 9$  Ma (HD182) together with an overall spread of single grain ages between  $16 \pm 10$  Ma (HD125) and  $202 \pm 36$  Ma (HD179) (Tab. 1, Fig 3). The detrital samples display distinctly younger ages compared to their deposition ages. All regional samples fail the  $\chi^2$ -test, which implies a deviation from a true cooling age (Tab. 1). One exception is the Upper Permian sample HD184 with a  $\chi^2$ -value of 6.27 %. The fault related samples show central ages ( $55 \pm 4$  Ma (HD128) and  $60 \pm 12$  Ma (HD129)) and single grain ages ( $13 \pm 8$  Ma (HD128) and  $176 \pm 134$  Ma (HD129); Fig. 3) comparable to the data set from the Kandern region.

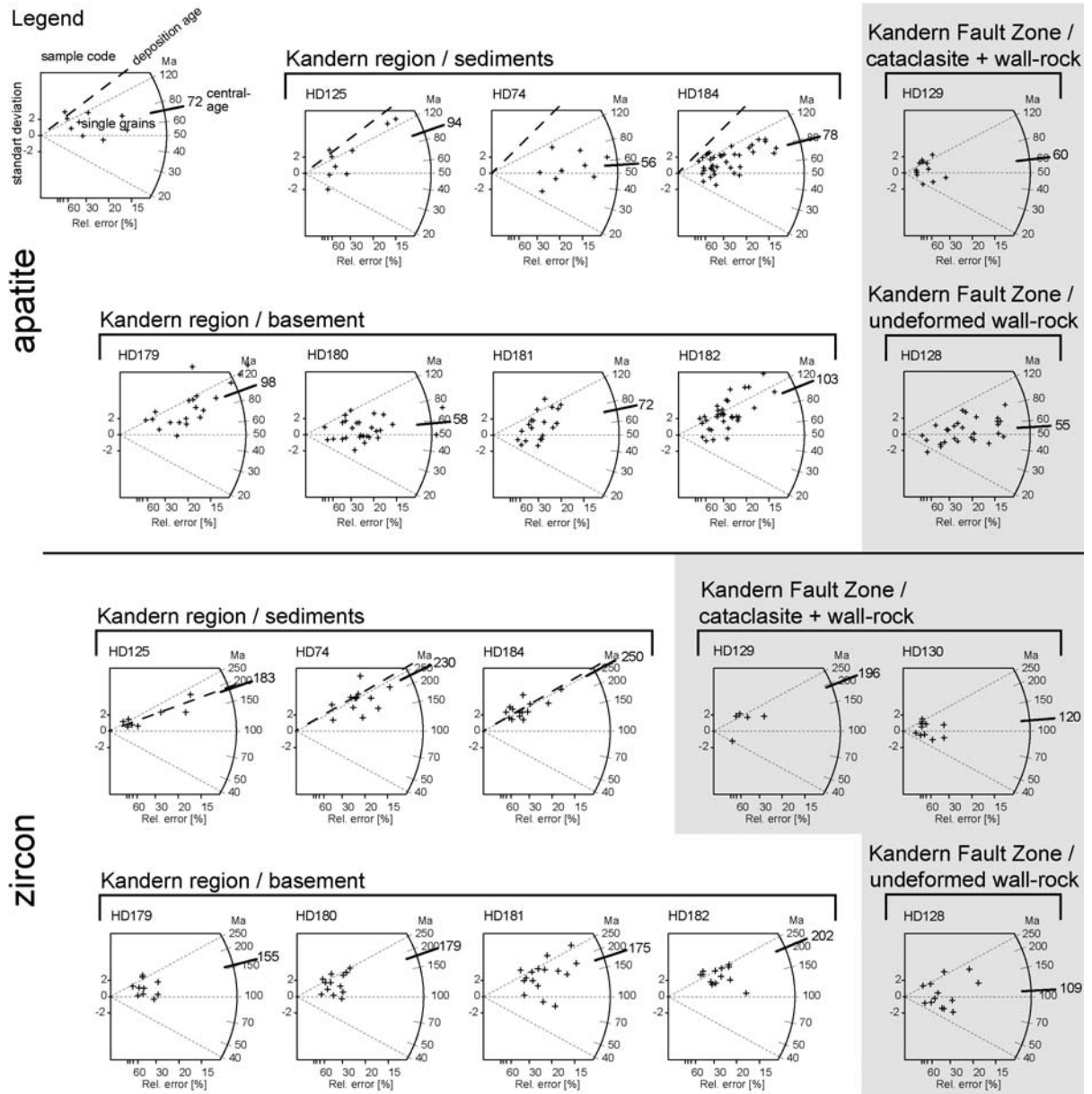


Fig. 3  
Apatite and zircon FT radial plots of the Kandern regional sample set and of the Kandern Fault Zone (shaded)

### ***Microstructural observations***

Two cataclastic deformation episodes can be distinguished for the Rhenish-striking faults of the Kandern Fault Zone. Evidence for the older episode (cataclasite I) are large, multi-component clasts, which have been healed and cemented before the formation of a younger cataclasite (cataclasite II; Fig. 4). In cataclasite I, quartz and feldspar are deformed by fracturing (Fig. 4). Quartz and feldspar clasts in discrete fractures are completely healed and have lost

their angular shapes (Fig. 4c,d). Instead, they appear as well-rounded (recrystallized) grains. In parts, this recrystallized material constitutes more than 30% of the volume of the cataclasite I. Some healed cracks are similar to narrow zones of bulging recrystallization (Fig. 4c,d; Stipp et al. 2002a, b), but other features of extensive crystal plastic deformation are missing.

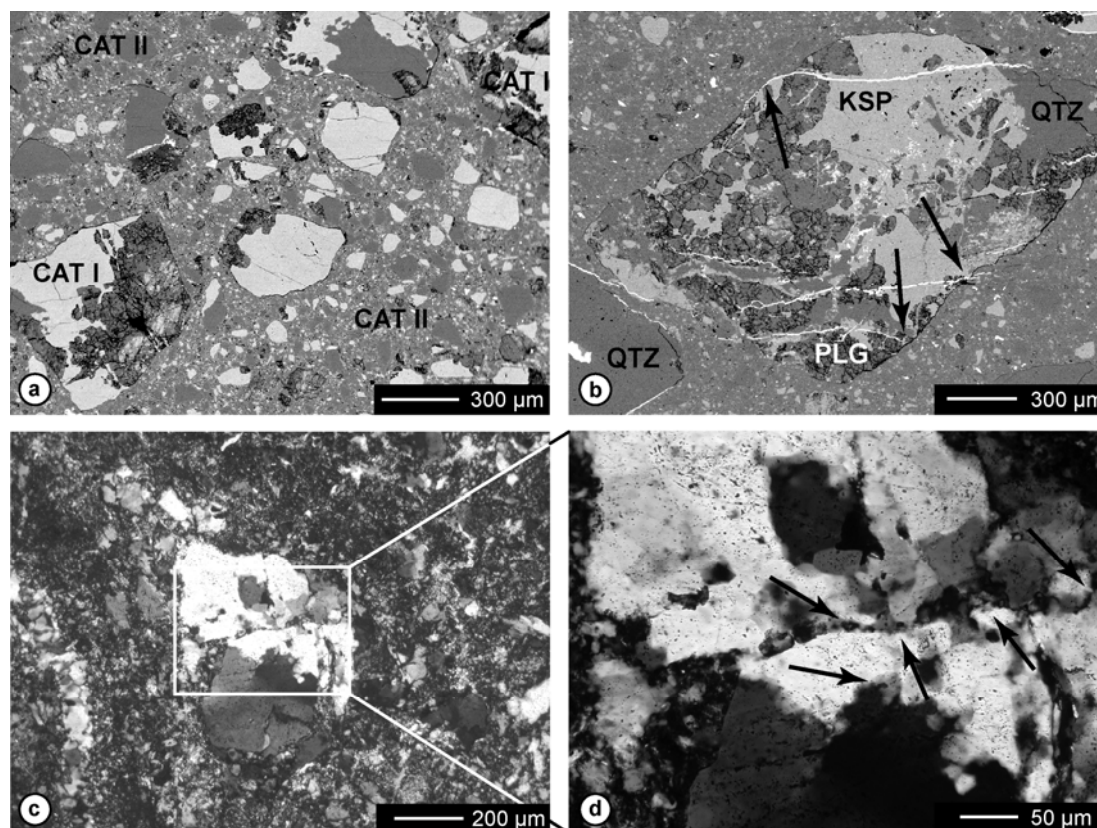


Fig. 4  
 Backscatter-contrast scanning electron micrographs (a,b) and crossed polarized light (c,d) showing typical microstructures from the Kandern Fault zone.  
 (a) Cataclasite-II, in which larger clasts consist of fractured and re-cemented clasts (Cataclasite-I)  
 (b) Thin barite veins (white, arrows) cut Cataclasite-I and do not continue into the matrix of Cataclasite-II.  
 KFS = K-feldspar, QTZ = quartz, PLG = plagioclase.  
 (c,d) Along a healed crack quartz has been deformed by bulging recrystallisation (arrows).

Kinking and gliding along (001) planes is observed in deformed biotite at the edges of cataclasite I clasts. In the cataclastic matrix and within some of the fractures in K-feldspar and quartz, hematite has been precipitated. After formation of cataclasite I, a set of thin barite veins cuts through the rocks (Fig. 4b). The barite veins are more localised phenomena than the hematite precipitations.



During formation of cataclasite II fragmented and granulated quartz, feldspar, biotite, muscovite, hematite, and multi-component fragments originating from cataclasite I form a fine-grained matrix. All minerals show only brittle deformation features. Cataclasite II forms clasts ranging from less than 1  $\mu\text{m}$  to about 10-20 mm in cross-section (Fig. 4a,b). The observed average size of the quartz fragments is slightly larger than for feldspar; most of the larger clasts are quartz minerals.

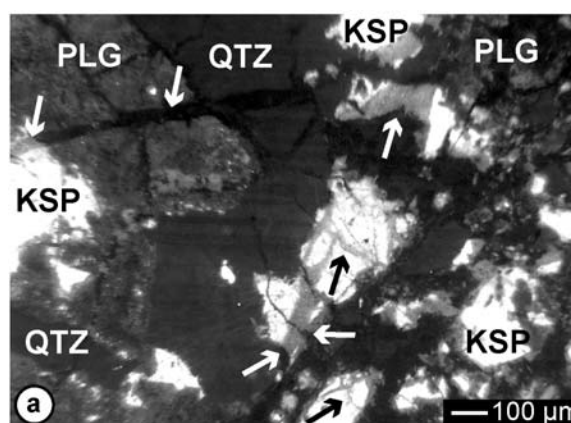
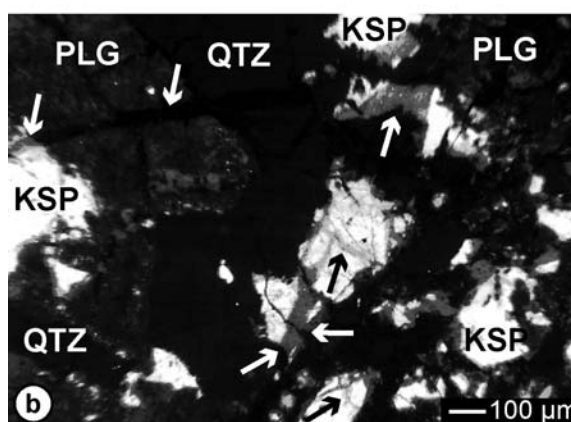


Fig. 5  
Crossed polarized light and cathodoluminescence camera micrographs of structures in the Kandern Fault zone.

(a) equivalent image to (b) with adjusted (inverted squared) grey-values.

(a) clasts of Cataclasite-I (K-feldspar, white) cemented with light grey luminescent material (black arrows). Later fractures cut through all minerals and are cemented with low-luminescent (dark-grey/black) material, indicated in (b) with white arrows.



Alteration reactions have been observed in the granitoid rock and are concentrated in the fine-grained fragments produced during the formation of cataclasite II. Inter-growths of chlorite with Fe-Ti-oxides have been observed in biotite. Chlorite and K-feldspar are formed at the expense of biotite and muscovite. Both K-feldspar and muscovite partly react to form kaolinite. K-feldspar is partly replaced by albite. A series of syntaxial silicate veins cuts through all other structures. The silica-rich veins consist of adularia when cutting through K-feldspar and of quartz within quartz or plagioclase minerals. By means of cathodoluminescence two generations of silicate deposition have

been observed. The first one cements fractures in quartz, plagioclase and K-feldspar with luminescent material of the same phase (Fig. 5a). The closed fractures have the same optical orientation as the minerals in which the fractures occur and are hardly visible with LM or SEM (BSE contrast). The second generation is represented by the late silicate veins described above and is low-luminescent (Fig. 5b). The change from quartz deposition to adularia deposition can be observed as a colour change of the vein material from black to dark grey (Fig. 5b).

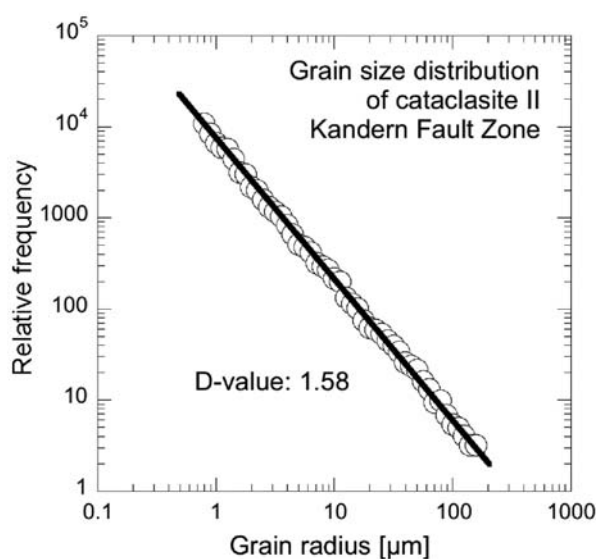


Fig. 6  
Frequency histogram for grain sizes determined in cataclasite II of the Kandern Fault Zone. The D-value indicates the slope of the log (frequency) - log (size) distribution.

The grain size distribution fits on a straight line in the log (frequency) - log (size) histogram (Fig. 6; D-value = 1.58). The minimum measured grain size has a radius of 1 μm and is the smallest grain size present with a statistically relevant resolution. The largest measured grain size is limited by the size of the thin section and is not the largest size of fragments in the rock.

## 5. Discussion and interpretation

### ***Regional temperature history***

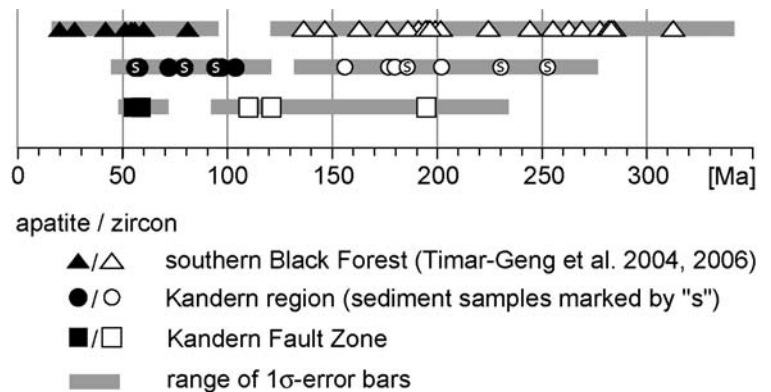
The zircon samples of the Kandern region in the south-western Black Forest show similar FT central ages and corresponding single grain ages as the dataset of Timar-Geng et al. (2004, 2006; Fig. 7, 8). The FT central ages and the single grain ages suggest a Mesozoic thermal overprint reaching the lower

boundary of the ZPAZ. Such a scenario has already been proposed by Timar-Geng et al. (2004) for the southern Black Forest, with temperatures of up to ~250 °C. The few pre-Mesozoic single grain ages in the basement samples (Fig. 8) indicate an incomplete resetting and therefore, that the Kandern area did not experience temperatures higher than the upper boundary of the ZPAZ (~350 °C; Tagami 2005) since Permian times. The youngest zircon FT central ages of the reference samples correspond to the Early Cretaceous (Fig. 7); thus indicating regional cooling through the ZPAZ at that time.

The apatite FT central ages presented here are about 30 Myr older than the youngest of Timar-Geng et al. (2006; Fig. 7). These could either indicate earlier cooling or a less pronounced late Eocene heating of the Kandern region in comparison to the area further North (Timar-Geng et al. 2006). Furthermore, the Middle Cretaceous apatite FT central ages suggest a resetting during the Triassic and Jurassic thermal pulse. The apatite FT ages show almost complete resetting of the detrital grains after deposition.

Fig. 7

Fission-track central-ages for apatite (black) and zircon (white) originating from Black Forest, Kandern region and the Kandern Fault Zone. Error bars (grey) indicate 1 $\sigma$ . The apatite FT central ages of the Kandern region are slightly older compared to that of Timar-Geng et al. (2006). Zircon samples of the Kandern Fault Zone yield the younger FT central-ages than the reference sample sets, while the apatite FT central-ages do not differ significantly from the regional sample set.



A couple of Miocene apatite single grain ages imply slow cooling up to the Miocene or a subordinate heating event followed by cooling below ZPAZ conditions, possibly related to Miocene volcanism. However, an accelerating cooling trend from early Miocene times onward seems probable and is a matter of debate (Timar-Geng et al. 2006, Ziegler and Dèzes 2007).

## ***Local temperature history of the Kandern Fault Zone***

### *Microstructures*

The fracturing and cementation structures of quartz resemble bulging recrystallization in cataclasite I. Similar microstructures have been observed at the transition between brittle and crystal-plastic deformation in natural rocks (Fitz Gerald and Stünitz 1993, van Daalen et al. 1999, Stipp et al. 2002, a, b, Trepmann and Stöckhert 2003). For bulging recrystallization in quartz, temperatures above approximately  $280\text{ °C} \pm 30\text{ °C}$  at strain rates of  $10^{-12}\text{ s}^{-1}$  have been inferred (Stipp et al. 2002a,b), whereas Trepmann and Stöckhert (2003) infer seismic pulses at ambient temperatures of 300-350 °C. In any case, the deformation temperature of cataclasite I appears to have been lower than about 280-300°C because of the lack of pervasive crystal-plastic deformation microstructures. Biotite grains inside cemented clasts of cataclasite I have been deformed by kinking and gliding. Laboratory experiments on granites under high strain rates ( $10^{-4}$  to  $10^{-6}\text{ s}^{-1}$ ) at 300 °C indicate that biotite deforms by a combination of fracturing, gliding and kinking (Tullis and Yund 1977, Kato et al. 2003, Keulen et al. 2007). The observed glide and kinking in biotite is consistent with slightly elevated temperatures of deformation, as inferred for quartz but below 280 °C.

In cataclasite II, all minerals have been deformed in a brittle manner. No evidence for aggregates of rounded quartz grains has been observed. Biotite is always fractured. Mainly brittle behaviour has been observed for biotites that have been experimentally deformed at 180°C under strain rates of  $10^{-4}$  to  $10^{-6}\text{ s}^{-1}$  (Kato et al. 2003). The transition from brittle to semi-brittle behaviour of biotite in natural fault zones is estimated at about 150 °C by Lin (1999).

After the formation of cataclasite II silica-rich veins have formed. Cataclasis has resulted in an enhanced permeability and a high grain surface area to grain volume ratio, which favours the dissolution of silica. As silica is very insoluble and, therefore, very immobile at temperatures below approximately 70 °C (e.g. Truesdell 1984), the temperature is assumed to have been higher than circa 70 °C. Temperatures below 150 °C are estimated for the formation of cataclasite II based on the veins, and the quartz and biotite microstructures.

Cathodoluminescence investigations confirm the presence of two generations of cataclasites formed under different temperature conditions. Two phases of vein cementation are observed in quartz and K-feldspar. In cataclasite I, fragments are grown together with newly deposited luminescent material; cataclasite II veins are filled with non-luminescent material (Fig. 5). Material precipitated under higher temperatures is luminescent, but vein filling precipitated under diagenetic temperatures does hardly show any luminescence (e.g. Ramseyer et al. 1992; Milliken and Laubach 2000).

The grain-size distribution of cataclasite II shows a D-value of 1.58 (Fig. 6). This value is the same as has been measured for parts of the San Andreas Fault ( $D = 1.60$ ; Sammis et al. 1987), the Qin-Ling Mountain, China ( $D = 1.59$ ; Shao and Zhou 1996), and the Nojima Fault Zone ( $D = 1.59$ ; Boullier et al. 2004, Keulen et al. 2008). In these three areas several earthquakes occurred during recorded history and their cataclasites are associated with pseudotachylytes, which are generally assumed to be the most likely indicator for seismic deformation (e.g. Magloughlin 1992). Keulen et al. (2008) have shown that for granitoid samples, experimentally deformed at a rate of  $10^{-4}\text{s}^{-1}$ , the D-values of 1.5 to 1.6 are the result of healing after heat treatment of the samples in presence of a fluid. The observed grain size distribution of cataclasite II in the Kandern Fault Zone is, therefore, most likely the result of healing of the cataclasite after deformation.

#### *Interpretation of the FT data in comparison with the microstructural analysis*

Apatite FT central ages (Fig. 7) of the fault-related samples plot at the young side of the age range of the reference sample set. Therefore, a similar cooling path is inferred for the Kandern Fault Zone samples and the regional sample set. However, the zircon FT central ages (Fig. 7) display different central ages for the fault-related samples HD128 ( $109 \pm 17$  Ma) and HD130 ( $120 \pm 20$  Ma) in comparison to the reference zircon FT central ages of the Kandern region, ranging between  $155 \pm 23$  Ma and  $202 \pm 23$  Ma. Furthermore, the two zircon FT ages from the Kandern Fault Zone are younger than the ages of the Black Forest determined so far (Timar-Geng et al. 2004, 2006). These points to somewhat higher temperatures possibly due to a fault related thermal overprinting and (partial) resetting of these samples. The central age of

sample HD129 ( $196 \pm 38$  Ma) is relatively uncertain, as only 5 grains have been dated.

As outlined above, formation of cataclasite I occurred under higher temperatures (less than  $280\text{ }^{\circ}\text{C}$ ) than cataclasite II (less than  $150\text{ }^{\circ}\text{C}$ ). These syn-deformational temperatures may have allowed for full annealing of fission tracks in apatite and partial annealing in zircon. Therefore, apatite FT central ages (Fig. 7) point to a pre-Cenozoic formation of cataclasite I. The combination of the estimated minimum overburden of the Kandern Fault Zone of about 1950 m (see above) for the late Jurassic with the inferred temperatures of approximately  $250\text{ }^{\circ}\text{C}$  to  $280\text{ }^{\circ}\text{C}$  for the presently exposed level of the Kandern Fault Zone implies a relatively high palaeo-geothermal gradient of about  $128\text{ }^{\circ}\text{C}/\text{km}$  to  $154\text{ }^{\circ}\text{C}/\text{km}$ . Such high gradients have possibly been established by the Late Palaeozoic emplacement of nearby outcropping granitic plutons (Echtler and Chauvet 1992, Schaltegger 2000), thus, suggesting formation of cataclasite I during the Late Variscan orogeny. Alternatively, hydrothermal activity during the Mesozoic (e.g. Wetzel et al. 2003) and related tectonic activity could also have provided the necessary temperature and fluid conditions to produce the observed microstructures.

Repeated fracturing after intermittent healing indicates reactivation of the faults within the Kandern Fault Zone. For cataclasite II a geothermal gradient of about  $77\text{ }^{\circ}\text{C}/\text{km}$  can be calculated by combining the estimated deformation temperatures of max.  $150\text{ }^{\circ}\text{C}$  with the inferred sample depth (1950 m). Such temperatures may allow for annealing of FTs in apatite, but are insufficient for annealing of FTs in zircon grains (e.g. Green et al. 1986, Yamada et al. 1995). Thus, it may be inferred that cataclasite II has formed after cooling through the ZPAZ. This lower limit is based on the youngest single grain age cluster, which comprises the thermally sensitive zircon grains (Brandon et al. 1998, Fügenschuh and Schmid 2003).

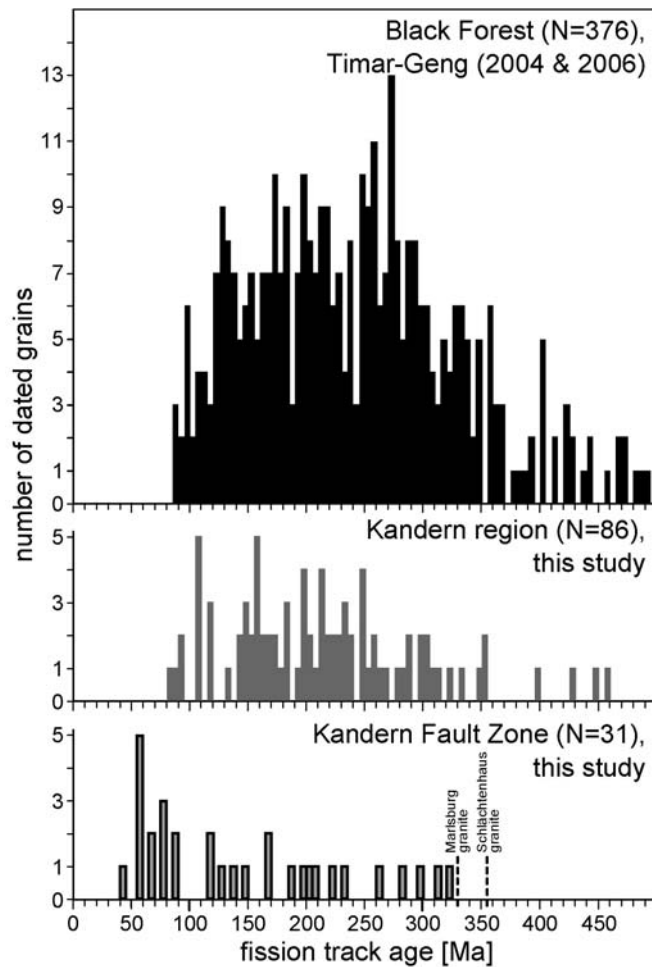


Fig. 8  
Zircon fission-track single grain ages; N = number of counted grains; width of bars 5 Ma; U/Pb age of the Marlsburg granite (Todt 1976) and of the Schlächtenhaus granite (Schaltegger 2000) are given for reference at the bottom.

The youngest zircon single grain ages from the Black Forest (Timar-Geng et al. 2004, 2006) and the Kandern region (this study) are dated at ca.  $80 \pm 16$  Ma (HD181) (Fig. 8). In contrast, one third of the zircon single grain ages of the fault related samples (HD128, HD129, HD130) yielded Late Palaeocene to Middle Eocene ages, thus, clearly younger than  $80 \pm 16$  Ma (HD181) (Figs. 3, 8). At first sight this seems to be contradicted by the apatite age spectrum of the same fault-related samples, which range between  $13 \pm 8$  Ma (HD128) and  $176 \pm 134$  Ma (HD129) (Figs. 3, 9). This unusual broad overlap, ranging in time between  $44 \pm 32$  Ma (HD129) (youngest zircon single grain age) and  $176 \pm 134$  Ma (HD129) (oldest apatite single grain age) asks for a more detailed inspection.

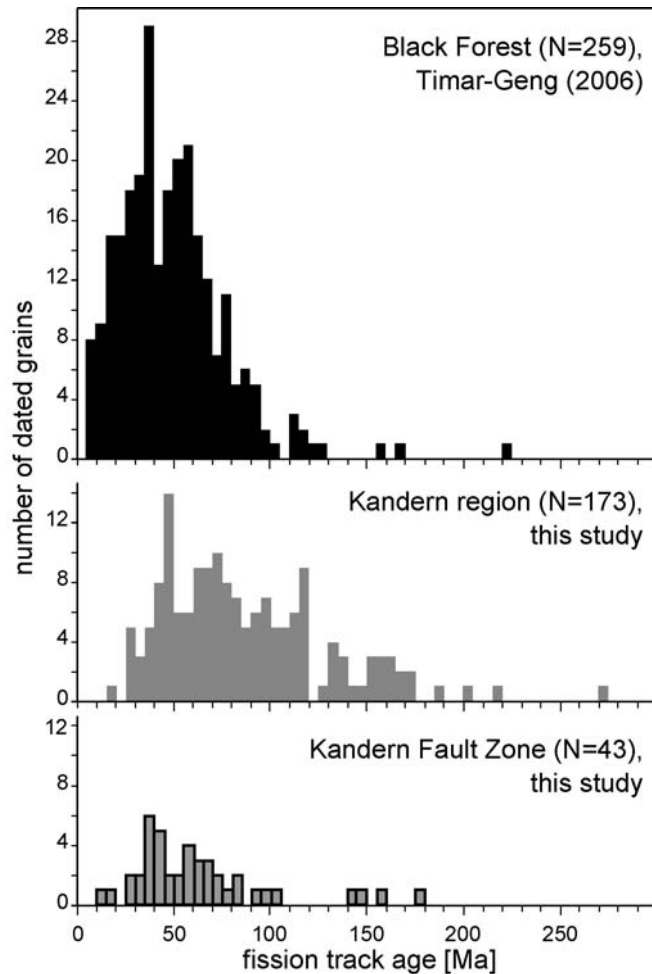


Fig. 9  
 Apatite fission-track single grain ages; N = number of counted grains; width of bars indicates 5 Ma

Generally, the partial annealing zones of zircon and apatite are well separated by a temperature gap of about 60°C (e.g. Wagner and van den Haute 1992, Tagami and Shimada 1996, Tagami et al. 1998). For a fast cooling through the ZPAZ and the APAZ the annealing kinetics of each grain and the individual error of the single grain age determination do not allow for a significant separation between single grain age distributions of apatite and zircon within one sample. Such an overlap can be observed in volcano-sedimentary layers (e.g. Odin et al. 1991) or in fast exhuming areas affected by meteoric fluids (e.g. Fügenschuh et al., 1997).

Alternatively, an overlap in the apatite and zircon single grain age distribution can result from an inhomogeneous temperature distribution on the scale of a few tens of centimetres. Such a steep temperature gradient can be produced by heating one side of the sample to temperatures valid for zircon annealing, followed by fast cooling.



Murakami and Tagami (2004) modelled a steep temperature gradient of 1000 °C to 200 °C within a distance of 1 cm in a pseudotachylyte and its adjacent fault gouge in the Nojima Fault, Japan. Within a few millimetres, they determine total-, partial- and no-resetting zones of zircon FTs for a short (5 s) seismically induced heating event followed by fast cooling (10 s). In the case of the Nojima Fault pseudotachylyte formation a background temperature of about 200 °C avoids further fast cooling into the APAZ.

This example illustrates that a steep temperature gradient over a short distance can be established only by a short localised heating event within a relatively cool environment. In such a scenario, a rock becomes heated at one side and different annealing areas should be discernible (Fig. 10), which comprise “hot” to “cold” areas documented by total-, partial- and no-resetting of both, apatite and zircon. The zircon total- and partial-resetting occurs within the apatite total-resetting area. Therefore, the earlier thermal history is stored at the sample’s “cold” side, whereas at the “hot” side the influence of the young heating episode is documented.

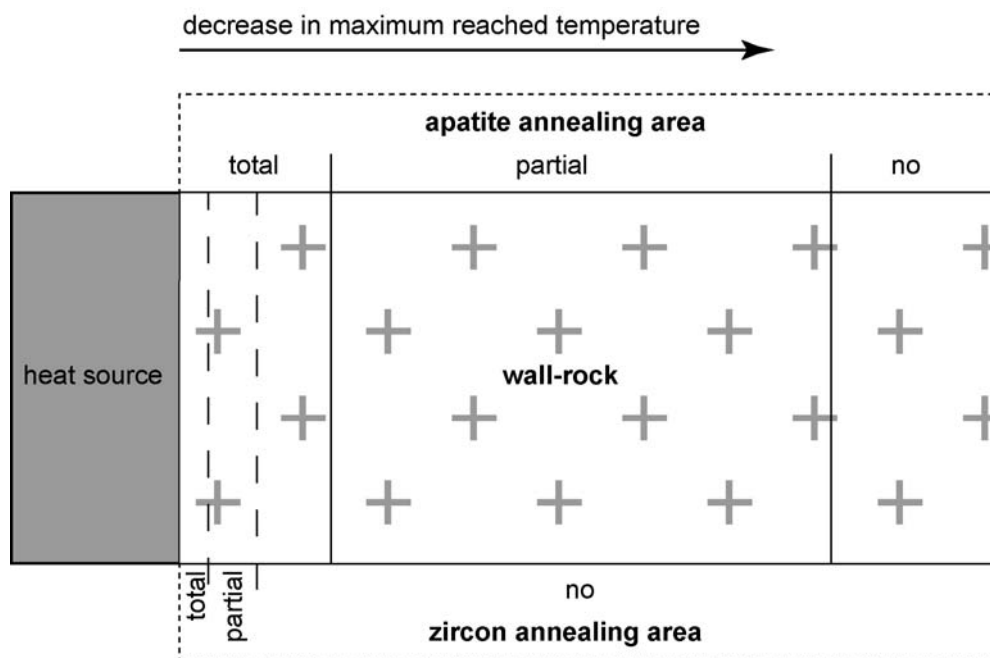


Fig. 10 Schematic sketch on hand-specimen scale of a wall-rock heated during short time period showing the influence on the FTs in apatite and zircon. The size of each zone depends on the duration of heating, on the thermal diffusivity, on the heat source temperature, on the environmental temperature and the three-dimensional shape of the contact between heat source and wall-rock

Assuming that cataclasite II formed while hot fluids percolated through it, they could have heated the (undisturbed) wall-rock conductively. Thus, a steep temperature gradient of some 20 cm width could have been established. The relevant parameters for conductive heat flow are the duration of heating, thermal diffusivity, heat source temperature, background temperature and the geometry of the contact between heat source and wall-rock.

For the Kandern Fault Zone a high fluid flow during and after the formation of cataclasite II, is suggested by the silicate veins. Fluid flux can increase along the fault zones before, during or after earthquakes (hours to days and sometimes for years) due to an enhanced permeability (e.g. Sibson 1990, Hill et al. 1993, Tokunaga 1999, Huang et al. 2004). For a relatively short time fluid temperature may increase as well (e.g. Mogi et al. 1989, Sibson 1990, Hamza 2001). Although no pseudotachylyte was observed at the Kandern Fault Zone, shear heating may eventually have occurred at larger depth. Since almost all mechanical work associated with movement on the fault plane is converted into heat (Scholz 1990) this may provide an additional heat source. Consequently, the heat can be transported to the studied part of the fault plane by means of fluid flow. The short duration of the heating event can be explained by fast sealing of the seismically induced pathways (Parry 1998). Sustained temperatures higher than 150 °C for extended periods of time during or after the formation of cataclasite II are unlikely. They would lead to recrystallisation of biotite and, at even higher temperatures, of quartz, and cause fast grain growth with luminescent material deposited around the fragmented gouge. However, temperatures of up to about 400°C might not lead to recrystallisation and grain growth if lasting only a very short period of time (in the order of hours or a few days). Therefore, for short durations the seismically induced fluid flow might have been sufficiently hot to start annealing of FTs in zircons without influencing the low-temperature microstructures.

## Numeric model

To combine the observed FT data with the data of FT annealing experiments a numerical model was designed, allowing for a rough estimate of the temperature and duration of the heating of cataclasite II and their wall-rock by a hot fluid.

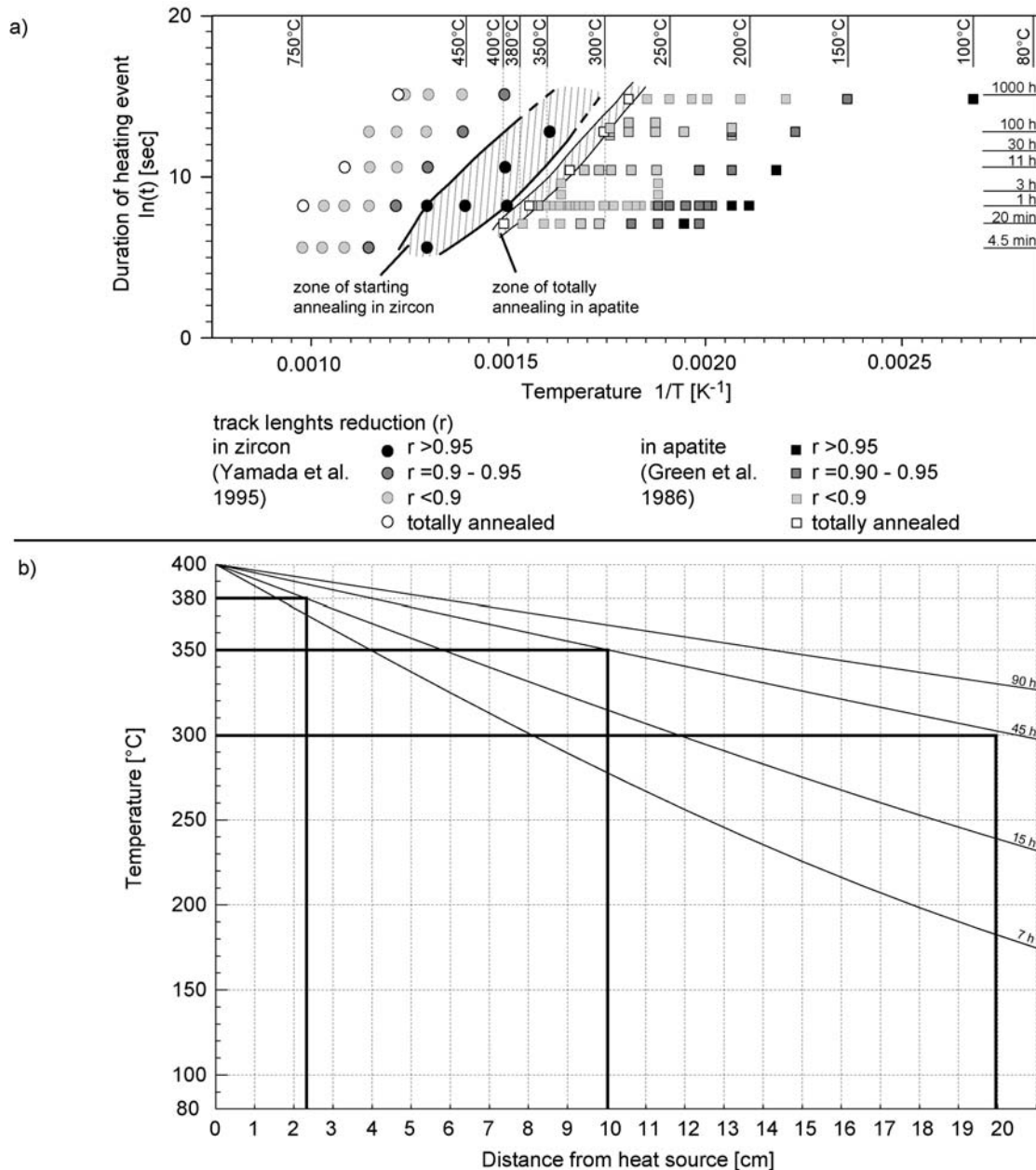


Fig. 11

Relationship between FT annealing experiments and modelled heat conduction within granite  
a) The Arrhenius diagram displays the FT lengths annealing behaviour of apatite (Green et al. 1986) and zircon (Yamada et al. 1995), respectively, depending on heating temperatures and heating durations. Hatched zones indicate the area of measurable annealing of track lengths in zircon and totally annealing of FTs in apatite, respectively.  $r$  = track lengths reduction ( $r = L/L_0$ ; with  $L$  = mean lengths of tracks and  $L_0$  = track lengths of the induced tracks).

b) Diffusion of heat around a heat source (400°C) into a rock (granite) at an ambient temperature of 80°C. Thin lines are isochronal time steps. For modelling procedure see Appendix.

Experimental FT annealing studies on zircon (e.g. Carpena 1992, Yamada et al. 1995, Tagami et al. 1998) and apatite (Green et al. 1986, Crowley et al. 1991, Ravenhurst et al. 2003) cover a large part of the temperature range typical for hydrothermal fluids.

The results of experimental data of Yamada et al. (1995) and Green et al. (1986) are plotted in an Arrhenius diagram (Fig. 11a), which displays the FT length annealing behaviour for apatite and zircon in relation to the temperatures and durations of a heating event. The experiments cover heating durations of a few minutes to 1000 hours and they show FT length reduction “r” (with:  $r=L/L_0$ ; L= mean lengths of tracks and  $L_0$  = track lengths of the induced *fresh* tracks) in zircon between 350 °C to 750 °C and in apatite between 100 °C to 398 °C. The annealing experiments show that track annealing increases with increasing temperature or increasing heating duration.

To correlate the observed FT data of the Kandern Fault Zone with the data of the annealing experiments a 1-D numerical model was designed. It simulates heat conduction through an undeformed “cold” wall-rock (granite) initiated by hot fluids flowing through the cataclasite II or along a discrete permeable fault plane (see Appendix for further details).

In the case of the annealing experiments, the temperatures were fixed after starting the experiments for the whole sample and for a distinct duration. In contrast, within the numerical model, heat enters the system at the cataclasite – wall-rock boundary and propagates into the wall-rock. Therefore, combinations of the annealing experiments with the numerical model offer only rough estimations to clarify the state of annealing of FTs in the conductive heated wall-rock.

In the model, the ambient temperature was set to 80 °C, which is estimated from the microstructures of cataclasite II and matches the observed FT data (see above). The heat source (fluid) temperature was set to 400 °C. Therefore, the model covers the whole temperature range used in the apatite annealing experiments (Green et al. 1986) and the “low” temperature annealing experiments in zircon (Yamada et al. 1995).

Immediately after the model start, the zircons at the contact reached temperatures exceeding the ZPAZ. The annealing experiments of Yamada et

al. (1995) on FTs in zircon, with an initial length of 11.4  $\mu\text{m}$ , show that track length reduction starts for a heating duration between 1 h to 11 h at ca. 400 °C (Fig. 11a). Such conditions are comparable with the contact zone (heat source - wall-rock) in the numerical model. Furthermore, the annealing experiments suggest the same degree of track annealing in zircon after ca. 30 h at 380 °C (Fig. 11a). In the numerical model the part of the wall-rock within a distance of ca. 2 cm from the heat source experienced 380 °C after 15 h. Within this 2 cm wide zone, track shortening is predicted to occur after 45 h.

The annealing experiments of Green et al. (1986) on FTs in apatite, with an initial length of 16  $\mu\text{m}$ , yield about 50 % ( $r = 0.49$ ) track shortening after 20 min at these conditions. Complete annealing occurred after ca. 1 h (Green et al. 1986). With respect to the 380 °C isotherm in the numerical model and after 15 h, the zone of total resetting in apatite propagated 2-3 cm into the wall-rock.

In order to estimate the possible distance from the heat source, which causes total resetting of apatite, the more relevant isotherm is at 350 °C. At 350 °C about 3 h were needed to reset apatite (Green et al. 1986) and, therefore, the zone of complete annealing expanded after 45 h to little less than 10 cm. After ca. 45 h the 300 °C isotherm reached a distance of 20 cm from contact. For FTs in apatite, Green et al. (1986) found that 20 min were needed to obtain about 14 % of track length reduction, for tracks with an initial length of 16  $\mu\text{m}$  at a fixed temperature of 300 °C.

To summarize, the numerical modelling compared to the FT annealing experiments suggest a short (~30-45 h) heating event with a heat source of 350 °C to 400 °C might be able to produce partial annealing of FTs in zircon and complete to partial annealing of FTs in apatite within a distance from heat source of up to 20 cm.

The temperature estimate is also affected by the still poorly defined low-temperature boundary of the ZPAZ. Accumulated radiation damage caused by alpha-decay can substantially lower the boundaries of the ZPAZ (Kasuya and Naeser 1988). This is especially the case for samples, which were heated up to temperatures well within the ZPAZ and remained there for a prolonged

period of time (Rahn et al. 2004, Timar-Geng et al., 2004). A good data set of annealing experiments on highly alpha-damaged zircons is still missing.

The initial mean track length within the fault related samples prior to reheating is not known. Yet initial track lengths heavily influence the FT ages, as short tracks disappear rapidly during reheating and lead to an apparent younging. A substantial amount of short tracks can be expected for zircons that remained in the ZPAZ for a long time, as it is the case within the wider working area (Timar-Geng et al. 2004).

The proposed temperature range of the fluid between 350 °C and 400 °C seems rather hot for the uppermost crustal level with a depth of approximately 1950 m. Fluid inclusion studies at the Cenozoic URG Main Border Fault at Guebwiller (Surma et al. 2003) and Badenweiler (Lüders 1994) show homogenisation temperatures of 195 °C to 225 °C in Triassic units, with a maximum depth of only 1300 m. The studied fault at Guebwiller is of a post-Early Triassic age and at Badenweiler a Cenozoic formation age is determined.

#### *Age estimation of the proposed short thermal event*

The youngest zircon single grain age cluster (44 ±32 Ma (HD129) to 59 ±22 Ma (HD128), Fig. 3) contains the grains with the lowest thermal stability. These grains are the last to close while cooling below the ZPAZ (Brandon et al. 1998, Fügenschuh et al. 2003). Thus, the maximum age of the high thermal anomaly can be estimated to be younger than ca. 60 Ma.

The proposed short-lived high temperature event is expected to have caused a high degree of FT annealing in apatite. Therefore, a large amount of single grains should show the age of the event. Depending on the post-event thermal history a further younging of the ages may occur.

The fact that only a negligible number of apatite single grain ages are younger than 35 Ma (Fig. 3) implies a pre-Oligocene age of the inferred thermal event. The initial rifting period during the late Eocene (Schumacher 2002) offers ideal conditions to generate high-thermal anomalies such as described above. Since the timing constraints derived by fission-track dating (35 Ma – 60 Ma) coincide with a time span of increased tectonic activity, the anomalous heating

event at the Kandern Fault Zone seems likely, to have occurred at late Eocene times

In terms of a possible indication of a heat source providing hot fluids to the Kandern Fault Zone the close structural relationship of the nearby, chronometrically so far undated, Feuerbach diatreme is worth mentioning.

## 6. Conclusions

The Kandern Fault Zone forms the intersection of two steeply dipping fault zones, namely the NNE trending URG Main Border Fault of Cenozoic age and the WNW-striking Palaeozoic Kandern-Hausen Fault (Fig. 1). Additionally, the Kandern Fault Zone is connected to the Feuerbach diatreme by a set of NW to NNW oriented faults (Fig. 1).

Microstructural analysis of the Kandern Fault Zone indicates repeated tectonic activity since the Variscan orogeny. The youngest cataclasite generation (II) has been formed in a seismic or fast a-seismic event accompanied by an enhancement of the fluid flow and the temperatures of the surrounding rocks, which have an ambient temperature below 150 °C.

FT analysis of fault-affected material yielded zircon FT central ages ( $109 \pm 17$  Ma and  $120 \pm 20$  Ma) distinctly younger than from surrounding (reference-) samples. The spread in zircon single grain ages ( $44 \pm 32$  Ma –  $284 \pm 99$  Ma) partially overlaps with the apatite FT single grain ages distributions ( $13 \pm 8$  Ma -  $176 \pm 134$  Ma). This significant deviation of the thermal history of the Kandern Fault Zone from the regional thermal evolution indicates a strong influence of a local short-lived thermal anomaly.

The comparison of the numerical model with the FT annealing experiments suggests that a local short-lived heat pulse (~30 - 45 h) with a heat source of 350 °C to 400 °C is capable to produce the observed FT age record. Such a thermal pulse can produce steep gradients causing complete and an incomplete resetting of FTs on the hand specimen scale as observed at the Kandern Fault Zone.

The time constraints derived by FT analyses provide a time range for the occurrence of such a thermal anomaly between about 60 Ma and 35 Ma.

These timing coincides with the initial rifting stage of the URG indicating a relationship of the anomalous heating event at the Kandern Fault Zone and tectonic events during the Late Eocene.

### **Acknowledgements**

This work has been supported by the Swiss National Science Foundation (Project Nos. 1509-NF 20020-105088/1.). We thank gratefully James R. Mackenzie † for all help; we will never forget him! A. Kounov, M. Tischler, T. Heijboer, E. Wosnitza and S. Kock are thanked for fruitful discussion, W. Tschudin for thin sections. R. Waite, L. Cartier and C. Seiler for sample preparation. K. Ramseyer (Univ. Bern) for the introduction into cathodoluminescence and the usage of his microscope. Central Microscope Centre of the University Basel for the use of their facilities. S. Hinsken for introduction into the local geology and K. Ustaszewski for providing structural data of the Kandern Fault Zone. The published parts of this chapter are substantial improved by reviews of B. Ventura und U. Glasmacher.

### **Appendix**

#### **Numerical modelling of heat conduction**

The parabolic partial differential equation

(1)

$$\frac{\partial T}{\partial t} = D \frac{\partial^2 T}{\partial x^2}$$

is the governing equation for conduction of heat in a 1-dimensional isotropic medium, where T is the temperature, t is the time, the quantity D is the thermal diffusivity, and x is the distance. This equation can be used to predict in a rudimentary fashion the change of temperature with time at a given point in space.



After discretisation employing the Crank-Nicolson scheme (Crank and Nicolson 1947) the flow of heat can be expressed in the form

(2)

$$\frac{T_m^{n+1} - T_m^n}{\Delta t} = \frac{D}{2(\Delta x)^2} (T_{m+1}^{n+1} - 2T_m^{n+1} + T_{m-1}^{n+1} + T_{m+1}^n - 2T_m^n + T_{m-1}^n)$$

with

$$\begin{aligned} T_m^n &= T(x_m, t_n) & T_m^{n+1} &= T(x_m, t_n + \Delta t) \\ T_{m+1}^n &= T(x_m + \Delta x, t_n) & T_{m+1}^{n+1} &= T(x_m + \Delta x, t_n + \Delta t). \\ T_{m-1}^n &= T(x_m - \Delta x, t_n) & T_{m-1}^{n+1} &= T(x_m - \Delta x, t_n + \Delta t) \end{aligned}$$

m and n correspond to the nodes of a regularly spaced grid with respect to the variables x and t, respectively.

The rearrangement of relation (2) and the consideration of initial and boundary conditions yields a set of simultaneous linear equations, which is solved for  $T_m^{n+1}$  at each time step by Gaussian elimination. Dirichlet-boundaries were implemented fixing the temperature at the inner and outer boundary to the initial values throughout the entire simulation. A 400°C hot heat source, which keeps a constant temperature, emits heat into a granitic host rock with 80°C ambient temperature. The size of the model was set to 15 m, and 1000 hours were chosen for the duration of the simulation. To guarantee appropriate precision,  $\Delta x$  and  $\Delta t$  were specified as ca. 2.5 mm and 60 s, respectively. Smaller values for  $\Delta x$  and  $\Delta t$  result in negligible changes of temperature but substantially increase the computational effort. A value of  $0.8 \cdot 10^{-6} \text{ m}^2 \text{ s}^{-1}$  was used for the thermal diffusivity of the host rock, which is within the range of typical values for crustal rocks.



## **II. Upper Jurassic to Early Cretaceous thermal pulse in the later Upper Rhine Graben area**

### Abstract

Hydrothermal mineralisations, mineral alterations as well as fission track (FT) analyses suggests accelerated hydrothermal activity during the Triassic and the Jurassic in the region of the future Upper Rhine Graben (URG). New FT analyses on Permian and Mesozoic deposits of the southern URG area have been carried out to get more insights in the thermal evolution during the Mesozoic. Additionally, to test the effect of heating of the Mesozoic sediments by burial several subsidence analyses have been performed. For this purpose, different hypothetical amounts of today missing Jurassic and Lower Cretaceous deposits were taken into account.

The Jurassic hydrothermal phase is confirmed by the FT analyses of the Permian and Lower Mesozoic sediments. The last intense regional hydrothermal phase, which reached temperatures of or above 180 °C occurred probably between 150 Ma and 140 Ma. FT age signatures indicate that during this time the affected Permian and Lower Triassic units reached abnormal geothermal gradients; higher than 110 °C/km. afterwards, during the Cretaceous the FT-results only show cooling. Accompanying the initial rifting of the URG at about 60 Ma a few localised thermal anomalies with temperatures in excess of 180 °C can be recognised along the eastern URG main border fault.

### **1. Introduction**

The southern Upper Rhine Graben (URG) is bordered by the Vosges (NE-France) in the west, the Black Forest (SW-Germany) in the east and the Jura Mountains (France/Switzerland) in the south (Fig. 1). The sedimentary record in this region comprises Upper Palaeozoic to Upper Jurassic strata and, after a large hiatus, sedimentation continues in the Eocene (Fig. 3). The reason for this stratigraphic gap is still a matter of debate; large-scale domal uplift

starting at the end of Jurassic led to a phase of non-deposition (Illies 1977, Geyer & Gwinner 2004) or, alternatively, Late Cretaceous domal uplift caused complete erosion of Cretaceous sediments (Ziegler 1990). However, additional information is provided by subsidence analysis that is generally documenting cooling of the lithosphere during the Mesozoic (e.g. Ziegler et al. 2004) and by fission track (FT) data of the Palaeozoic basement. The latter suggests complex and possibly rapidly changing thermal conditions in the upper crust from the Permian to the Neogene (Fig. 2, Timar-Geng et al. 2004, 2006a,b).

Based on Mesozoic FT ages, Timar-Geng et al. (2004) concluded that substantial heating of the upper crust mainly during a Jurassic hydrothermal phase was followed by cooling during the Cretaceous. Temperatures up to 250 °C just below the contact between crystalline basement and Mesozoic sedimentary cover were proposed. Considering normal geothermal gradients (~30 °C/km) that cannot be explained with burial alone since the maximum thickness, of Mesozoic strata is on the order of 1500 m (Timar-Geng et al. 2004). Comparable thermal conditions were reported by Madritsch et al. (2008) from the Massif de la Serre (NE-France) about 100 km SW of the Vosges. The recurrent enhanced basement temperatures during the Jurassic in the Vosges, Black Forest and Massif de la Serre (e.g. Timar-Geng et al. 2004, Madritsch et al. 2008) appear to contradict the overall cooling of the European lithosphere (Ziegler et al. 2004). However, there is ample evidence of hydrothermal activity affecting this area during Triassic, Jurassic and partially Cretaceous times (e.g. Wetzel et al. 2003, Brockamp et al. 2003).

A more moderate thermal pulse affected the uppermost crystalline basement of the Vosges and Black Forest during the Eo-Oligocene, simultaneous to the first rifting of the URG. Temperatures in excess of 120 °C within the uppermost crystalline basement were hardly reached on a regional scale, as demonstrated by apatite FT modelling results (Timar-Geng et al. 2006a,b). Additionally, for the northernmost Jura a thermal event related to the URG rifting during the Oligocene and Early Miocene was proposed by vitrinite analyses of Todorov et al. (1993).

In this study new fission track data from the Permian and Mesozoic sediment cover provide the advantage to discriminate between a pre-depositional

thermal history of provenance regions and a post-depositional basin-related thermal history of the subsidence dominated environment in the investigation area during Mesozoic. FT analyses on detrital apatite and zircon grains that experienced considerable post-depositional heating offer the potential to investigate the Mesozoic to Cenozoic thermal conditions of the upper crust in more detail. To test the effect of burial-related thermal overprint of the sampled Permian to Jurassic strata, the Mesozoic subsidence history of the investigated area was taken into account. Especially in the light of the late Jurassic to late Eocene sediment hiatus and the sparse evidences of the upcoming URG, a better knowledge of the Mesozoic thermal history may lead to better understanding of the regional geologic evolution.

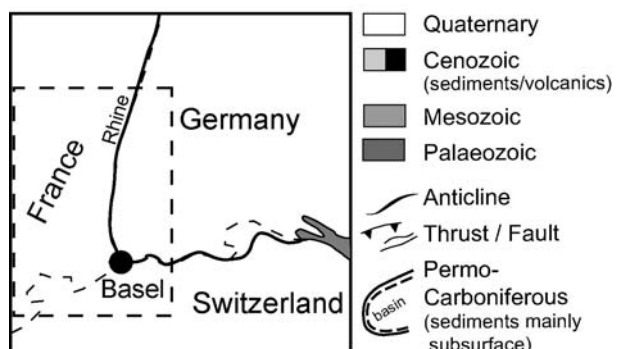
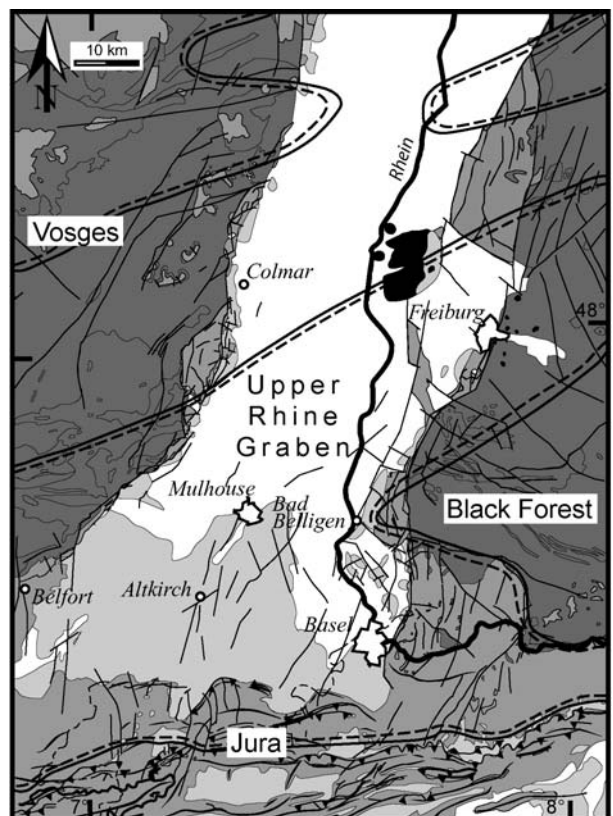


Fig. 1  
Geologic map of the southern URG  
and adjacent areas  
(changed after Metz and Rein 1957,  
Chantraine et al. 1996, Ustaszewski  
et al. 2005)

## 2. Geological background

Metamorphism, large-scale thrust tectonics as well as extensive magmatic activity affected the region of the later URG and its flanks during the Variscan orogeny (e.g. Edel & Fluck 1989, Eisbacher et al. 1989, Echtler & Chauvet 1992, Schaltegger et al. 1996, 2000, Hann et al. 2000). Exhumation and rapid cooling of the crystalline basement rocks introduce a phase of crustal consolidation during the Permian (Fig. 2). At the end of the Variscan orogeny, numerous grabens and half-grabens formed, including a graben system that extends from the Burgundy to the Lake Constance (Fig. 1), mainly documented in the subsurface (Diebold 1989, Laubscher & Noack 1997). Further intramontane basins are positioned to the north, crossing the Black Forest in the same direction (WSW to ENE) (Boigk & Schöneich 1970).

Deposition of Permian strata leads again to increasing temperatures at the top of the basement and the successive deeper and deeper buried sediment layers especially within the Permo-Carboniferous basins. Sedimentation continues during the Mesozoic generally controlled by thermal subsidence (Loup et al. 1999). In addition, opening of the Atlantic and Tethys oceans caused a stretching of the lithosphere of the area in-between, including the study area (Ziegler 1990). The extensional stress regime and the thermal subsidence during the Triassic and Jurassic account for deposition of several hundreds of meters of continental and marine sediments (e.g. Wetzel et al. 2003, Ziegler & Dezes 2005). Subsidence curves from the northern alpine molasse basin, the northern Jura and the southern URG show comparable subsidence histories during Triassic and Jurassic times (Fig. 6 und Wildi et al. 1989, Schegg & Leu 1998, Wetzel et al. 2003, Ziegler et al. 2004, Mazurek et al. 2006). Beside a subtle pattern of numerous subordinate subsidence phases, two main periods of enhanced subsidence are obvious, an early Triassic (about 240-220 Ma) and a middle to late Jurassic (about 180-140 Ma). The last one possibly continued during the Early Cretaceous.

Several periods of accelerated hydrothermal activity that have been recognized by enhanced vein materialisations on the flanks of the later URG until the Neogene (Werner & Franzke 1994, 2001, and references therein,

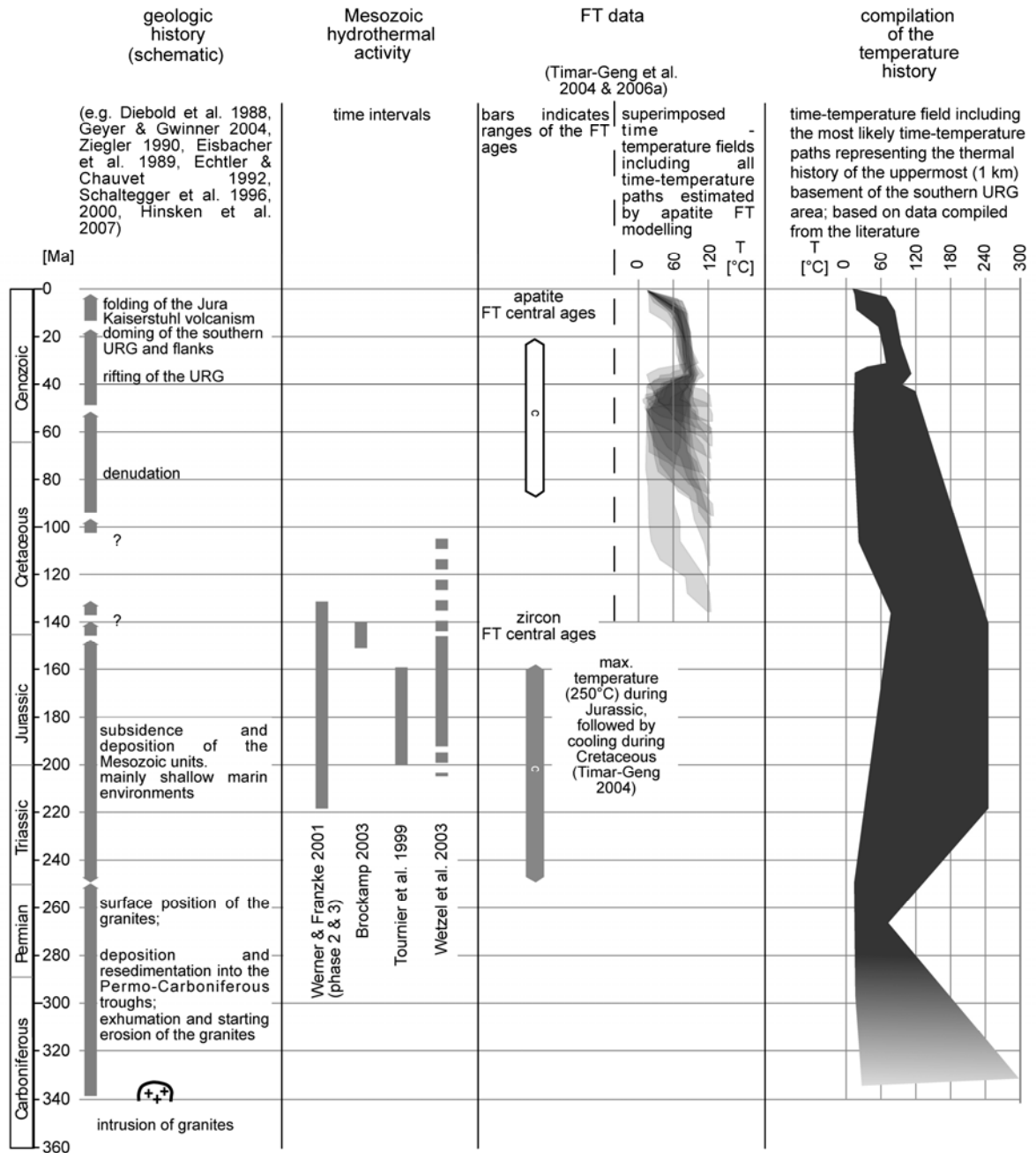


Fig. 2  
Compilation (right column) of geologic history, Mesozoic hydrothermal activity and FT data of the uppermost (1 km) basement of the southern URG area

Brockkamp et al. 2003) are partly contemporaneous to the estimated phases of enhanced subsidence rates (e.g. Wetzel et al. 2003).

After a strong Variscan hydrothermal activity an Upper Permian to Lower Triassic phase is only weakly expressed. From the late Triassic to the late Jurassic localised hydrothermal activity can be recognized in the Vosges and the Black Forest (Werner & Franzke 1994, 2001, Tournier et al. 1999, Wetzel et al. 2003 and references therein). These hydrothermal episodes coincide

with the modal values of zircon FT central ages in the southern Black Forest and Vosges, leading to the interpretation of a regional thermal pulse caused by hydrothermal activity with temperatures up to 250 °C (Timar-Geng et al. 2004, 2006a). Locally in the Black Forest formation-water could be responsible for a lowering of these temperatures to values of 150 °C and 80 °C (Werner & Franzke 2001).

Local fluid inclusion study in the Lower Triassic strata at Guebwiller (Vosges/France) yielded fluid temperatures of about 240 °C (Surma et al. 2003), therefore, maximum temperatures of 250 °C (Timar-Geng et al. 2004) occurring in the Lower Triassic units cannot ruled out.

During the Late Jurassic and the Early Cretaceous a widespread hydrothermal phase is expressed by the regional occurrence of vein materialization and alteration of minerals in the Black Forest (e.g. Werner & Franzke 1994 and references therein, Brockamp et al. 2003)

Wetzel et al. (2003) account the opening of the Atlantic and the extensional stress regime in between (Ziegler 1990) as responsible, for the reactivation of pre-existing structures and related hydrothermal activity in Jurassic times.

Starting in the Late Jurassic (Illies 1977, Geyer & Gwinner 2004) or, alternatively during the Late Cretaceous (Ziegler 1990), uplift of several parts of the northern Alpine foreland related to intraplate compressional stresses (Ziegler & Dezes 2005) led to continental conditions in the region of the later southern URG. Consequently, erosion probably started sometime between the Late Jurassic and Palaeogene. Sporadic pre-rift volcanism occurred since the early Palaeocene (Keller et al. 2002), pointing to a thermal weakening of the lithosphere (Ziegler et al. 2004). However, the maximum of volcanic activity, represented by the Kaiserstuhl volcano complex, developed after the first strong rifting phase at least during the Miocene (19 Ma – 14 Ma; Keller et al. 2002, Wimmenauer 2003).

The initial rifting of the URG is recognized by reworked palaeo and fresh-water limestones of Middle Eocene age (Illies 1967). A pronounced relief developed along the graben margins from the Late Eocene/Early Oligocene onwards when extensional sub-basins formed (e.g. Düringer 1988, Schumacher 2002, Hinsken et al. 2007, Roussé 2006).



The thermal regime of the underground accompanying the initial rifting period of Eocene to Late Oligocene times was known by a temperature increase affecting the crystalline basement of the Vosges, the Black Forest and the northern Switzerland, as suggested by apatite FT modelling (Timar-Geng et al. 2006a,b). Additionally, vein mineralizations have been found to be associated with the early syn-rift tectonic activity during the Palaeogene (Werner & Franzke 2001). Moreover, for the northern Jura palaeo-geothermal gradients during the URG rifting were estimated by vitrinite analyses at about 40 to 100 °C/km.

Regarding the apatite FT analyses by Timar-Geng et al. (2006a,b) the temperatures in the uppermost basement rocks reached in their maximum about 120 °C (Fig. 2). The FT data suggest only cooling afterwards. Although a doming of the Moho is documented below the Kaiserstuhl complex (Rousset et al. 1993) a second regional thermal pulse accompanying the Miocene Volcanism of the Kaiserstuhl is not observable within the FT dataset.

However, today absent sediments, which were deposited during the Oligocene and Early Miocene have been largely eroded in the southern URG documenting uplift of the southern URG area since the Early Miocene (e.g. Roll 1979). Laubscher (1992, 2003) interpreted the uplift of parts of the Black Forest, Vosges and the southern URG along a WSW-striking arc structure through the vicinity of the Kaiserstuhl volcano complex as a response to the alpine orogeny. The reasons of this Miocene up lift are still under discussion (Ziegler & Dezes 2007, Hinsken et al. 2007, Bourgeois et al. 2007). Up to recent times the exposed flanks of the graben were intensely denudated while subsidence of the graben starts again (Illies 1967).

### **3. Sample material**

In the southern URG twenty-seven detrital samples were collected (Fig. 3), covering a stratigraphic range from the Lower Permian (ca. 296 Ma) to the Middle Jurassic (ca. 175 Ma). Due to the low relief of the study area most of the samples have been collected along the escarpments of the URG, which provides acceptable outcrops.



sampled units experienced burial after deposition during the Mesozoic and depending on their geographic position on the graben flanks or along the escarpments possibly during the formation of the URG.

#### **4. Methods**

##### ***FT method***

FT analysis on apatite and zircon is a low-temperature thermochronological method widely used to quantify the thermal history of igneous, metamorphic and clastic sedimentary rocks (e.g. Wagner and van den Haute, 1992, Reiners & Ehlers, 2005).

Fission-track analysis on apatite and zircon was carried out applying the external detector method according to Naeser (1976) and Gleadow (1981).

Apatite and zircon grains were separated from each sample (2 to 8 kg rock material) following standard mineral separation procedure including crushing, magnetic and heavy liquid separation. The zircon samples were mounted in the Teflon PFA®, while the apatite samples were embedded in epoxy resin. After polishing, the apatites were etched for 40 s in 6.5 % HNO<sub>3</sub> at ~18 °C and the zircons for 5 to 14 h in an eutectic-melt of KOH-NaOH (220 °C). Muscovite was used as an external detector (Naeser 1976, Gleadow 1981) and CN-5 (apatite) and CN-1 (zircon) standards as dosimeter glasses. Irradiation with thermal neutrons was carried out at the Australian Nuclear Science and Technology Organisation facility (ANSTO).

Muscovite detectors were etched in 40 % HF for 40 min at ~18 °C. Tracks in apatite, zircon and detector muscovites were counted on a Zeiss (Axioplan2) optical microscope with a 1600x magnification (dry) using a computer-controlled motorised scanning stage, run by the "FT-STAGE 3.11" software (Dumitru, 1993). The FT age determination followed the zeta calibration method (Hurford & Green 1983) with a zeta value of  $380.67 \pm 10.58$  (Durango, CN-5) for apatite and  $145 \pm 6.88$  (Fish Canyon Tuff, CN-1) for zircon.

The FT single grain ages, central ages, analytical errors and chi-square values were calculated using the TRACKKEY software (Dunkl 2002).

To interpret the FT data basic statistical methods were used. To test whether more than one age-population was present the chi-square was used

(Galbraight & Laslett 1993). Samples that have failed the chi-square test ( $P_{\chi^2} < 5\%$ ) are commonly thought to indicate a mixed age composition (e.g. Brandon 1998, Garver et al. 2000, Stewart & Brandon 2004). For such samples the BinomFit® software (e.g. Brandon et al. 1992, Brandon 2005) applying the binominal "peak-fitting" method (Galbraight & Green 1990, Galbraight & Laslett 1993) has been used for peak age (population) calculation. The BinomFit® software determines the optimal number of significant age peaks by using the F-Test, which calculates the improvement of the binominal peak-fitting statistic after each added age peak (e.g. Brandon 1992, 1996, 1998, Stewart & Brandon 2004).

The FT method is sensitive for temperatures between about 40°C to 350°C. (Tagami 2005). Regarding the fission track partial annealing zones (PAZ) used here the temperature brackets given by Gleadow & Duddy (1981) and Green et al. (1989) for apatite (APAZ) 60 to 120 °C and Tagami (2005) for zircon (ZPAZ) are 180 to 350 °C), respectively.

It has been suggested that the annealing temperature for FT's in apatite is controlled mainly by their chemical composition (e.g. Gleadow & Duddy 1981; Green et al., 1985, 1986). One of the important factors influencing the annealing properties of zircon is the radiation damage of the crystal lattice by alpha decay (alpha-damage; Kasuya & Naeser 1988, Rahn et al. 2004). Accumulated radiation damage can lower the temperature boundary of the zircon PAZ (Kasuya & Naeser 1988, Rahn et al. 2004). Unfortunately, a quantification of the lowering of this boundary seems not possible at the moment. According to Tagami (2005), who used natural zircon for his estimations, the 180°C isotherm was used as the lower temperature boundary for the interpretation here.

Sediment samples usually contain detrital grains coming from different source areas bearing different thermal histories within their grain population. If these samples have not been heated significantly after deposition, the peak-fitting method (Galbraith & Green 1990, Galbraith & Laslett 1993) has the potential to discriminate different FT age groups eventually corresponding to different provenance regions (e.g. Brandon 1998, Carter 1999, Garver et al. 2000, Bernet & Garver 2005). Otherwise, every relevant post-depositional heating

event should cause an overprint of the inherited FT signature and offer the potential to investigate the post-depositional thermal history.

The degree of influence of post-depositional events on the FT data depends on the different annealing characteristics of the individual grains. Supposing that the possible spectrum of annealing characteristics of single grains within one detrital sample was well represented, an interpretation of the FT single grain ages deliver a high potential for interpretation of thermal histories.

During cooling through the PAZ, thermal low sensitive grains should close at first while thermal high sensitive grains close at last representing the best approximation of the age of the last cooling below the lower boundary of the PAZ (Fügenschuh and Schmid 2003).

Therefore, the younger age peaks estimated from the single grains of the apatite and zircon samples probably contain the grains with the lowest thermal stability. After a post-depositional heating event, these grains will be the last to start their FT clock when they cool down trough the APAZ or ZPAZ respectively (Brandon et al. 1998). The youngest age peak then is indicative of the maximum age for the last cooling below the specific PAZ after a significant heating event (e.g. Fügenschuh & Schmid 2003).

If the zircon FT peak age of samples documents post-depositional reheating ( $T > 180\text{ °C}$ ), total resetting of the apatite FT system in these samples can be assumed. In this case the old apatite FT peak ages represent the minimum age of the cooling into the APAZ.

### ***Subsidence analysis***

Subsidence analysis was carried out on representative sections of the Mesozoic sediment column (Fig. 3). Two deposition scenarios have been considered assuming different amounts of missing Late Mesozoic deposits.

Deposition scenario I comprise the sediment column up to the end of Jurassic. The amount of today locally eroded Middle and Upper Jurassic sediments has been evaluated considering the thickness of these units within boreholes in the southern URG in a probably complete stratigraphic column (e.g. Otterbach II, Häring 2002; Hirtzbach, Vonderschmidt 1942), the known thickness in the adjacent Swabian Alb (Geyer & Gwinner 2004) and the Swiss Jura (Müller et

al. 1984, Bitterli-Brunner 1987). Thus, Upper Jurassic strata were estimated to be in the thickness range of 350 m.

Deposition scenario II comprises the sediment columns used in scenario I plus 450 m of Lower Cretaceous deposits. This number is based on subsidence analysis and thermo-chronological data from central northern Switzerland (Mazurek et al., 2006). These authors proposed a maximum thickness of 450 m of Lower Cretaceous deposits.

Considering the deposition scenarios, between well-reported boreholes and vertical sections, N-S directed transects along the western and eastern margin of the URG were constructed (Fig.3, 4). The sample position of each FT samples were projected onto these transects according to their stratigraphic position, to estimate the burial of each sample within the different deposition scenarios at the given time. These burial values of each sample was determined using standard decompaction and backstripping methods (see below)

The subsidence analyses on several vertical sections were prepared by using a Microsoft excel™ spreadsheet called EASYSUB (primary Backstripp89; by Uriate & Schegg 1991 and modified by Borel 1995), which uses the standard backstripping and decompaction techniques (e.g. Van Hinte 1978, Sclater and Christie 1980, Funk 1985, Wildi 1989, Allen & Allen 1990). The lithological parameters (porosity and compaction coefficients) are included from Sclater & Christie (1980), Sawyer et al (1982), Schmoker & Halley (1982) and Borel (1995) (Tab. 4, Appendix).

Due to the geographic position of the samples along the graben margins and on top of the flanks only minor or no eroded Cenozoic deposits are expected. Furthermore, eroded Upper Jurassic and Cretaceous deposits are responsible for compaction of the underlying units, which, during a possible Cenozoic burial, are not or only moderately affected by a continued compaction. Therefore, the Cenozoic accumulation of syn-rift deposits was not considered. The Bathymetric changes during the Mesozoic in the study area with max. water depths of up to 150 m were considered according to Allia (1996) and Wetzel and Allia (2003).



Estimation of the palaeo-surface temperature influences the palaeo-gradient calculations. Due to significant climatic changes and changes between marine and continental surface condition as well as the probably not linear character of thermal gradients at shallow depths (< ~500m) it is difficult to find a single and representative value. Fully aware, that this problem was not solved palaeo-surface temperatures of 20 °C during the Permian, Mesozoic and Cenozoic and for the Quaternary 10 °C was chosen. If the surface temperature varies by  $\pm 10^{\circ}\text{C}$ , the gradients vary as well within the first 3000m with values of up to  $\pm 10^{\circ}\text{C}/\text{km}$ . It has to be noted that these calculations of hypothetical gradients are only rough estimations for getting an overview onto the thermal stage at the investigated age levels. There are a lot of factors influencing the estimation of the palaeo-geothermal gradients, which cannot be quantified. For instance the water content of the sediments, which is an important factor considering the conductivity of an unit is unknown. It has to paid attention, considering the various not quantifiable uncertainties influencing these calculations, no errors were calculated.

## 5. Results

### ***FT data***

Twenty-seven samples yielded 16 apatite and 25 zircon data (Tab. 1; apatite, Tab. 2; zircon, Fig. 5; the peak ages, central ages and deposition ages).

Apatite samples:

The apatite FT peaks calculated by the BINOMFIT® software and central ages range between  $21 \pm 3$  Ma (HD77) and  $195 \pm 19$  Ma (HD57) (Tab. 1). All apatite samples show post-depositional peak ages.

Zircon samples:

The zircon FT peak and central ages ranges between  $55 \pm 13$  Ma (HD169) and  $349 \pm 112$  Ma (HD79) (Tab. 2). All sampled stratigraphic units yielded FT central or peak ages ( $\pm 1\sigma$  error), which are younger and older than the deposition age. Especially the samples of the Permian and Triassic strata show a significant younging of many zircon FT peak and central ages in respect to the deposition age (Fig. 5).



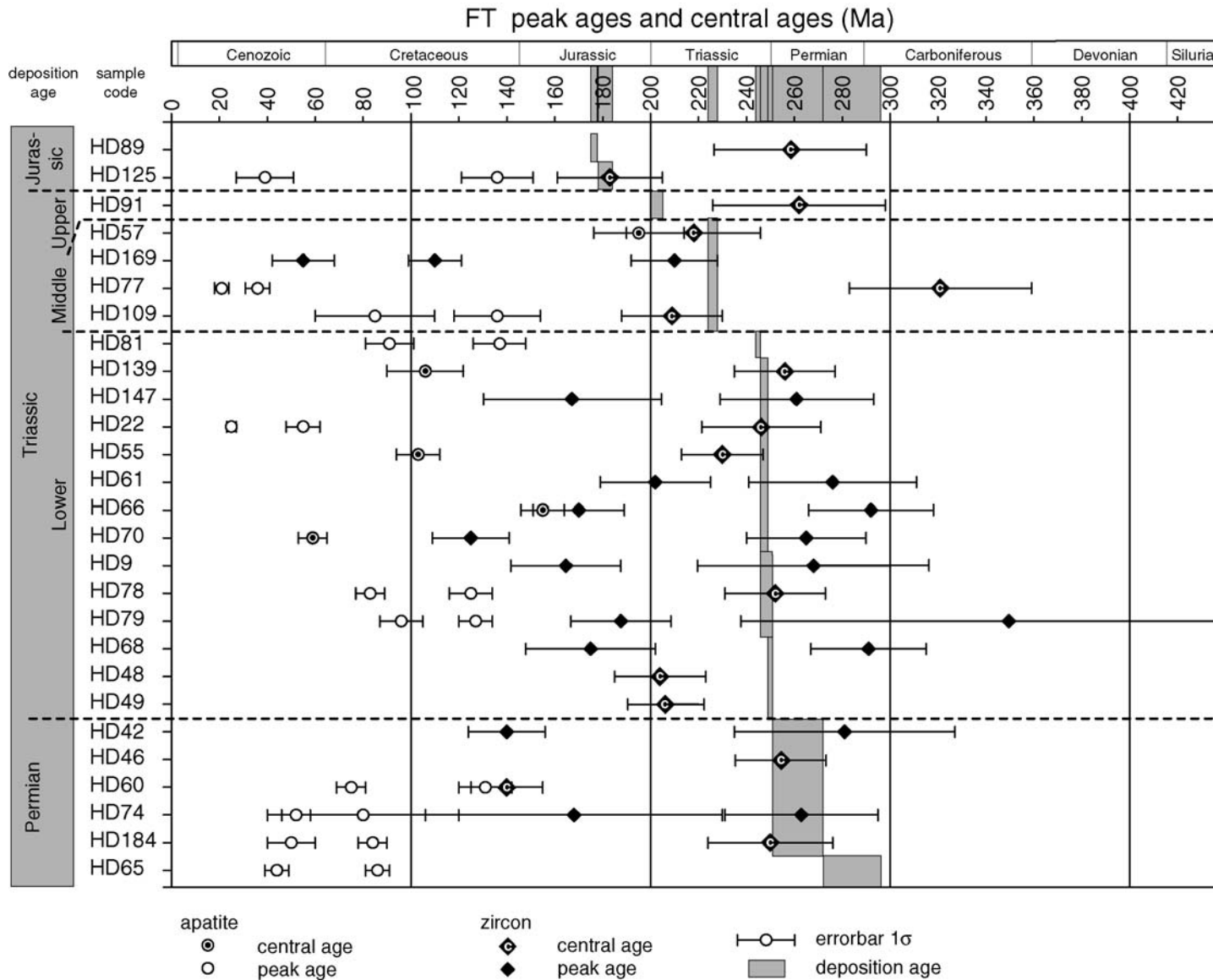


Fig. 5  
Apatite and zircon FT peak and central ages and sample deposition age

| Deposition age<br>Ma | Stratigraphy    | Lithology  | sample code | Coordinates<br>(G K Zone3) | elev.<br>[m] | No. of crystals counted<br>(n) | Spontaneous tracks<br>$\rho_s$ (Ns) | Induced tracks<br>$\rho_i$ (Ni) | $P(\chi^2)$<br>(%) value | Dosimeter<br>$\rho_d$ (Nd) | Disp. | Central-age<br>Ma $\pm 1\sigma$ | peak age 1 (Mio-Oligocene)<br>Ma $\pm 1\sigma$ (n) | peak age 2 (Eocene)<br>Ma $\pm 1\sigma$ (n) | peak age 3 (Late Cretaceous)<br>Ma $\pm 1\sigma$ (n) | peak age 4 (Early Cretaceous)<br>Ma $\pm 1\sigma$ (n) |
|----------------------|-----------------|------------|-------------|----------------------------|--------------|--------------------------------|-------------------------------------|---------------------------------|--------------------------|----------------------------|-------|---------------------------------|--|---|--|---|
| 178-184              | Lower Jurassic  | silt-stone | HD 125      | 3400540,<br>5287135        | 350          | 9                              | 14 (209)                            | 23 (331)                        | 0<br>32                  | 9.15<br>(2648)             | 0.52  | 93 $\pm$ 20                     |  | 39<br>(3) $\pm$ 12                          |  | 136<br>(6) $\pm$ 15                                   |
| 224-226              | Middle Triassic | sandstone  | HD 57       | 3396320,<br>5266390        | 370          | 15                             | 13 (314)                            | 15(372)                         | 14<br>20                 | 12.3<br>(1648)             | 0.16  | 195 $\pm$ 19                    |  |   |  |   |
| 224-226              | Middle Triassic | sandstone  | HD 77       | 3400560,<br>5295030        | 550          | 33                             | 3 (291)                             | 20 (1796)                       | 2<br>51                  | 8.8 (2730)                 | 0.25  | 27 $\pm$ 3                      | 21<br>(18) $\pm$ 3                                 | 36<br>(15) $\pm$ 5                          |  |   |
| 224-226              | Middle Triassic | sandstone  | HD 109      | 3409530,<br>5312230        | 395          | 18                             | 11 (409)                            | 19 (686)                        | 2<br>31                  | 10 (2648)                  | 0.24  | 110 $\pm$ 11                    |  |   | 85<br>(9) $\pm$ 25                                   | 136<br>(9) $\pm$ 18                                   |
| 246-249              | Lower triassic  | sandstone  | HD 22       | 3406225,<br>5306400        | 365          | 46                             | 8 (1068)                            | 30 (4195)                       | 0<br>180                 | 6.3 (3641)                 | 0.37  | 31 $\pm$ 2                      | 25<br>(34) $\pm$ 2                                 | 55<br>(12) $\pm$ 7                          |  |   |
| 246-249              | Lower triassic  | sandstone  | HD 55       | 3408230,<br>5308860        | 305          | 7                              | 13 (244)                            | 29 (526)                        | 15<br>9                  | 11.8<br>(2730)             | 0.00  | 103 $\pm$ 9                     |  |   |  |   |
| 246-249              | Lower triassic  | sandstone  | HD 66       | 3365143,<br>5308233        | 510          | 13                             | 31 (986)                            | 41 (1296)                       | 28<br>14                 | 10.9<br>(1648)             | 0.06  | 155 $\pm$ 9                     |  |   |  |   |
| 246-249              | Lower triassic  | sandstone  | HD 70       | 3368521,<br>5343075        | 840          | 4                              | 12 (130)                            | 37 (385)                        | 77<br>1                  | 9 (2730)                   | 0.00  | 59 $\pm$ 6                      |  |   |  |   |
| 246-251              | Lower triassic  | sandstone  | HD 78       | 3421180,<br>5275990        | 838          | 20                             | 28 (1782)                           | 43 (2764)                       | 0<br>71                  | 8 (3641)                   | 0.21  | 98 $\pm$ 7                      |  |   | 83<br>(12) $\pm$ 6                                   | 125<br>(8) $\pm$ 9                                    |
| 246-251              | Lower triassic  | sandstone  | HD 79       | 3421250,<br>5274410        | 800          | 18                             | 33 (1682)                           | 52 (2685)                       | 5<br>28                  | 10 (1648)                  | 0.12  | 117 $\pm$ 7                     |  |   | 84<br>(12) $\pm$ 7                                   | 126<br>(8) $\pm$ 10                                   |
| 244-246              | Lower triassic  | sandstone  | HD 81       | 3401145,<br>5272780        | 360          | 30                             | 24 (1291)                           | 37 (1976)                       | 0<br>66                  | 9.5 (1648)                 | 0.22  | 116 $\pm$ 8                     |  |   | 85<br>(12) $\pm$ 8                                   | 127<br>(8) $\pm$ 11                                   |
| 246-249              | Lower triassic  | sandstone  | HD 139      | 3413350,<br>5316325        | 330          | 6                              | 14 (78)                             | 28 (151)                        | 35<br>6                  | 11 (2797)                  | 0.10  | 106 $\pm$ 16                    |  |   |  |   |
| 251-272              | Permian         | arose      | HD 60       | 3341870,<br>5289149        | 490          | 28                             | 12.98 (932)                         | 26.7<br>(1920)                  | 0<br>77                  | 10.8<br>(2730)             | 0.27  | 103 $\pm$ 8                     |  |   | 75<br>(13) $\pm$ 6                                   | 131<br>(15) $\pm$ 11                                  |
| 296-272              | Permian         | arose      | HD 65       | 3347442,<br>5287860        | 400          | 28                             | 8 (1216)                            | 24 (3032)                       | 0<br>91                  | 9.7 (2730)                 | 0.28  | 70 $\pm$ 5                      |  | 44 (9) $\pm$ 5                              | 86<br>(19) $\pm$ 5                                   |   |
| 251-272              | Permian         | arose      | HD 074      | 3401245,<br>5285735        | 530          | 10                             | 19 (504)                            | 44 (1172)                       | 0<br>24                  | 6.9 (3641)                 | 0.21  | 56 $\pm$ 5                      |  | 52 (8) $\pm$ 6                              | 80<br>(2) $\pm$ 40                                   |   |
| 251-272              | Permian         | arose      | HD 184      | 3405170,<br>5285095        | 435          | 40                             | 13 (869)                            | 28 (1931)                       | 5<br>55                  | 9.17<br>(2797)             | 0.16  | 78 $\pm$ 5                      |  | 49 (7) $\pm$ 10                             | 84<br>(33) $\pm$ 6                                   |   |

Tab. 1  
Apatite FT data

Coordinates (x, y) of Gauss Krüger DHDN Zone 3, Elevation (elev.) in metres above sea level, Number of grains counted (n).  $\rho_s$ ,  $\rho_i$  and  $\rho_d$  are spontaneous, induced and dosimeter track densities in  $10^5$  tracks/cm<sup>2</sup>. N are number of tracks counted shown in brackets. Analyses by external detector method using 0.5 for the  $4\pi/2\pi$  geometry correction factor. Disp., Dispersion, according to Galbraith and Laslett (1993). Ages calculated as central ages according to Galbraith and Laslett (1993) using dosimeter glass CN5 for apatite with  $\zeta_{CN5} = 380.67 \pm 10.58$  (H. Dresmann).  $P(\chi^2)$  is the probability of obtaining  $\chi^2$  value for  $\nu$  degrees of freedom where  $\nu =$  number of crystals-1. Samples that have failed the chi-square test ( $P\chi^2 < 5\%$ ) the BinomFit® software (e.g. Brandon et al. 1992, Brandon 2005) applying the binominal "peak-fitting" method (Galbright & Green 1990, Galbright & Laslett 1993) has been used for peak age calculation.

| Deposition age Ma | Stratigraphy    | Litho. code | sample code | Coordinates (G K Zone3) | elev. [m]       | No. of crystals counted (n) | Spontaneous tracks ps (Ns) | Induced tracks pi (Ni) | P( $\chi^2$ ) (%) value | Dosimeter pd (Nd) | Disp. | Central-age Ma $\pm 1\sigma$ | peak age 1 (Cenozoic) Ma $\pm 1\sigma$ (n) | peak age 2 (Cretaceous) Ma $\pm 1\sigma$ (n) | peak age 3 (Jurassic) Ma $\pm 1\sigma$ (n) | peak age 4 (Triassic) Ma $\pm 1\sigma$ (n) | peak age 5 (Palaeozoic) Ma $\pm 1\sigma$ (n) |
|-------------------|-----------------|-------------|-------------|-------------------------|-----------------|-----------------------------|----------------------------|------------------------|-------------------------|-------------------|-------|------------------------------|--|--|--|--|--|
| 178-175           | Middle Jurassic | 1           | HD 89       | 3383611, 5250426        | 660             | 11                          | 205 (1671)                 | 16 (133)               | 20<br>13                | 2.92 (1625)       | 0.18  | <b>259</b> $\pm$ <b>32</b>   |  |  |  |  |  |
| 178-184           | Lower Jurassic  | 2           | HD 125      | 3400540, 5287135        | 360             | 8                           | 232 (731)                  | 34 (106)               | 85<br>3                 | 3.71 (1338)       | 0.01  | <b>183</b> $\pm$ <b>22</b>   |  |  |  |  |  |
| 200-205           | Middle Triassic | 1           | HD 91       | 3384254, 5250063        | 570             | 8                           | 235 (738)                  | 24 (76)                | 39<br>7                 | 3.8 (936)         | 0.10  | <b>262</b> $\pm$ <b>36</b>   |  |  |  |  |  |
| 224-226           | Middle Triassic | 1           | HD 109      | 3409530, 5312230        | 395             | 18                          | 179 (1290)                 | 24 (170)               | 67<br>14                | 3.87 (1338)       | 0.01  | <b>209</b> $\pm$ <b>21</b>   |  |  |  |  |  |
| 224-226           | Middle Triassic | 1           | HD 169      | 3400375, 5281420        | 410             | 45                          | 151 (4882)                 | 24 (770)               | 0<br>147                | 3.4 (1338)        | 0.42  | <b>155</b> $\pm$ <b>15</b>   | <b>55</b> (2) $\pm$ <b>13</b>              | <b>110</b> (14) $\pm$ <b>11</b>              |  | <b>210</b> (29) $\pm$ <b>18</b>            |  |
| 224-226           | Middle Triassic | 1           | HD 57       | 3396320, 5266390        | 370             | 7                           | 214 (663)                  | 29 (88)                | 58<br>5                 | 4.07 (936)        | 0.01  | <b>218</b> $\pm$ <b>28</b>   |  |  |  |  |  |
| 224-226           | Middle Triassic | 1           | HD 77       | 3400560, 5295030        | 550             | 13                          | 181 (1183)                 | 16 (103)               | 78<br>8                 | 3.95 (936)        | 0.00  | <b>321</b> $\pm$ <b>38</b>   |  |  |  |  |  |
| 246-249           | Lower Triassic  | 1           | HD 139      | 3413350, 5316325        | 330             | 19                          | 156 (3000)                 | 16 (304)               | 68<br>15                | 3.63 (1338)       | 0.05  | <b>256</b> $\pm$ <b>21</b>   |  |  |  |  |  |
| 246-249           | Lower Triassic  | 1           | HD 147      | 3371291, 5323818        | 590             | 19                          | 265 (2952)                 | 29 (325)               | 5<br>29                 | 3.5 (936)         | 0.20  | <b>223</b> $\pm$ <b>22</b>   |  | <b>167</b> (5) $\pm$ <b>37</b>               |  | <b>261</b> (14) $\pm$ <b>32</b>            |  |
| 246-249           | Lower Triassic  | 1           | HD 22       | 3406225, 5306400        | 365             | 30                          | 258 (2656)                 | 19 (202)               | 6<br>42                 | 2.69 (1625)       | 0.25  | <b>246</b> $\pm$ <b>25</b>   |  |  |  |  |  |
| 249-251           | Lower Triassic  | 1           | HD 48       | 3368117, 5330714        | 670             | 11                          | 253 (1547)                 | 37 (224)               | 52<br>9                 | 4.14 (936)        | 0.01  | <b>204</b> $\pm$ <b>19</b>   |  |  |  |  |  |
| 249-251           | Lower Triassic  | 1           | HD 49       | 3367885, 5330935        | 720             | 20                          | 200 (2972)                 | 28 (424)               | 36<br>21                | 4.11 (936)        | 0.02  | <b>206</b> $\pm$ <b>16</b>   |  |  |  |  |  |
| 246-249           | Lower Triassic  | 1           | HD 55       | 3408230, 5308860        | 305             | 23                          | 221 (3804)                 | 28 (482)               | 78<br>17                | 4.09 (936)        | 0.02  | <b>230</b> $\pm$ <b>17</b>   |  |  |  |  |  |
| 246-249           | Lower Triassic  | 1           | HD 61       | 3349644, 5290132        | 410             | 32                          | 182 (5800)                 | 23 (720)               | 3<br>47                 | 4.06 (1338)       | 0.14  | <b>232</b> $\pm$ <b>17</b>   |  |  |  | <b>202</b> (17) $\pm$ <b>23</b>            | <b>276</b> (15) $\pm$ <b>35</b>              |
| 246-249           | Lower Triassic  | 1           | HD 66       | 3365143, 5308233        | 510             | 22                          | 269 (5652)                 | 32 (671)               | 0<br>74                 | 4 (936)           | 0.29  | <b>228</b> $\pm$ <b>22</b>   |  | <b>170</b> (9) $\pm$ <b>19</b>               |  | <b>292</b> (13) $\pm$ <b>26</b>            |  |
| 249-251           | Lower Triassic  | 1           | HD 68       | 3372978, 5338278        | 360             | 30                          | 302 (8156)                 | 24 (646)               | 0<br>59                 | 2.9 (1625)        | 0.22  | <b>246</b> $\pm$ <b>20</b>   |  | <b>175</b> (8) $\pm$ <b>27</b>               |  | <b>291</b> (22) $\pm$ <b>24</b>            |  |
| 246-249           | Lower Triassic  | 1           | HD 70       | 3368521, 5343075        | 840             | 20                          | 248 (3029)                 | 33 (403)               | 0<br>71                 | 3.97 (936)        | 0.33  | <b>234</b> $\pm$ <b>26</b>   |  | <b>125</b> (2) $\pm$ <b>16</b>               |  | <b>265</b> (18) $\pm$ <b>25</b>            |  |
| 246-251           | Lower Triassic  | 1           | HD 78       | 3421180, 5275990        | 838             | 14                          | 320 (5097)                 | 25 (403)               | 15<br>18                | 2.83 (1625)       | 0.11  | <b>252</b> $\pm$ <b>21</b>   |  |  |  |  |  |
| 246-251           | Lower Triassic  | 1           | HD 79       | 3421250, 5274410        | 800             | 15                          | 238 (2132)                 | 32 (287)               | 5<br>24                 | 3.93 (936)        | 0.19  | <b>211</b> $\pm$ <b>21</b>   |  | <b>187</b> (12) $\pm$ <b>21</b>              |  | <b>349</b> (3) $\pm$ <b>112</b>            |  |
| 246-251           | Lower Triassic  | 1           | HD 9        | 3395140, 5271935        | 1830-1840<br>bs | 16                          | 251 (1764)                 | 32 (226)               | 5<br>25                 | 3.5 (1625)        | 0.21  | <b>193</b> $\pm$ <b>21</b>   |  | <b>164</b> (10) $\pm$ <b>23</b>              |  | <b>268</b> (6) $\pm$ <b>49</b>             |  |
| 251-272           | Permian         | 3           | HD 42       | 3401565, 5281035        | 435             | 24                          | 197 (3226)                 | 24 (396)               | 0<br>66                 | 3.26 (1502)       | 0.35  | <b>208</b> $\pm$ <b>23</b>   |  | <b>140</b> (10) $\pm$ <b>16</b>              |  | <b>281</b> (14) $\pm$ <b>46</b>            |  |
| 251-272           | Permian         | 3           | HD 46       | 3418335, 5330440        | 250             | 36                          | 231 (5527)                 | 20(474)                | 36<br>37                | 3.06 (1625)       | 0.10  | <b>254</b> $\pm$ <b>19</b>   |  |  |  |  |  |
| 251-272           | Permian         | 3           | HD 60       | 3341870, 5289149        | 490             | 6                           | 299 (796)                  | 46 (123)               | 71<br>3                 | 3.01 (1625)       | 0.00  | <b>140</b> $\pm$ <b>16</b>   |  |  |  |  |  |
| 251-272           | Permian         | 3           | HD 74       | 3401245, 5285735        | 530             | 12                          | 310 (3335)                 | 27 (290)               | 1<br>25                 | 2.86 (1625)       | 0.22  | <b>230</b> $\pm$ <b>24</b>   |  | <b>168</b> (3) $\pm$ <b>62</b>               |  | <b>263</b> (9) $\pm$ <b>32</b>             |  |
| 251-272           | Permian         | 3           | HD 184      | 3405170, 5285095        | 435             | 14                          | 268 (1639)                 | 25 (153)               | 68<br>10                | 3.28 (936)        | 0.01  | <b>250</b> $\pm$ <b>26</b>   |  |  |  |  |  |

Tab. 2 Zircon FT data; Lithology code: 1=sandstone, 2=Siltstone, 3=arcose; bs = below surface

Coordinates (x, y) of Gauss Krüger DHDN Zone 3, Elevation (elev.) in metres above sea level, Number of grains counted (n).  $\rho_s$ ,  $\rho_i$  and  $\rho_d$  are spontaneous, induced and dosimeter track densities in  $10^5$  tracks/cm<sup>2</sup>. N are number of tracks counted shown in brackets. Analyses by external detector method using 0.5 for the  $4\pi/2\pi$  geometry correction factor. Disp., Dispersion, according to Galbraith and Laslett (1993). Ages calculated as central ages according to Galbraith and Laslett (1993) using dosimeter glass CN1 for zircon with  $\zeta_{CN1} = 145 \pm 6.88$  (H. Dresmann).  $P(\chi^2)$  is the probability of obtaining  $\chi^2$  value for  $\nu$  degrees of freedom where  $\nu$  = number of crystals-1. Samples that have failed the chi-square test ( $P_{\chi^2} < 5\%$ ) the BinomFit® software (e.g. Brandon et al. 1992, Brandon 2005) applying the binominal "peak-fitting" method (Galbright & Green 1990, Galbright & Laslett 1993) has been used for peak age calculation.

### **Subsidence curves**

The modelled subsidence curves of the Triassic and Jurassic periods are in agreement with the previously published subsidence curves from the southern URG and adjacent areas (Fig. 6; Wildi et al. 1989, Schegg & Leu 1998, Wetzler et al. 2003, Ziegler et al. 2004, Mazurek et al. 2006). All investigated sections show accelerated subsidence in the Early and Middle Triassic and additionally in the Middle Jurassic, which continued during the Cretaceous, depending on the estimate about the amount of Cretaceous sediments (Fig. 6).

The determined palaeo-depths of the samples ranges between some hundred meters considering no Cretaceous deposits and up to 1890 m by supposing 450 m of Cretaceous sediment thickness according to deposition scenario II (Tab. 3, Fig. 8 Appendix).

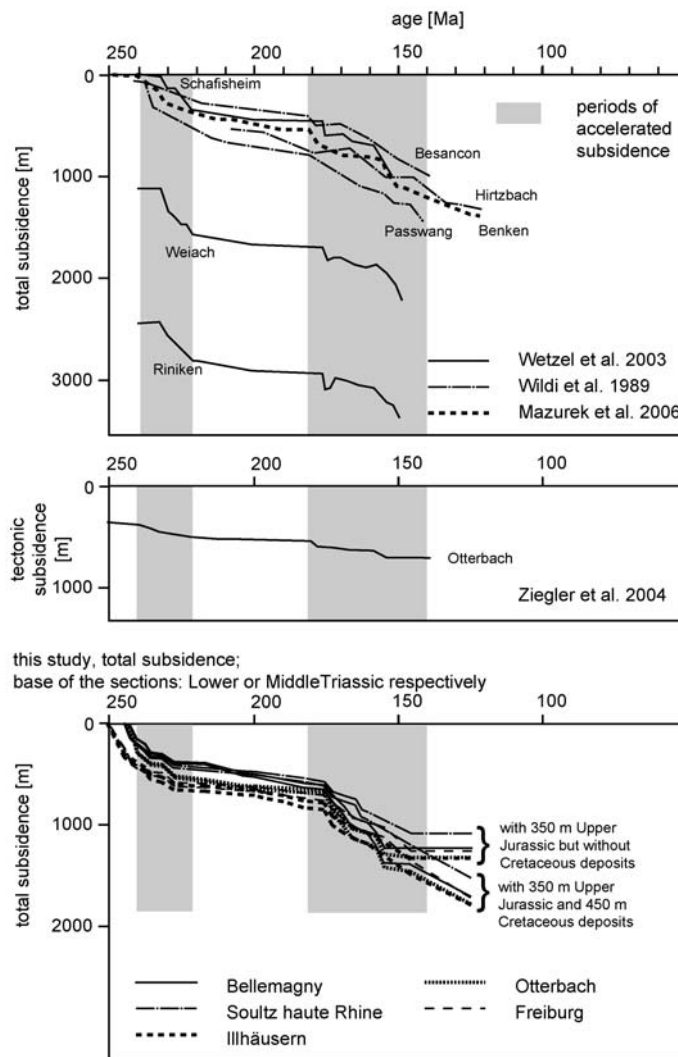


Fig. 6  
Subsidence curves of the base of the Mesozoic from the southern URG and adjacent areas

### ***Palaeo-geothermal gradients***

Related to the deposition scenarios two distinct age levels were studied for the integration with the new FT data. The first investigated age level is at 166 Ma coeval to the end of deposition of the Middle Jurassic Hauptrogenstein Formation (Gonzales and Wetzel 1996). Timar-Geng et al. (2004) estimated a thermal pulse affecting the uppermost crystalline basement with temperatures of up to 250 °C approximately at this time. Additionally, this top Hauptrogenstein horizon is a regional wide marker, which is easily to identify with in borehole logs of the region. The second age level is at 125 Ma, an Early Cretaceous age, which is supposed as the age of maximum sediment thickness during deposition scenario II. This age correspond to a distinct significant Mesozoic thermal pulse recognised in the central northern Swiss by Mazurek et al (2006).

The calculated palaeo-depths of the samples combined with the FT data, provide an estimate of hypothetical post-depositional palaeo-geothermal gradients (Tab. 3). Considering annealing of FTs in zircon and the same deposition scenario as estimated for the northern Switzerland by Mazurek et al. (2006), palaeo-geothermal gradients of 85 °C/km to 108 °C/km can be estimated for the Cretaceous at 125 Ma, which are significantly lower compared to 134 °C/km to 333 °C/km estimated for the Middle Jurassic at ca. 166 Ma. Without Cretaceous deposits gradients increase to values between 111 °C/km to 211 °C/km and to 142 °C/km to 381 °C/km for 125 Ma and 166 Ma respectively.

Additionally, the table 3 shows the necessary overburden of each sample, if a Cretaceous (at ~125 Ma) palaeo-geothermal gradient of about 40 °C/km, as estimated for the central Swiss Molasse Basin (Mazurek et al. 2006), should be transferred to the URG. About 2500 m thick Cretaceous deposits are necessary to reach the required burial of the individual samples.

|                                 | Deposition scenario | II<br>with Upper Jurassic (350m)<br>and Cretaceous (450m) |                   |  | II<br>with Upper Jurassic (350m)<br>and Cretaceous (450m) |                   |  | I<br>with Upper Jurassic (350m)<br>without Cretaceous |                   |  | I<br>with Upper Jurassic (350m)<br>without Cretaceous |                   |  | according to the thermal regime<br>of the central Swiss Molasse<br>Basin (Mazurek et al. 2006);<br>with Upper Jurassic (350m) and<br>Cretaceous (2500m) |                   |  |        |  |  |
|---------------------------------|---------------------|---|-------------------|--|---|-------------------|--|---|-------------------|--|---|-------------------|--|---|-------------------|--|--------|--|--|
|                                 |                     | investigated age  |                   |  | 125 Ma  |                   |  | 166 Ma  |                   |  | 125 Ma  |                   |  | 166 Ma  |                   |  | 125 Ma |  |  |
|                                 |                     | sample code   | sample depth<br>m | geothermal gradient<br>necessary to reach at<br>temperatures of: |   | sample depth<br>m | geothermal gradient<br>necessary to reach at<br>temperatures of: |   | sample depth<br>m | geothermal gradient<br>necessary to reach at<br>temperatures of: |   | sample depth<br>m | geothermal gradient<br>necessary to reach at<br>temperatures of: |   | sample depth<br>m | geothermal gradient<br>necessary to reach at<br>temperatures of: |        |  |  |
| 180 °C                          | 120 °C              |   |                   | 180 °C   | 120 °C  |                   | 180 °C   | 120 °C  |                   | 180 °C   | 120 °C  |                   | 180 °C   | 120 °C  |                   |  |        |  |  |
| western margin and<br>Vosges    | HD 70 (zr /ap)      | 1740  | 92                | 57   | 960   | 167               | 104  | 1160  | 138               | 86   | 850   | 188               | 118  | 3810  | 42                | 26   |        |  |  |
|                                 | HD 68 (zr)          | 1890  | 85                |  | 1100  | 145               |  | 1300  | 123               |  | 940   | 170               |  | 3940  | 41                |  |        |  |  |
|                                 | HD 48 (zr)          | 1800  | 89                |  | 1030  | 155               |  | 1240  | 129               |  | 970   | 165               |  | 3850  | 42                |  |        |  |  |
|                                 | HD 49 (zr)          | 1800  | 89                |  | 1030  | 155               |  | 1240  | 129               |  | 970   | 165               |  | 3850  | 42                |  |        |  |  |
|                                 | HD147 (zr)          | 1610  | 99                |  | 860   | 186               |  | 1100  | 145               |  | 840   | 190               |  | 3660  | 44                |  |        |  |  |
|                                 | HD 66 (zr/ap)       | 1480  | 108               | 68   | 760   | 211               | 132  | 1020  | 157               | 98   | 810   | 198               | 123  | 3530  | 45                | 28   |        |  |  |
|                                 | HD 61 (zr)          | 1640  | 98                |  | 950   | 168               |  | 1210  | 132               |  | 920   | 174               |  | 3690  | 43                |  |        |  |  |
|                                 | HD 60 (zr/ap)       | 1710  | 94                | 58   | 1020  | 157               | 98   | 1270  | 126               | 79   | 980   | 163               | 102  | 3760  | 43                | 27   |        |  |  |
|                                 | HD 65 (- /ap)       | 1750  |                   | 57   | 1070  |                   | 93   | 1310  |                   | 76   | 1010  |                   | 99   | 3800  |                   | 26   |        |  |  |
| eastern margin and Black Forest | HD 46 (zr)          | 1760  | 91                |  | 1040  | 154               |  | 1300  | 123               |  | 970   | 165               |  | 3810  | 42                |  |        |  |  |
|                                 | HD139 (zr/ap)       | 1590  | 101               | 63   | 860   | 186               | 116  | 1140  | 140               | 88   | 810   | 198               | 123  | 3640  | 44                | 27   |        |  |  |
|                                 | HD109 (zr/ap)       | 1200  | 133               | 83   | 480   | 333               | 208  | 760   | 211               | 132  | 420   | 381               | 238  | 3250  | 49                | 31   |        |  |  |
|                                 | HD 55 (zr/ap)       | 1640  | 98                | 61   | 920   | 174               | 109  | 1190  | 134               | 84   | 860   | 186               | 116  | 3690  | 43                | 27   |        |  |  |
|                                 | HD 22 (zr/ap)       | 1650  | 97                | 61   | 930   | 172               | 108  | 1200  | 133               | 83   | 880   | 182               | 114  | 3700  | 43                | 27   |        |  |  |
|                                 | HD 77 (- /ap)       | 1200  |                   | 83   | 530   |                   | 189  | 800   |                   | 125  | 450   |                   | 222  | 3250  |                   | 31   |        |  |  |
|                                 | HD125 (zr/ap)       | 1180  | 136               | 85   | 480   | 333               | 208  | 760   | 211               | 132  | 430   | 372               | 233  | 3230  | 50                | 31   |        |  |  |
|                                 | HD 74 (zr/ap)       | 1840  | 87                | 54   | 1170  | 137               | 85   | 1420  | 113               | 70   | 1090  | 147               | 92   | 3890  | 41                | 26   |        |  |  |
|                                 | HD184 (zr/ap)       | 1850  | 86                | 54   | 1180  | 136               | 85   | 1420  | 113               | 70   | 1100  | 145               | 91   | 3900  | 41                | 26   |        |  |  |
|                                 | HD169 (zr)          | 1230  | 130               |  | 550   | 291               |  | 825   | 194               |  | 490   | 327               |  | 3280  | 49                |  |        |  |  |
|                                 | HD 42 (zr)          | 1850  | 86                |  | 1190  | 134               |  | 1440  | 111               |  | 1110  | 144               |  | 3900  | 41                |  |        |  |  |
|                                 | HD 78 (zr/ap)       | 1820  | 88                | 55   | 1170  | 137               | 85   | 1410  | 113               | 71   | 1130  | 142               | 88   | 3870  | 41                | 26   |        |  |  |
|                                 | HD 81 (- /ap)       | 1790  |                   | 56   | 1140  |                   | 88   | 1380  |                   | 72   | 1050  |                   | 95   | 3840  |                   | 26   |        |  |  |
|                                 | HD 79 (zr/ap)       | 1820  | 88                | 55   | 1170  | 137               | 85   | 1410  | 113               | 71   | 1130  | 142               | 88   | 3870  | 41                | 26   |        |  |  |
| HD 9 (zr)                       | 1830                | 87  |                   | 1190   | 134   |                   | 1430   | 112   |                   | 1100   | 145   |                   | 3880   | 41  |                   |  |        |  |  |
| eastern<br>margin<br>and Jura   | HD 89 (zr)          | 1160  | 138               |  | 500   | 320               |  | 750   | 213               |  | 430   | 372               |  | 3210  | 50                |  |        |  |  |
|                                 | HD 91 (zr)          | 1210  | 132               |  | 560   | 286               |  | 810   | 198               |  | 480   | 333               |  | 3260  | 49                |  |        |  |  |
|                                 | HD 57 (zr)          | 1260  | 127               |  | 590   | 271               |  | 850   | 188               |  | 520   | 308               |  | 3310  | 48                |  |        |  |  |

Tab. 3

Estimated sample depth and calculated palaeo-geothermal gradients for different deposition scenarios at the investigated ages 125 Ma and 166 Ma. The shaded geothermal-gradients are of samples, which showed a clear post-depositional influence on the zircon FT system causing partial annealing.

## 6. Discussion and interpretation

Nearly all analysed apatite samples (except HD57) have been reset by at least one phase of post-depositional heating up to temperatures of the APAZ or above. The old apatite FT peak ages (all less than 137 Ma) suggest a resetting during Cretaceous. Especially Permian samples show Late Cretaceous to Early Cenozoic peak ages. The period of elevated temperatures accompanies the initial rifting of the URG (Timar-Geng et al. 2006) are obviously responsible for annealing of FTs within the deeply buried layers. Only samples with a close spatial relationship to the URG main border fault (HD22 and HD77) are heavily influenced by a Cenozoic syn-rift thermal pulse leading to complete resetting, which is probably related to ascending hot hydrothermal fluids. But at these locations temperatures of the ZPAZ were not reached since the zircon FT data of these samples show no clear post-devotional younging.

Since all zircon samples have a relatively large spread of single grain ages with some younger and some older than the related age of their deposition it can be assumed that they have not been fully reset. Therefore the sample ages are considered as partially reset and the apparent central age being older than the age of the thermal event which induced the annealing. The large age spread reflects on the one hand the pre-depositional thermal history preserved partially in the less thermally sensitive grains and, on the other hand, the post-depositional thermal processes which have affected the minerals more sensitive to annealing. The zircon single grain ages of Permian strata, which are older than the deposition age indicate that no sampled stratigraphic unit was heated to temperatures higher than the upper temperature limit of the ZPAZ at about 350 °C (Tagami 2005). This also agrees with temperature estimates for the uppermost basement rocks during the Jurassic hydrothermal period of 150 °C to 250 °C (Brockamp et al. 2003, Timar-Geng et al. 2004).

### ***Time vs. temperature paths***

To outline the thermal history of (1) the Permian and Lower Triassic deposits (Fig. 7a) and (2) the Upper Triassic and Middle Jurassic deposits (Fig. 7b) on

the base of the FT dataset the probable time-temperature fields were constructed in which the real palaeo-temperature paths lay.

In a first approximation the thermal history of the basement (Fig. 2) provides the time vs. temperature limits (Fig. 7a, dashed line) for the overlying Permian to Lower Triassic deposits. This approximation is additionally refined by FT analyses on the sediment samples. The Permian to Early Triassic thermal evolution in turn provides the constraints for a first approximation for the time vs. temperature limits (Fig. 7b, dashed line) of the Middle Triassic to Middle Jurassic depositional intervals.

The geographic distribution of the common temperature distribution in a distinct depth ranges probably within an unknown temperature array. Therefore, in each individual case it is hard to decide whether a local event or a regional thermal trend affects a FT sample. In a first view it is assumed, that all FT results determined in this study are reflecting regional rather than local effects.

However, if zircon starts to record its FT age finally, due to cooling below the lower boundary of the ZPAZ (~180 °C), it is thought, that the temperatures fall below the 180°C isotherm and of course the proposed maximum temperature of 250 °C (Timar-Geng et al. 2004) were no longer reached on a regional scale. Moreover, the final cooling below the 180 °C isotherm is necessary before the first apatite samples cool below the upper temperature boundary of the APAZ at 120 °C. As shown here, the apatite samples were completely reset, this is independently proven by the partial annealing of the zircon FT system. In such a case, the oldest old-peak-ages display the ages closest to the cooling below the upper temperature boundary of the APAZ (120°C).

#### *Permian and Early Triassic deposits (Fig. 7a)*

By combining the results of all Permian and Lower Triassic FT samples, a wide region can be covered (Fig. 3) allowing for the construction of the time vs. temperature field valid for a regional scale.

As described above, the old apatite FT peak age at  $137 \pm 11$  Ma (sample HD81; Tab. 1), marks approximately the entrance into the APAZ from temperatures above 120 °C. Considering a similar regionally thermal



evolution, the oldest peak at  $137 \pm 11$  Ma marks the apatite FT age closest to the final cooling below the  $180^\circ\text{C}$  isotherm. This fits quite well with the cooling below the ZPAZ estimated by the young peak ages of the zircon FT dataset at  $125 \pm 16$  Ma (HD70) and clustering between  $140 \pm 16$  Ma (HD42) and  $175 \pm 27$  Ma (HD68).

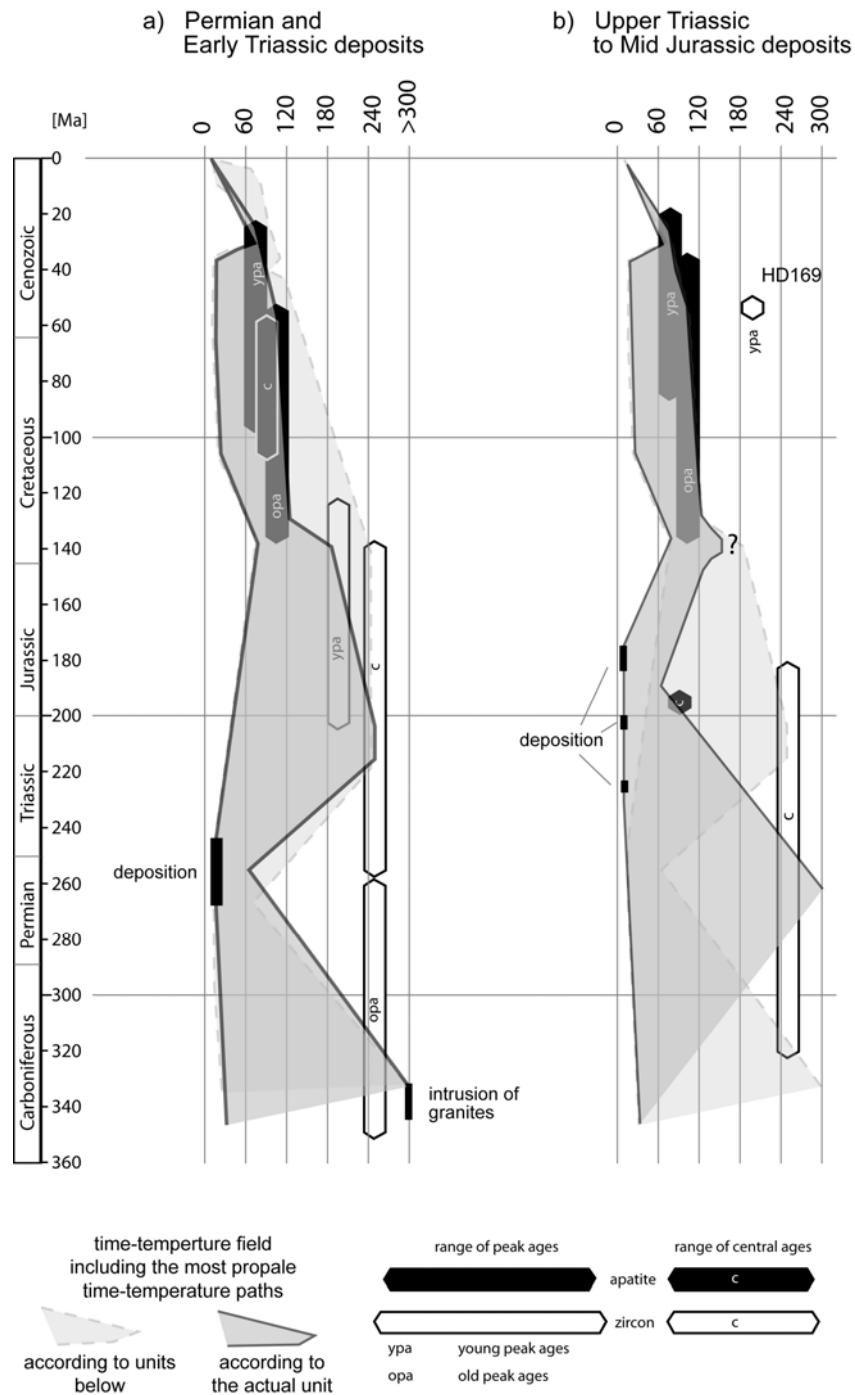


Fig. 7 a,b  
Outline of the time-temperature field including the most likely time-temperature paths representing the thermal history of the a) Permian and Lower Triassic deposits and b) Upper Triassic and Middle Jurassic deposits of the Southern URG area. Ages after ICS (Gradstein et al. 2004)

The range of the apatite FT peak ages of the Permian and Lower Triassic are in the range of the already known apatite FT central ages of the crystalline basement (Michalski 1987, Wyss 2001, Timar-Geng et al. 2006a). Therefore a similar low temperature (<120 °C) evolution is inferred. As also shown by Timar-Geng et al. (2006a) the relative broad scattering of the apatite FT data prove a long remaining within the APAZ between about 137 Ma and 25 Ma. Modelled time vs temperature paths (Timar-Geng et al. 2006a) may show periods of minor cooling below APAZ temperature conditions before a short Eo-Oligocene heating period occurred, which was followed by a last cooling. Thereby, the young apatite FT peak age of  $25 \pm 2$  Ma (HD22) of the Lower Triassic deposits reflects possibly the last cooling below 60 °C in the region. This age coincides with the onset of uplift of the southern URG. The reason and the amount of the uplift and the amount of eroded material is still a matter of debate (Laubscher 1992, 2003, Ziegler 1994, Ziegler & Dezes 2007, Hinsken et al. 2007).

#### *Late Triassic to Middle Jurassic deposits (Fig. 7b)*

Upper Triassic and Middle Jurassic samples come from the eastern part of the study area. Nevertheless, information about the underlying units and on a local scale is preserved.

The sampled Upper Triassic and Middle Jurassic sediments were deposited in three time steps between 226 Ma and 224 Ma and between 205 Ma and 200 Ma and the Lower to Middle Jurassic between 184 Ma and 175 Ma.

Inspection of the FT data (Fig. 5) very obviously reveals that sample HD169 is an outlier of the young zircon FT peak ages. This sample yielded three zircon FT peak ages, in which the young FT peak age at 55 Ma represents the youngest zircon FT peak age of the whole dataset. This young age does not match the possible time vs temperature paths recognized in the Permian to Lower Triassic deposits (Fig. 7a) or the crystalline basement (Fig. 2). Therefore, it is suggestive of a localized thermal anomaly, which disturbed the regional temperature field significantly. A similar high temperature anomaly was also detected about 4 km away near Kandern, Germany related to the URG Main Border Fault for the same time (Dresmann et al. 2009). The

sample HD169 (Middle Triassic sandstone) was taken about 100 m west of the URG Main Border Fault. Therefore, a relationship to hot hydrothermal fluid flow related to tectonic activity as proposed in the Kandern Fault Zone (Dresmann et al. 2009) seems very likely.

Except for sample HD169, no Middle Triassic to Middle Jurassic sample yielded zircon FT ages younger than their deposition age. Hence, apart from local thermal anomalies the temperature range of the ZPAZ was not reached in the stratigraphic units younger than Middle Triassic on a regional scale. Therefore, these samples mainly reflect the thermal evolution of their source regions.

The apatite FT data show approximately the same age pattern as shown for the underlying units, implying a similar low-temperature (<120 °C) evolution. Except, sample HD57, which yielded a relative old FT central age. Several old FT apatite peak ages at ca. 128 Ma to 137 Ma suggest cooling from temperatures higher than 120 °C during Cretaceous as estimated for the underlying units.

### ***Subsidence analysis and FT data***

The calculated hypothetical palaeo-geothermal gradients, which displays the necessary temperature conditions to influence the FT data characterises the thermal history at the investigated age levels. According to the two proposed deposition scenarios these hypothetical palaeo-geothermal gradients should now be discussed.

#### *Thermal evolution during deposition scenario 1 (without Cretaceous deposits)*

Deposition scenario I was subdivided into two thermal sub-scenarios (a) and (b). First (a), according to Timar-Geng et al. (2004), a Jurassic, about 55 Myr long hydrothermal phase affected the crystalline basement as well as the Permian and Lower Triassic deposits with temperatures of at least 180 °C. To reach the 180°C isotherm palaeo-geothermal gradients of about 144 °C/km (sample HD42, Permian arcose) are necessary during the investigated age level at 166 Ma. The proposed maximum temperature of about 250 °C requires geothermal gradients in excess of 144°C/km during Middle Jurassic. Due to the decreasing overburden of the analysed horizons (Permian to Lower Triassic) the expected gradients tend to elevated values, if hypothetical

thermal events ( $\geq 180$  °C) predate the deposition age of Middle Jurassic sediments (166 Ma). After the main phase of hydrothermal activity the geothermal-gradients decreased in their intensity during the Late Jurassic and were followed by cooling until the Late Eocene.

Considering the required abnormal high geothermal-gradients during this scenario, a regional heating of Mesozoic sediments up to temperatures corresponding to the ZPAZ seems highly unlikely since no signs of magmatism are recognized during Triassic and Jurassic times.

The second thermal sub-scenario (b) is in contrast to the first (a) related to a relative short (about 10-15 Myr) high thermal pulse during Late Jurassic and Early Cretaceous. It is suggested, that such a hypothetical thermal event occurred simultaneously to the stage of maximal burial. Therefore, the hypothetical geothermal-gradient needed during this relative short time window indicate values in excess of about 111 °C/km (sample HD42, Permian arcose) to reach temperatures of the ZPAZ.

The necessary palaeo-gradients are substantial lower than in sub-scenario (a), but still, abnormal elevated. Nevertheless, such a thermal scenario at the transition from the Jurassic to the Cretaceous is in line with the last documented Mesozoic hydrothermal activity recognized on a regional scale (Werner und Franzke 2001, Brockamp et al. 2003, Wetzels et al. 2003). By the absence of signs of magmatism, a regional-wide hydrothermal activity has to be assumed as an additional heat source to explain the high gradients during the Late Jurassic and Early Cretaceous.

#### *Thermal evolution during deposition scenario II*

Considering an additional burial by 450 m of Early Cretaceous deposits, the required palaeo-geothermal gradients are below 100 °C/km during the middle Early Cretaceous (125 Ma). Deposition scenario II allows the lowermost and therefore most realistic palaeo-geothermal gradients. Nevertheless, the old apatite FT peak ages indicate a cooling below the 180 °C isotherm before about 140 Ma (lower most Early Cretaceous), contradicting a thermal pulse of at least 180°C simultaneous to the proposed maximum burial at the end of Early Cretaceous. Additionally, extensive hydrothermal activity that could have

caused such a late Early Cretaceous (~125 Ma) thermal pulse is up to now not observed in the southern URG area (e.g. Wetzel et al. 2003). In neighbouring regions like the central northern Switzerland for Middle Cretaceous times a thermal pulse was recognized (Mazurek et al. 2006). Unfortunately, the estimated geothermal gradient of about 42 °C/km is not comparable with the needed values here. Assuming such a palaeo-geothermal gradient for the URG area, a burial related to about 2500 m of an Early Cretaceous sediment thickness would be required to allow for the observed annealing of FTs in zircon in the Lower Triassic and Permian strata (Tab. 3). Deposition of 2500 m thick Early Cretaceous sediments is geologically not reasonable. There are neither structural nor sedimentological evidences in the region in favour of such high values.

Concluding the considerations above it is clear, that independent of the time at which post-depositional heating to temperatures of the lower ZPAZ boundary (180 °C) and above occurred, an elevated heat flux from the depth is crucial on a regional scale.

By the excluding arguments of a heating event related to deposition scenario II and the abnormal high gradients needed during the first thermal sub-scenario (a) of deposition scenario I, only the second thermal sub-scenario (b) is probable.

Therefore, the most reasonable set-up is constraint by a thermal pulse causing hydrothermal activity simultaneous to the maximum of burial at the transition between Jurassic and Cretaceous between about 150 Ma and 140 Ma.

An increased heat flow may activate a convective hydrothermal system, which transports heat very fast from the deeper crust to more shallow depths. Considering the repeated hydrothermal activity since the Variscan orogeny (Werner & Franzke 1994, 2001, Wetzel et al. 2003), it could be possible that within the upper crust a huge amount of fluids persisted since then. That may explain the chance for a quick rise of temperatures in the upper crust on a regional scale. Additionally, the described scenario does not exclude increased temperatures in relationship to localized hydrothermal activity during Jurassic and Triassic times. Moreover, a localized Jurassic and Triassic hydrothermal overprint supports the development of the observed

heterogeneous zircon FT central ages, peak ages and single grain age distributions.

In the light of the regional geologic evolution some points remains unclear. Although, extension of basins south, west to north of central Europe during the Early Cretaceous was well documented (e.g. Stampfli & Marchant 1997, Montadert et al. 1979, Hanisch 1984, Ziegler 1990), especially the geologic regime in the area of the later URG during the Cretaceous is still under discussion. Some authors (e.g. Illies 1977, Ziegler 1990, Geyer & Gwinner 2004) point out the changed stress regime as responsible for uplift of parts of the northern Alpine foreland. While Illies (1977) and Geyer & Gwinner (2004) proposed continental conditions since Late Jurassic, Ziegler (1990) argued for uplift leading to continental conditions during the Late Cretaceous (Ziegler 1990).

Unfortunately, on the base of the presented data it is not possible to fix only one opportunity. Thermal effects on the crust are manifold and it is possible to find argues for both proposed theories of Early Cretaceous as well as Late Cretaceous uplift. Nevertheless, the FT data suggest strongly a modification of the thermal conditions within the upper crust probably related to a basic change of the regional tectonic conditions at the Jurassic - Cretaceous transition.

## **7. Conclusions**

Cenozoic and Mesozoic FT ages within the Permian and Mesozoic sediments of the URG area prove a post-depositional thermal overprint of the apatite and zircon FT system. By integration of FT data and the geo-history analyses a preferred scenario has been evaluated.

Triassic to Jurassic overall cooling of the lithosphere led to thermal subsidence in the southern URG area after the Variscan orogeny. Related to the reactivation of pre-existing faults in the crystalline basement Triassic and mainly Jurassic hydrothermal activity led to a local strong disturbance of the thermal regime within the upper crust; locally the temperature conditions of the ZPAZ were reached. Within the time frame between Late Jurassic to Early

Cretaceous (150 Ma - 140 Ma) the thermal regime of the studied area changed substantially. The combination of burial metamorphism and hydrothermal activity led to a regional-wide rise of the temperatures, which can be recognized by the observed younging of zircon FT ages and the complete reset of the apatite FT system of samples from Lower Mesozoic sediments. Such a regional wide heating episode was characterized by geothermal gradients in the range of 150 °C/km to 110 °C/km and a duration of at least 10 My. In Permian and Lower Triassic strata temperatures of at least 180 °C have been reached while Late Triassic to Middle Jurassic units were subjected to at least 120 °C.

After this Late Jurassic to Early Cretaceous heating pulse the thermal regime of the upper crust cools rapidly to temperatures below 120 °C.

During a short heating phase accompanying the initial rifting of the URG the cooling trend was interrupted in the Late Eocene to Early Oligocene. During this phase temperatures of up to 120 °C were reached in the uppermost crystalline basement and the Permian to Lower Triassic sediments.

Related to the URG rifting hydrothermal anomalies developed locally leading to temperatures inside the ZPAZ ( $\geq 180$  °C). On a regional scale no thermal overprint of the zircon FT system within the Mesozoic deposits occurred during the Cenozoic.

The sampled stratigraphic units most probably cooled below the APAZ at around 25 Ma (Oligocene to Miocene transition).

## Acknowledgments

This work is a contribution of the EUCOR-URGENT Project (Upper Rhine Graben, Evolution and NeoTectonics). It has been supported by the Swiss National Science Foundation (Project Nos. 21-57038.99 and 20-64567.01). We thank gratefully Philippe Elsass (BRGM Strasbourg) for providing access to unpublished well data. Special thanks go to Gilles Borel for providing the spreadsheet EASYSUB and permission to use it. Alexandre Kounov, Mathias Tischler, Nynke Keulen, and Elmar Wosnitza are thanked for very fruitful discussions and proof readings.

## Appendix

| Lithology  | Initial porosity | Lithological coefficient | Sediment grain density | Reference                   |
|------------|------------------|--------------------------|------------------------|-----------------------------|
|            | $\Phi_0$         | $c [km^{-1}]$            | $\rho [kg m^{-3}]$     |                             |
| Limestone  | 0.45             | 0.54                     | 2710                   | Sawyer et al (1982)         |
| Sandstone  | 0.49             | 0.27                     | 2650                   | Sclater and Christie (1980) |
| Shale      | 0.63             | 0.51                     | 2720                   | Sclater and Christie (1980) |
| shaly Sand | 0.56             | 0.39                     | 2680                   | Sclater and Christie (1980) |
| Dolomite   | 0.31             | 0.22                     | 2860                   | Schmoker and Halley (1982)  |
| Evaporite  | 0.15             | 0.10                     | 3000                   | Borel 1995                  |
| Siltite    | 0.56             | 0.39                     | 2680                   | Sclater and Christie (1980) |

Tab. 4  
Lithological parameters used during the subsidence analyses



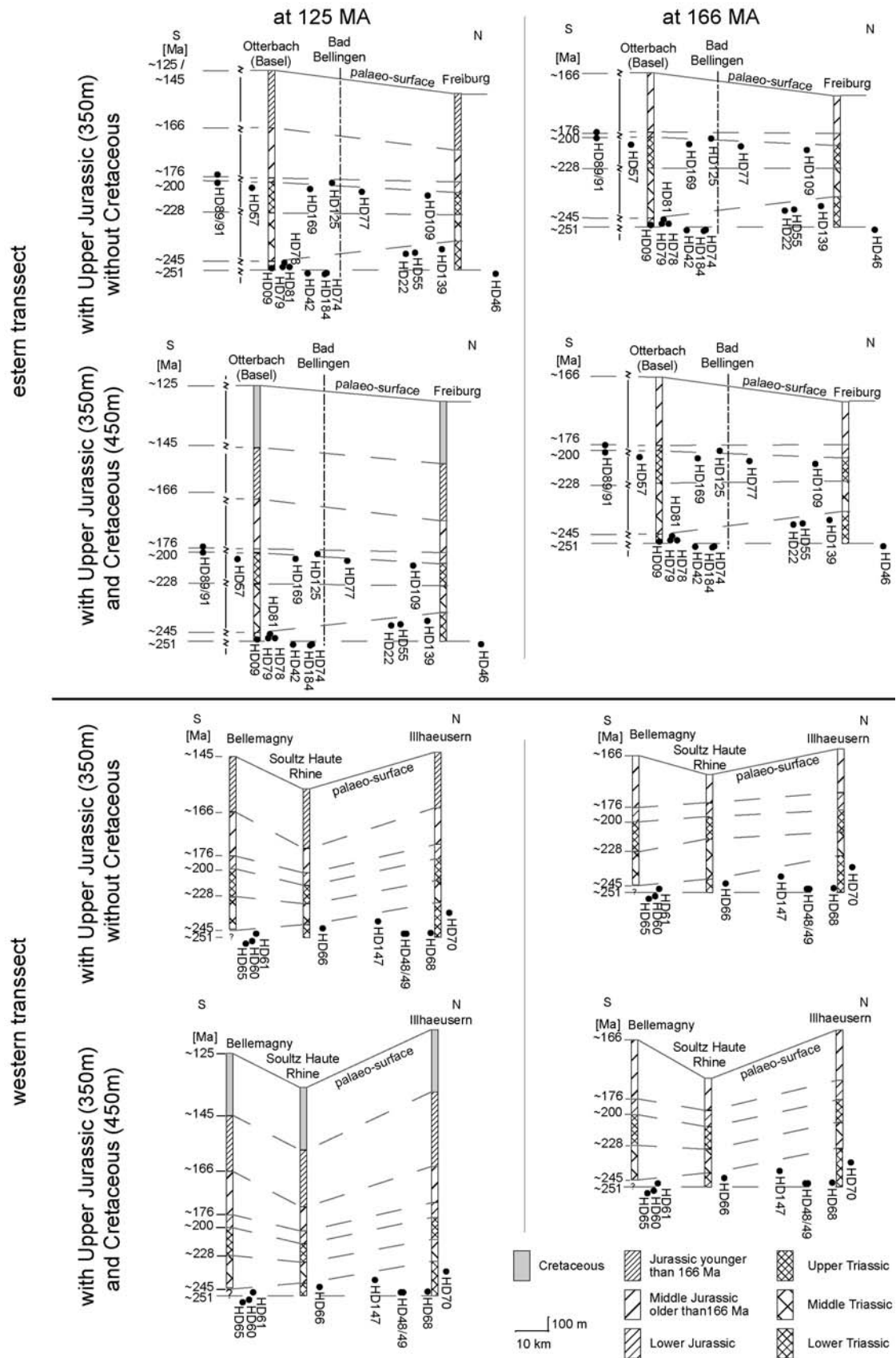


Fig. 8 North-south oriented transects (Fig. 3) delivers the overburden thickness of each sample at 166 Ma and 125 Ma depending on the deposition scenario which were studied by the subsidence analyses.



### **III. Thermal evolution and provenance regions of Cenozoic sediments from the southern Upper Rhine Graben**

#### Abstract

During the rifting of the Upper Rhine Graben (URG) various fluvial drainage systems developed, were changed and later some disappeared during the Cenozoic. Several hundreds of meters of sediments related to temporary marine transgression and to dominant fluvial and lacustrine environments were deposited.

Fission track (FT) analyses show that the Cenozoic units of the southern URG were not significantly reheated after their deposition. The analyses on zircon grains showed no young thermal overprint, while at least the geographic position and the related burial of syn-rift sediments of the graben are the main factor for a thermal overprint of the FT system in apatite. Therefore, the FT analyses on detrital samples from the southern Upper Rhine Graben (URG) area led to the identification of their source regions. Where palaeo-fluvial systems recognized in the southern URG area can be separated and characterised as "local" with source areas on the graben flanks or "regional" from rivers that drain areas far from the rift. Especially, their typical FT signature can easily identify material derived from the Alps. Time intervals dominated by "local" systems are the Eocene - Early Oligocene period and again after a short (about 5 Ma) interval of marine transgression until the Middle Pliocene. More or less simultaneous to the marine transgression from the North Sea into the URG, a connection in the South of the URG with the northern Alpine Molasse basin was developed. This is indicated by the Alpine FT signature in the "Meeressand" unit, which is the lower, most proximal facies of the early marine Grey Marl Formation. During the Early Miocene erosion was dominant in the southern URG area. Deposits were transported once again into the southern graben area by "local" river systems between Middle and Late Miocene. Alpine material was transported by the palaeo-Aare into the southern URG at about 4.2 Ma, proving the establishment of "regional" river systems originating in the Alps.

#### **1. Introduction**

Foreland deposits provide information on the denudation and exhumation history of the hinterland. The temporal evolution of geodynamic processes acting in the hinterland can be recorded from the changing characteristics of the foreland deposits. Detrital samples taken from the foreland consist of grains obtained of the whole drainage area and yield, depending on their stratigraphic age, information on their earlier provenance regions and on

(palaeo-) fluvial systems (Bernet and Garver 2005). Additionally, also a post-depositional basin-related thermal history has been archived in such sediments, (e.g. Brandon 1998, Carter 1999). Fission-track (FT) analyses on selected bedrock samples of potential source regions deliver thermo-chronological information on localised areas and contain the low temperature signature of currently outcropping rocks (e.g. Wagner & Van Den Haute 1992).

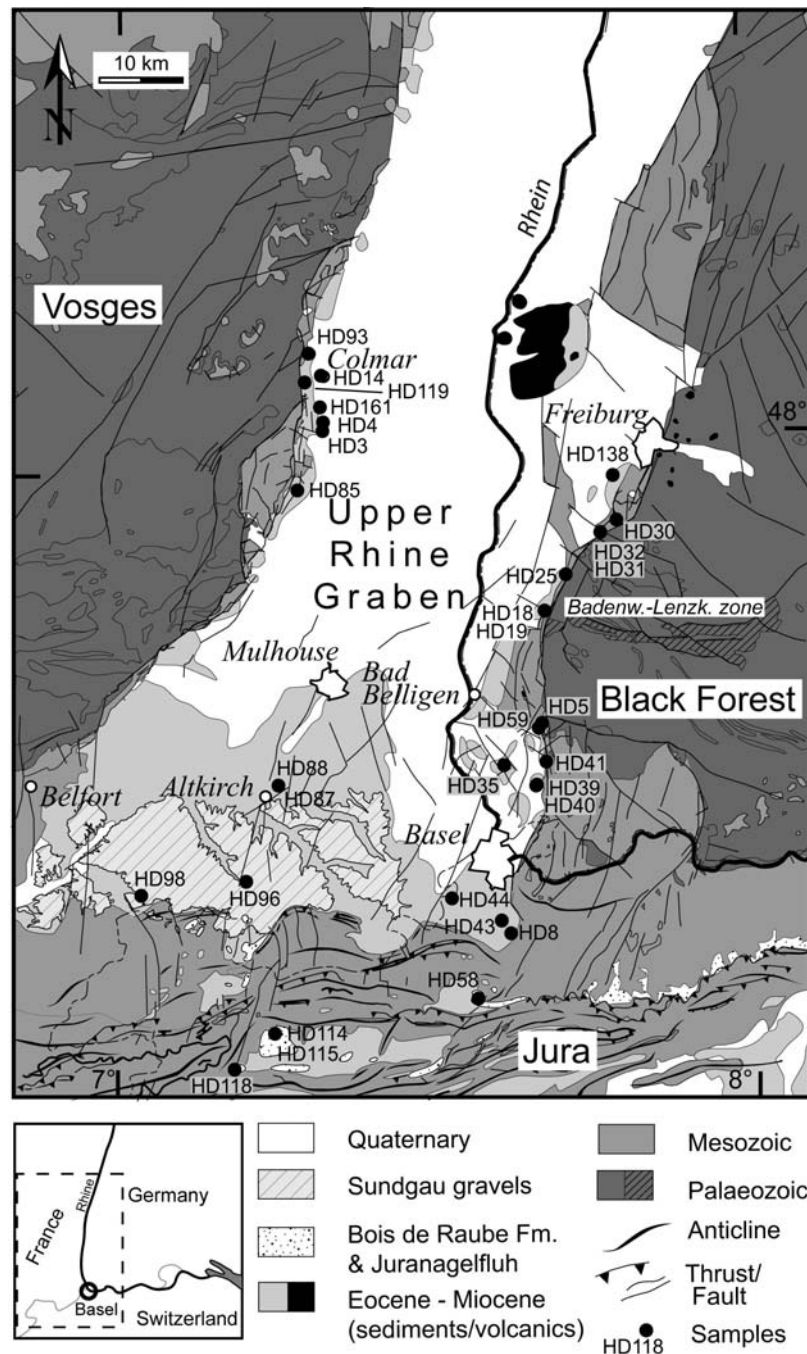


Fig. 1  
Geologic map of the southern URG area and sample location

Applying FT analyses on detrital samples of syn-rift deposits from the southern Upper Rhine Graben (URG) area gives the possibility to discriminate between their different source regions. Furthermore, their thermal history can still contain information on palaeo-geodynamic processes of the hinterland, which is documented in these sediments, even when their source rocks have been lost by erosion.

In this study we are trying to establish the provenance regions of the various marine and fluvial detrital deposits of the southern URG area as well as the cooling and denudation history of the flanks of the southern URG by analysing the apatite and zircon FT grain-age distributions.

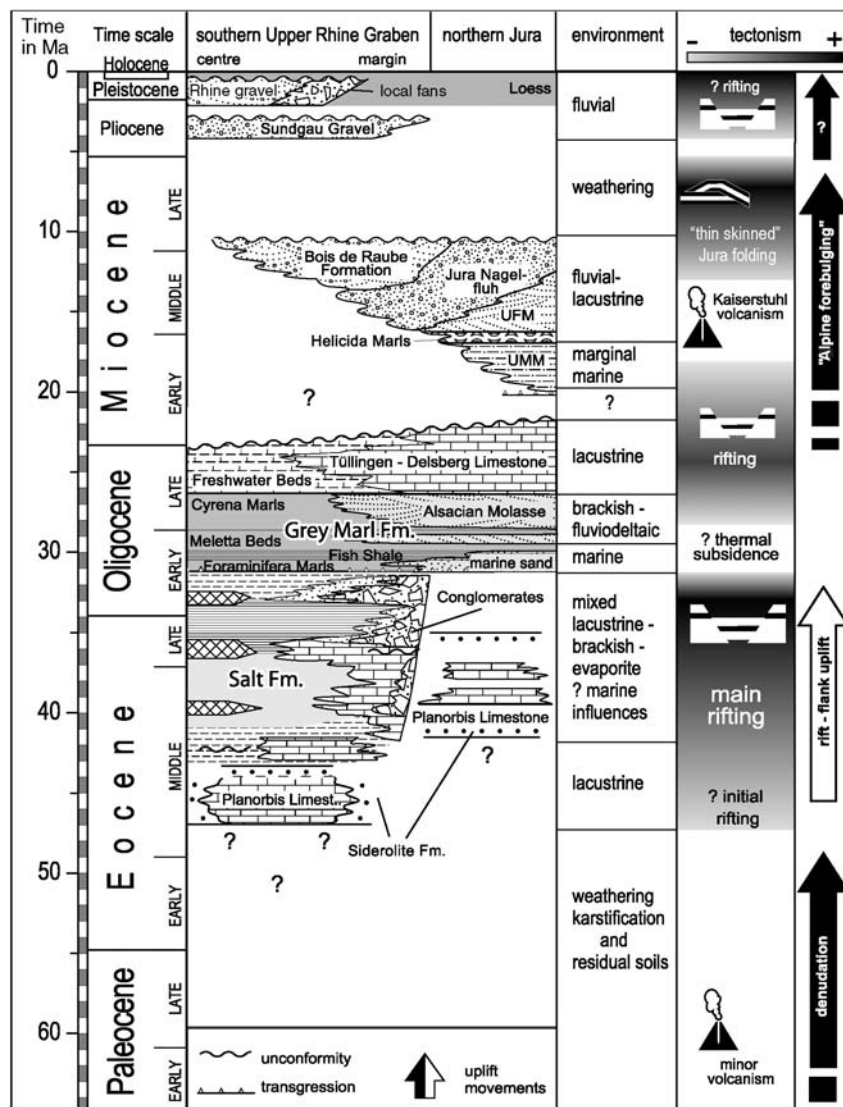


Fig. 2 Stratigraphic chart illustrating the Cenozoic evolution of the southern URG and northern Jura (slightly modified after Hinsken et al. 2007 and own observations; numerical ages after Gradstein et al. 2004).

## 2. Drainage systems attributed to the southern URG area

Since the beginning of rifting in the Late Eocene, various fluvial systems have developed in the southern URG. First, small rivers flew from the flanks into several lakes within the graben delivering coarse fan-like deposits along the evolving rift escarpments (Fig. 1, 2, 3; Salt Formation; Düringer 1988, Hinsken 2003).

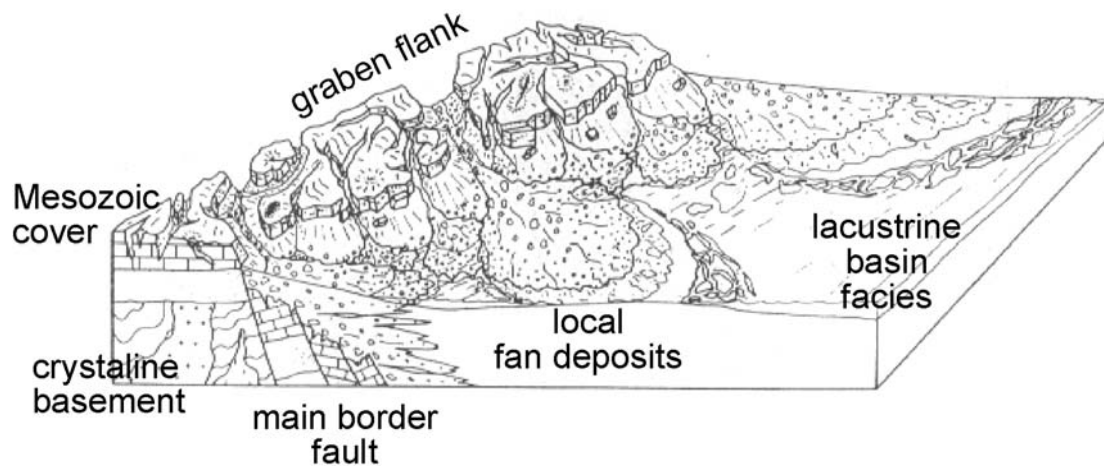


Fig. 3  
Eocene to Oligocene, Salt Formation; local fans in front of the graben flank (after Düringer 1988)

A less pronounced relief and the receding of the coarse proximal facies accompanied a marine transgression starting during the Rupelian. A marine connection to the North-Sea was developed as well as a link to the Swiss Molasse basin from where clastic material was delivered (Fig. 1, 2, 4; Grey Marl Formation, including Alsacian Molasse and “Meeressand”; Fischer 1965, Doehl 1967, Spiegel et al. 2007).

During the Miocene a large hiatus within the sedimentary record witness a period of strong erosion in the southern URG, while deposition continued in the northern part (Sissingh 1998). This phase of erosion is caused by the regional uplift of the Black Forest - Vosges dome (e.g. Roll 1979, Laubscher 1992, 2003, Ziegler 1994, Ziegler & Dezes 2005), which is accompanied by the activity of the Kaiserstuhl volcanic complex localised at the culmination of this dome (Keller et al. 2002).

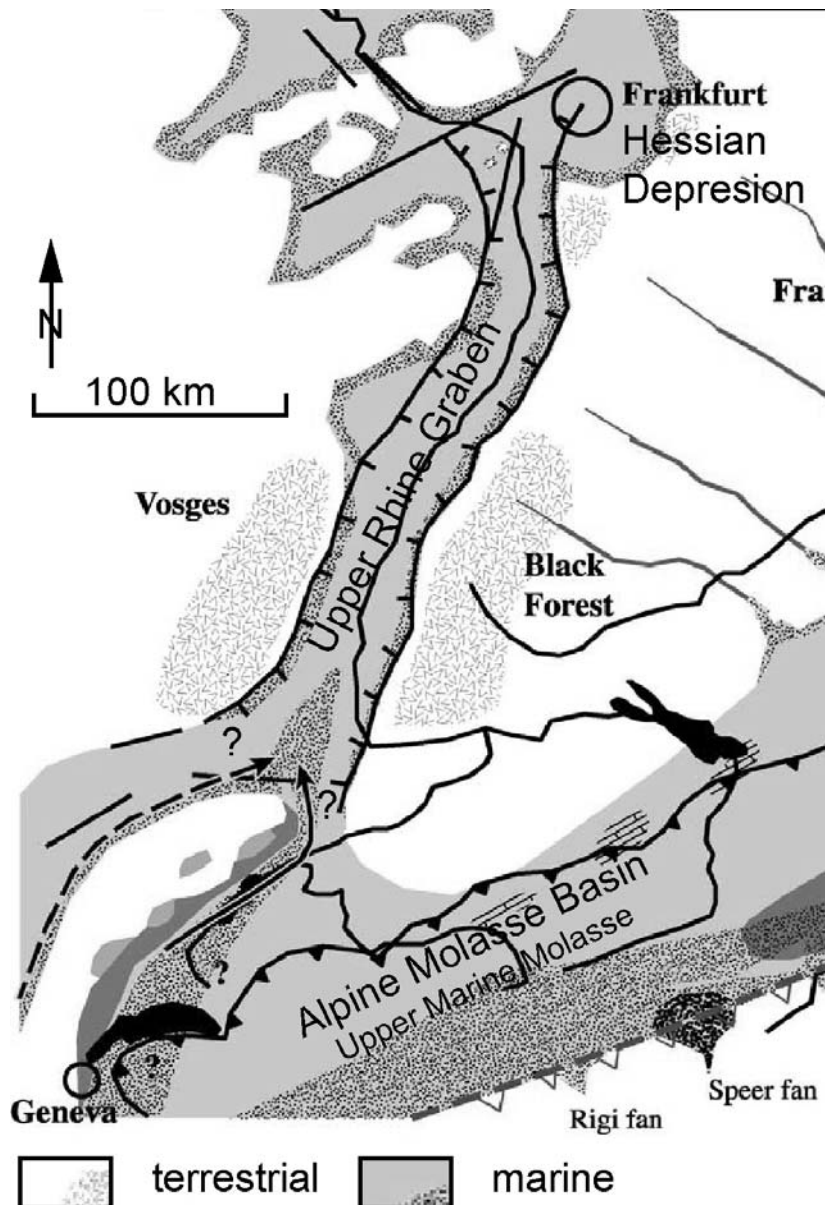
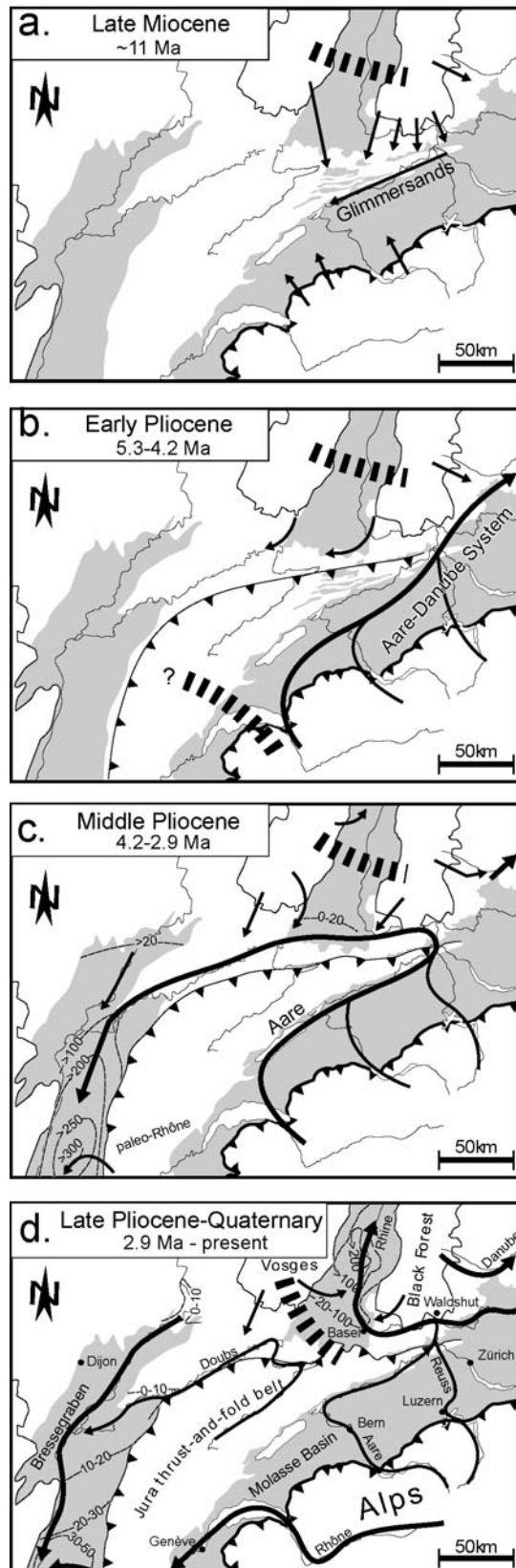


Fig. 4  
 Early Oligocene;  
 Marine transgression into the URG via the Hessian Depression, and probably from the South, palaeo-geography at ca. 31 Ma (slightly changed after Kuhlemann and Kempf 2002)

In the Early Miocene a new fluvial system developed draining the area. Especially the deposits derived from south-directed alluvial systems coming from the Black-Forest –Vosges-dome cover wide areas in the southernmost URG, the Tabular and later Folded Jura (Fig. 1, 2, 5; Bois de Raube Formation, Jura Nagelfluh including the Heuberg gravels and “Wanderblock Formation”)

Fig. 5



Drainages system of the southern URG area and the north-western Alpine foreland since Late Miocene (changed after Kálin 1990, Giamboni 2004, Ziegler 2007)

Therefore, their deposition age delimit the maximum age of the Jura folding.

The Middle Pliocene deposits present along the northern front of the Jura contain Alpine material, which imply the development of a new fluvial drainage system. Coming from the Alps the palaeo-Aare river changed its flowing direction and dewatered into the Bresse graben by crossing the southern URG in a westward direction (Fig.1, 2, 5; Sundgau gravels; Villinger 1998, Giamboni et al. 2004).

Since the Late Pliocene developed a new watershed between the URG and the Bresse Graben. The river Rhine becomes the dominant river and the present drainage system established. (Fig. 5d; Villinger 1998, Giamboni et al. 2004).

A large amount of material derived from the Alps has accumulated in the URG and partially further to the North (e.g. Pflug 1982). Additionally, the exposed flanks of the graben were intensely denudated (Illies 1967).



### 3. Fission Track (FT) Method

The FT technique is a geochronological method used on igneous, metamorphic and clastic sedimentary rocks, which contain the analysed minerals zircon and apatite. FTs are linear damages within the crystal lattice caused by the spontaneous nuclear fission of  $^{238}\text{U}$ . These damages are stable at low temperatures and they anneal at high temperatures. Within the used zircon and apatite the annealing temperatures of the tracks range between 180 °C to 350 °C for zircon (Tagami 2005) and between 60 °C and 110 °C for apatite (e.g. Gleadow and Brown 2000). (for a detailed overview see Reiners 2005).

Different types of FT ages should be taken into account. The FT central ages, analytical errors and chi-square values were calculated using the TRACKKEY software (Dunkl 2002). The chi-square value was used to evaluate whether the single grain ages from one sample belong to one or several age populations. All samples are reported as central ages (Galbraight & Laslett 1993). Additionally, samples that have failed the chi-square test ( $P_{\chi} < 5\%$ ) are commonly thought to indicate a mixed age composition (e.g. Brandon 1998, Garver et al. 2000, Stewart & Brandon 2004). For such samples the BinomFit® software (e.g. Brandon et al. 1992, Brandon 2005) applying the binominal "peak-fitting" method (Galbright & Green 1990, Galbright & Laslett 1993) has been used for peak age calculation. The BinomFit® software determines the optimal number of significant age peaks by using the F-Test (Brandon 1992), which calculates the improvement of the binominal peak-fitting statistic after each added age peak (e.g. Brandon 1996, 1998, Stewart & Brandon 2004). Furthermore, to get a better overview of the characteristics of single stratigraphic units all samples of a specific unit were compiled and the composite peak ages were calculated by the BinomFit® software. The analytical procedure is described within the appendix.

#### 4. Sample Material

Most of the syn-rift formations containing coarse siliciclastic detrital components of the southern URG area were sampled. The samples were taken at representative outcrops (Fig. 1, Tab. 1). Several samples contain large amounts of carbonate material, which are normally scarce on zircon and apatite grains. Therefore, from several samples only a relative low number of countable grains could be separated.

| denotation              | stratigraphy  | codes                                   | locations / facies<br>(for coordinates see table 2 & 3)   | lithology   |
|-------------------------|---|---|---|---|
| Pleistocene gravels     | Pleistocene<br>< 2 Ma<br>(Zollinger 1982)   | HD 30, 31, 32, 41                       | local fans along the eastern border fault                 | siliciclastic sands and gravels   |
| Sundgau gravels         | Pliocene<br>2.9 - 4.2 Ma<br>(Petit et al. 1996)   | HD 87, 96, 98                           | braided river deposits in the Ajoie and Sundgau           | siliciclastic sands and gravels, subordinate carbonate material                         |
| Bois de Raube Formation | Middle to Late Miocene,<br>11 -14 Ma<br>(Kählin 1997)   | HD 114,115                              | fluvial deposits of the basin of Delemont                 | mainly siliciclastic sands and gravels  |
| Juranagelfluh           | Middle to Late Miocene,<br>11 -14 Ma<br>(Wittmann 1988, Kählin 1997, Kemna & Becker-Haumann 2003) | HD 38, 39<br>(Juranagelfluh)            | fluvial deposits at the Schloss Rötteln, Lörrach          | calcareous gravels to cobbles, subordinate siliciclastic gravels to cobbles             |
|                         |   | HD 5, 59<br>(Heuberg gravels)           | fluvial deposits at the Heuberg, Kandern                  | siliciclastic sand and gravels to cobbles   |
|                         |   | HD 58<br>(Wanderblock "Fm.")            | fluvial deposits of Breitenbach, basin of Laufen          | cobbles and boulders of Lower Triassic sandstone  |
| Filling of karst pocket | Early to Middle Miocene,<br>13 - 17 Ma<br>(Hug et al. 1997)                                       | HD 118                                  | Molasse deposits, Glovelier, Folded Jura                  | sandstone, marls  |
| Grey Marl Formation     | Early to Late Oligocene,<br><br>26.5 – 31 Ma<br>(Berger et al. 2005)                              | HD 35, 40, 43, 44<br>(Alsacian Molasse) | brackish fluvial; south eastern URG                       | mica rich siliciclastic sand  |
|                         |   | HD 8, 14, 161<br>(Meeressand)           | brackish to marine; SE-URG and area of Eguisheim (Colmar) | calcareous and siliciclastic sandstones   |
| Salt Formation          | Middle Eocene to Early Oligocene, 31 – 40 Ma (Berger et al. 2005)                                 | HD 3, 4, 18, 19, 25, 85, 93, 119,138,   | local fans along the URG margins                          | calcareous conglomerate and sandstone including siliciclastic sand, pebbles and cobbles |
|                         |   | HD 88                                   | basin facies at Altkirch                                  | calcareous sandstone  |

Tab. 1  
sample description

## 5. Potential provenance regions

The mostly coarse grained deposits in the URG area, which have been analysed for this study, emanate from various fluvial systems and from the input related to marine transgressions. Ideally, the potential source areas of these deposits can be identified on the basis of their characteristic FT grain-age distributions, when three conditions are fulfilled: 1. The thermal history and therefore, the FT grain-age distribution of all potential source areas are known; 2. These FT grain-age distributions differ sufficiently from each other to provide their clear distinction; 3. The samples should not have experienced significant post-depositional heating. Such a reheating up to temperatures that are high enough to anneal FTs would overprint the source area signature, leading to a new basin related signature.

The published FT age signatures of potential source regions are illustrated and listed in Fig. 6, 7 and in Tab. 2. The Alps as well as the realms of the southern URG (Black Forest, Vosges and Jura) must be considered as the most important source regions. This was already evidenced by the petrography of selected pebbles and the investigation of heavy minerals (e.g. Liniger and Hofmann 1965, Düringer 1988, Hagedorn 2004). Furthermore, this hypothesis is strongly supported by the known palaeo-drainage system of the area (e.g. Villinger 1998).

### *Black Forest, Vosges and Jura*

Due to extensive erosion of the Black Forest and the Vosges as well as a subordinate sedimentary input from the Jura, large amounts of sediment were transported and accumulated into the Graben area. The sedimentary input from the Black Forest and the Vosges comprises Palaeozoic crystalline basement as well as Mesozoic strata. Material, which originates from the Jura Mountains consist of Mesozoic stratigraphic ages (e.g. Düringer 1988, Pflug 1982). The published zircon FT central ages from the Palaeozoic crystalline basement range between 127 Ma and 312 Ma (Timar-Geng et al. 2004, 2006a&b, Dresmann et al. 2009, Spiegel et al. 2007). FT ages obtained from investigations of apatite range between 20 Ma and 107 Ma (Michalski 1987,

Wyss 2001, Timar-Geng et al. 2006a & b, Dresmann et al. 2009). Whereas the FT central and peak ages obtained from zircons of the Mesozoic sedimentary cover of the southern URG range about between 125 Ma and 349 Ma, investigations of apatite grains from similar stratigraphic units yield ages between 27 Ma and 155 Ma (Dresmann 2009). Additionally, thermal anomalies are likely to have been occurred locally during initial URG rifting. In such cases, this would have led to a significant disturbance of the regional thermal signature. In a former study, such anomalies were determined at the eastern graben margins, where Late Palaeocene to Early Eocene zircon FT ages are obtained for Upper Triassic sandstones and fault related crystalline basement rocks (Dresmann et al. 2009, Dresmann 2009). Furthermore, widespread Cenozoic volcanic activity is recognised related to the URG rifting (e.g. Keller et al. 2002), which also represents considerable local occurring thermal disturbances of the regional thermal pattern.

### *Alps*

FT investigations on apatite of bedrock samples from the Alps provide a broad scattering from Mesozoic to Quaternary ages (e.g. Hunziker et al. 1992, Brügel et al. 2003). Therefore, the apatite FT age signatures bear only a low potential to characterize a distinct Alpine source region. In particular, the pre-Miocene apatite FT ages that are of Alpine origin differ hardly from ages obtained from the investigation of the Black Forest and the Vosges (Michalski 1987, Wyss 2001, Timar-Geng et al. 2006a, Dresmann et al. 2009).

However, contrary to the apatite FT ages the zircon FT age signature of bedrock samples of the Alps clusters into several distinct age domains (e.g. Hunziker et al. 1992, Fügenschuh et al. 2000, Fügenschuh and Schmid 2003). Originating from the bedrock, south of the Mont Blanc Massif young zircon FT ages cluster between about 7 Ma and 30 Ma and older zircon FT ages between about 50 Ma and 90 Ma (Fügenschuh and Schmid 2003). In the Eastern Alps, bedrock samples yielding zircon FT ages in the range of 10-20 Ma only from rocks of the Tauern Window (Fügenschuh et al. 1997) and from localities at the eastern-most extensions of the Alps (Brügel et al. 2003).

| region   | apatite FT ages  | zircon FT ages  | literature  |
|--|--|---|---|
| Fenoscandian shield (Oslo rift)  | 128 - 284 Ma   | 181 - 665 Ma  | Rohrmann et al. 1994  |
| Bohemian Massif  | western: 28 - 195 Ma   | north-western: 256 - 305 Ma,<br>Western: 215 - 283  | Wagner 1989, Hejl et al. 1997<br>Thomson & Zeh 2000,  |
| Rhenish Massif   | north-western & Ruhr Basin: 136 - 291 Ma,<br>North-Eastern: 130 - 239 Ma   |   | Glasmacher et al. 1997,<br>Karg et al. 2005   |
| Black Forest & Vosges  | 20 - 107 Ma  | 127 - 312 Ma and subordinate at ca. 60 Ma<br><br>(for details see text)   | Michalski 1987, Wyss 2001,<br>Timar-Geng et al. 2004, 2006;<br>Spiegel et al. 2007; Dresmann et al. 2009  |
| Massif de la Serre   | 48 – 65 Ma   | 227 – 131 Ma  | Madritsch et al 2008  |
| Odenwald   | 50 - 200 Ma  |   | Wagner 1989,  |
| Massif Central   | south-eastern 25 - 207 Ma  | 24 Ma, 103 Ma and 181 Ma  | Barbarand et al. 2001,<br>Bernet et al. 2004  |
| Alps   | Determined in the bedrock of the Alps 1 Ma to approx. Palaeozoic ages  | Alpine material recognized in the pre-Miocene northern & western Alpine Molasse: 256 Ma, 147 Ma, 76 Ma, 42 Ma and 30 Ma<br>additional in post-Oligocene Alpine Molasse deposits: 10 Ma, 15 Ma, 20 Ma<br>Determined in the bedrock of the Eastern Alps: 10-20 Ma scarce, >20 Ma are common<br>Determined in the bedrock of the central and western Alps: 7 Ma to 30 Ma and 50 Ma and 90 Ma<br><br>(for details see text) | Spiegel et al. 2000, 2001 & 2007,<br>Bernet 2002,<br>Bernet et al. 2004,<br><br>Brügel et al. 2003<br><br>Brügel et al. 2003, Hunziker et al. 1992, Fügenschuh & Schmid 2003, Fügenschuh et al. 1997 & 2000 |
| Mesozoic sediments of the southern URG area and the northern Switzerland | Upper Rhine Graben area, Triassic to Early Jurassic: 27 - 155 Ma; northern Switzerland Opalinuston 165-203 Ma, Stubensandstein 247 Ma, | Upper Rhine Graben area, Triassic to Early Jurassic: 140 - 349 Ma, Northern Switzerland and SW Germany: 219 – 285 Ma  | Köppen & Carter 2000,<br>Mazurek et al. 2006,<br>Dresmann et al. 2009, Dresmann 2009  |

Tab. 2  
Potential source areas of the deposits in the URG area and their apatite and zircon FT age signatures. (bedrock samples: central ages, detrital samples: peak ages)

Early to Middle Cenozoic ages (20 Ma to 50 Ma) are scarce and ages older than 60 Ma scatter broadly within the Eastern Alps (Brügel et al. 2003).

The zircon FT age signature of eroded Alpine material that stems from the early Alpine phase is recorded in Miocene and Oligocene Alpine Molasse sediments. The detrital FT ages of Miocene and Oligocene Molasse sediments clusters at ~256 Ma, 147 Ma, 76 Ma, and 42 Ma (e.g. Spiegel et al. 2006). A younger age group, which yields ~33 Ma, is solely determined in rocks from the foreland of the Western Alps (Bernet 2002). A similar age group is not known from the Oligocene Sediments of the northern Alpine foreland.

Zircon FT investigations of post-Early Miocene Alpine Molasse deposits and recent fluvial systems originating from the Alps yield age groups between 9 Ma and 15 to 20 Ma (Spiegel et al. 2000, Bernet 2002, Bernet et al. 2004). In general, zircon FT analyses on samples from the Miocene and Oligocene foreland Molasse of the eastern Alps yield ages older than 16 Ma (Brügel et al. 2003).

## **6. Results**

32 samples yielded 19 apatite and 31 zircon samples for FT analyses (Tab. 3, 4). During the first step FT central ages of each sample were calculated, accompanied by applying the chi-square test, which gives information on the potential to contain more than one age population within one single sample. Generally, the apatite FT central ages are similar to the known age ranges of the proposed source areas. All apatite samples failed the chi-square test ( $P_{\chi} < 5\%$ ) and didn't recommend a detailed interpretation of the FT central ages. The analyses of the single grain age distributions by the peak fitting method using the BinomFit<sup>®</sup> software (e.g. Brandon et al. 1992, Brandon 2005) yield 6 separate peak ages (P1-6) for apatite (Tab. 5) of the Cenozoic sediments from the URG. The apatite peak ages bases on relative broad grain age distributions within separated ranges, older than  $260 \pm 18$  Ma (P6), between  $226 \pm 26$  Ma and  $155 \pm 23$  Ma (P5),  $128 \pm 9$  Ma and  $98 \pm 9$  Ma (P4),  $84 \pm 5$  Ma and  $68 \pm 6$  Ma (P3),  $58 \pm 5$  Ma and  $38 \pm 2$  Ma (P2) and at  $25 \pm 3$  Ma

(P1). For a regional wide characterisation of distinct stratigraphic units the binominal peak fitting method (Galbright & Green 1990, Galbright & Laslett 1993) was applied to a composite data set, which contains all single grain analyses of one investigated unit. This calculation of composite peak ages should suppress outliers, which probably represents local anomalies. However, in spite of the low number of counted grains in several samples the calculated peak ages of single samples are in a good agreement with the calculated peaks of the composite data sets of each stratigraphic unit.

| deposition<br>age<br>Ma | stratigraphy |                         | lithology                | sample<br>code | coordinates<br>(G K Zone3) | no. of<br>crystals<br>counted<br>(n) | spontaneous<br>tracks<br>$\rho_s$ (Ns) | induced<br>tracks<br>$\rho_d$ (Ni) | $P(\chi^2)$<br>%<br>value | dosimeter<br>$\rho_d$ (Nd) | disp. | central<br>age<br>Ma $\pm 1\sigma$ |
|-------------------------|--------------|-------------------------|--------------------------|----------------|----------------------------|--------------------------------------|--|------------------------------------|---------------------------|----------------------------|-------|------------------------------------|
| < 2                     | Pleistocene  | Pleistocene<br>gravel   | gravels                  | HD 32          | 3407755,<br>5308240        | 9                                    | 12 (336)                               | 42 (1158)                          | 2<br>19                   | 13 (2370)                  | 0.19  | 69 $\pm$ 7                         |
| < 2                     | Pleistocene  | Pleistocene<br>gravel   | sandstone                | HD 31          | 3407755,<br>5308240        | 19                                   | 14 (1331)                              | 53 (5105)                          | 0<br>74                   | 13 (2730)                  | 0.22  | 64 $\pm$ 4                         |
| 2.9 - 4.2               | Pliocene     | Sundgau<br>gravel       | sand                     | HD 96          | 3364120,<br>5267376        | 5                                    | 9 (103)                                | 30 (354)                           | 1<br>12                   | 12 (2648)                  | 0.35  | 54 $\pm$ 12                        |
| 11 - 14                 | Miocene      | Bois de<br>Raube        | sand                     | HD 114         | 3367318,<br>5249252        | 20                                   | 11 (1162)                              | 21 (2279)                          | 0<br>154                  | 10 (2648)                  | 0.45  | 98 $\pm$ 11                        |
| 11 - 12 ?               | Miocene      | Juranagelfluh           | boulder<br>(L. Triassic) | HD 58          | 3392016,<br>5253009        | 5                                    | 26 (770)                               | 44 (1282)                          | 0<br>32                   | 11 (2730)                  | 0.25  | 119 $\pm$ 15                       |
| 11 - 14                 | Miocene      | Juranagelfluh           | conglomerate             | HD 39          | 3399485,<br>5278245        | 20                                   | 19 (1245)                              | 33 (2176)                          | 0<br>51                   | 9 (3641)                   | 0.20  | 100 $\pm$ 7                        |
| 11 - 14                 | Miocene      | Juranagelfluh           | conglomerate<br>(gneiss) | HD 38          | 3399485,<br>5278245        | 20                                   | 17 (1253)                              | 17 (1253)                          | 0<br>53                   | 9 (3641)                   | 0.22  | 79 $\pm$ 6                         |
| 13 - 17                 | Miocene      | karst pocket            | sand                     | HD 118         | 3362346,<br>5245050        | 18                                   | 9 (752)                                | 23 (1987)                          | 0<br>112                  | 10 (26489)                 | 0.44  | 70 $\pm$ 9                         |
| 26.5 - 28.5             | Oligocene    | Grey Marl Fm.           | sandstone                | HD 40          | 3399540,<br>5278310        | 19                                   | 12 (770)                               | 28 (1885)                          | 0<br>67                   | 8 (3641)                   | 0.32  | 64 $\pm$ 6                         |
| 26.5 - 28.5             | Oligocene    | Grey Marl Fm.           | sandstone                | HD 35          | 3395590,<br>5280665        | 23                                   | 8 (392)                                | 28 (1340)                          | 0<br>55                   | 8 (3641)                   | 0.34  | 47 $\pm$ 5                         |
| 26.5 - 28.5             | Oligocene    | Grey Marl Fm.           | sandstone                | HD 43          | 3395023,<br>5262233        | 20                                   | 7 (381)                                | 23 (1275)                          | 0<br>98                   | 7 (3641)                   | 0.49  | 49 $\pm$ 7                         |
| 26.5 - 28.5             | Oligocene    | Grey Marl Fm.           | sandstone                | HD 44          | 3389003,<br>5264994        | 39                                   | 8 (1336)                               | 22 (3524)                          | 0<br>138                  | 7 (3641)                   | 0.32  | 48 $\pm$ 4                         |
| 29.5 - 31               | Oligocene    | Grey Marl Fm.           | sandstone                | HD 14          | 3374212,<br>5327453        | 46                                   | 26 (2413)                              | 64 (6041)                          | 0<br>122                  | 9 (3641)                   | 0.22  | 67 $\pm$ 4                         |
| 32 - 34                 | Oligocene    | Salt Fm.<br>(basin)     | sandstone                | HD 88-1        | 3368249,<br>5278697        | 24                                   | 24 (2011)                              | 39 (3306)                          | 0<br>82                   | 9 (648)                    | 0.25  | 96 $\pm$ 7                         |
| 32 - 34                 | Oligocene    | Salt Fm.<br>(basin)     | sandstone                | HD 88-2        | 3368249,<br>5278697        | 18                                   | 28 (935)                               | 24 (803)                           | 0<br>80                   | 10 (3641)                  | 0.45  | 212 $\pm$ 28                       |
| 31 - 40                 | Oligocene    | Salt Fm.<br>(local fan) | sandstone                | HD 93          | 3372779,<br>5330065        | 11                                   | 14 (282)                               | 14 (266)                           | 0<br>26                   | 12 (2648)                  | 0.33  | 223 $\pm$ 32                       |
| 31 - 40                 | Oligocene    | Salt Fm.<br>(local fan) | sandstone                | HD 119         | 3372286,<br>5326644        | 25                                   | 27 (1816)                              | 46 (3112)                          | 0<br>136                  | 9 (2648)                   | 0.30  | 102 $\pm$ 8                        |
| 31 - 40                 | Oligocene    | Salt Fm.<br>(local fan) | conglomerate             | HD 3           | 3374300,<br>5320851        | 36                                   | 8 (731)                                | 24 (2349)                          | 1<br>60                   | 10 (3541)                  | 0.21  | 56 $\pm$ 4                         |
| 31 - 40                 | Oligocene    | Salt Fm.<br>(local fan) | conglomerate<br>(gneiss) | HD 85          | 3371140,<br>5313819        | 39                                   | 31 (2667)                              | 58 (5058)                          | 0<br>173                  | 7 (3641)                   | 0.26  | 67 $\pm$ 4                         |

Tab. 3 Apatite FT data

Coordinates (x, y) of Gauss Krüger DHDN Zone 3, Number of grains counted (n).  $\rho_s$ ,  $\rho_i$  and  $\rho_d$  are spontaneous, induced and dosimeter track densities in  $10^5$  tracks/cm<sup>2</sup>. N are number of tracks counted shown in brackets. Analyses by external detector method using 0.5 for the  $4\pi/2\pi$  geometry correction factor. Disp., Dispersion, according to Galbraith and Laslett (1993). Ages calculated as central ages according to Galbraith and Laslett (1993) using dosimeter glass CN5 for apatite with  $\zeta_{CN5} = 380.67 \pm 10.58$  (H. Dresmann).  $P(\chi^2)$  is the probability of obtaining  $\chi^2$  value for  $\nu$  degrees of freedom where  $\nu = \text{number of crystals} - 1$ .

| deposition age | stratigraphy |                      | lithology             | sample code | coordinates (G K Zone3) | no. of crystals counted (n) | spontaneous tracks ps (Ns) | induced tracks pi (Ni) | P( $\chi^2$ ) % value | dosimeter pd (Nd) | disp. | central age Ma $\pm 1\sigma$ |
|----------------|--------------|----------------------|-----------------------|-------------|-------------------------|-----------------------------|----------------------------|------------------------|-----------------------|-------------------|-------|------------------------------|
| < 2            | Pleistocene  | Pleistocene gravel   | gravels               | HD 30       | 3409770, 5309695        | 16                          | 183 (1648)                 | 35 (314)               | 0                     | 3 (1625)          | 0.99  | 95 $\pm$ 25                  |
| < 2            | Pleistocene  | Pleistocene gravel   | gravels               | HD 31-1     | 3407755, 5308240        | 11                          | 269 (1267)                 | 23 (110)               | 26                    | 3 (1625)          | 0.10  | 205 $\pm$ 24                 |
| < 2            | Pleistocene  | Pleistocene gravel   | gravels               | HD 31-2     | 3407755, 5308240        | 10                          | 184 (1880)                 | 15 (157)               | 5                     | 3 (1625)          | 0.21  | 268 $\pm$ 33                 |
| < 2            | Pleistocene  | Pleistocene gravel   | gravels               | HD 32       | 3407755, 5308240        | 15                          | 224 (1764)                 | 23 (181)               | 0                     | 3 (1625)          | 0.38  | 206 $\pm$ 29                 |
| < 2            | Pleistocene  | Pleistocene gravel   | gravels               | HD 41       | 3400775, 5281080        | 37                          | 201 (7083)                 | 19 (653)               | 0                     | 3 (1625)          | 0.27  | 246 $\pm$ 20                 |
| 2.9 - 4.2      | Pliocene     | Sundgau gravel       | gravels               | HD 87       | 3368249, 5278697        | 19                          | 145 (4923)                 | 18 (609)               | 0                     | 4 (1338)          | 1.38  | 147 $\pm$ 48                 |
| 2.9 - 4.2      | Pliocene     | Sundgau gravel       | gravels               | HD 96       | 3364120, 5267376        | 56                          | 111 (6968)                 | 58 (3633)              | xx                    | 3 (1625)          | 1.01  | 29 $\pm$ 4                   |
| 2.9 - 4.2      | Pliocene     | Sundgau gravel       | gravels               | HD 98       | 3351385, 5265931        | 40                          | 87 (2820)                  | 70 (2256)              | 0                     | 4 (1338)          | 0.66  | 33 $\pm$ 4                   |
| 11 - 14        | Miocene      | Bois de Raube        | sand                  | HD 114      | 3367318, 5249252        | 8                           | 133 (931)                  | 23 (166)               | 48                    | 4 (1338)          | 0.00  | 154 $\pm$ 16                 |
| 11 - 14        | Miocene      | Bois de Raube        | sand                  | HD 115      | 3367318, 5249252        | 20                          | 138 (2040)                 | 19 (276)               | 0                     | 4 (1338)          | 0.86  | 174 $\pm$ 37                 |
| 11 - 14        | Miocene      | Juranagelfluh        | boulder (porphyr)     | HD 5        | 3399900, 5285100        | 10                          | 258 (1637)                 | 19 (121)               | 82                    | 3 (1502)          | 0.00  | 313 $\pm$ 34                 |
| 11 - 14        | Miocene      | Juranagelfluh        | sand                  | HD 59-1     | 3400290, 5285650        | 20                          | 200 (3605)                 | 32 (570)               | 0                     | 4 (1338)          | 0.32  | 182 $\pm$ 18                 |
| 11 - 14        | Miocene      | Juranagelfluh        | sand                  | HD 59-2     | 3400290, 5285650        | 7                           | 229 (1232)                 | 41 (220)               | 0                     | 4 (936)           | 0.36  | 179 $\pm$ 31                 |
| 11 - 12 ?      | Miocene      | Juranagelfluh        | boulder (L.Triassic)  | HD58        | 3392016, 5253009        | 27                          | 242 (5335)                 | 25 (550)               | 5                     | 3 (1625)          | 0.16  | 200 $\pm$ 16                 |
| 11 - 14        | Miocene      | Juranagelfluh        | conglomerate (gneiss) | HD 38       | 3399485, 5278245        | 10                          | 279 (1386)                 | 27 (138)               | 2                     | 3 (1625)          | 0.28  | 219 $\pm$ 31                 |
| 11 - 14        | Miocene      | Juranagelfluh        | gravels               | HD 39       | 3399485, 5278245        | 10                          | 232 (968)                  | 30 (124)               | 3                     | 3 (1625)          | 0.24  | 173 $\pm$ 24                 |
| 13 - 17        | Miocene-     | karst pocket         | sand                  | HD 118      | 3362346, 5245050        | 11                          | 125 (1117)                 | 25 (221)               | 1                     | 4 (1338)          | 0.26  | 136 $\pm$ 18                 |
| 26.5 - 28.5    | Oligocene    | Grey Marl Fm.        | sandstone             | HD 40       | 3399540, 5278310        | 20                          | 149 (2725)                 | 21 (390)               | 0                     | 3 (1625)          | 0.32  | 161 $\pm$ 17                 |
| 26.5 - 28.5    | Oligocene    | Grey Marl Fm.        | sanstone              | HD 43       | 3395023, 5262233        | 16                          | 261 (16)                   | 34 (244)               | 0                     | 3 (1625)          | 0.37  | 158 $\pm$ 20                 |
| 26.5 - 28.5    | Oligocene    | Grey Marl Fm.        | sanstone              | HD 44       | 3389003, 5264994        | 32                          | 203 (32)                   | 24 (479)               | 0                     | 3 (1625)          | 0.46  | 181 $\pm$ 20                 |
| 29.5 - 31      | Oligocene    | Grey Marl Fm.        | sandstone             | HD 8-1      | 3396111, 5260713        | 12                          | 70 (631)                   | 25 (226)               | 0                     | 4 (1338)          | 0.37  | 83 $\pm$ 13                  |
| 29.5 - 31      | Oligocene    | Grey Marl Fm.        | sandstone             | HD 8-2      | 3396111, 5260713        | 17                          | 103 (1844)                 | 32 (580)               | 0                     | 3 (1625)          | 0.63  | 65 $\pm$ 11                  |
| 29.5 - 31      | Oligocene    | Grey Marl Fm.        | sandstone             | HD 161      | 3374086, 5323630        | 28                          | 192 (4498)                 | 19 (450)               | 21                    | 3 (1338)          | 0.07  | 247 $\pm$ 19                 |
| 32 - 34        | Oligocene    | Salt Fm. (basin)     | sandstone             | HD 88       | 3368249, 5278697        | 19                          | 225 (3755)                 | 26 (430)               | 0                     | 3 (1625)          | 0.66  | 153 $\pm$ 26                 |
| 31 - 40        | Oligocene    | Salt Fm. (local fan) | sandstone             | HD 119      | 3372286, 5326644        | 26                          | 292 (5003)                 | 34 (578)               | 0                     | 3 (1625)          | 0.57  | 159 $\pm$ 21                 |
| 31 - 40        | Oligocene    | Salt Fm. (local fan) | conglomerate          | HD 138      | 3409395, 5314990        | 18                          | 141 (1539)                 | 12 (133)               | 54                    | 4 (1338)          | 0.11  | 301 $\pm$ 33                 |
| 31 - 40        | Oligocene    | Salt Fm. (local fan) | sandstone             | HD 18       | 3400840, 5299040        | 7                           | 147 (909)                  | 14 (85)                | 54                    | 3 (1625)          | 0.03  | 259 $\pm$ 33                 |
| 31 - 40        | Oligocene    | Salt Fm. (local fan) | sandstone             | HD 19       | 3400840, 5299040        | 7                           | 123 (409)                  | 15 (50)                | 26                    | 3 (1625)          | 0.13  | 203 $\pm$ 34                 |
| 31 - 40        | Oligocene    | Salt Fm. (local fan) | conglomerate          | HD 25       | 3403450, 5303275        | 10                          | 187 (756)                  | 20 (81)                | 4                     | 3 (1625)          | 0.36  | 230 $\pm$ 40                 |
| 31 - 40        | Oligocene    | Salt Fm. (local fan) | conglomerate          | HD 4        | 3374435, 5321844        | 10                          | 202 (806)                  | 36 (144)               | 0                     | 3 (1502)          | 0.59  | 111 $\pm$ 25                 |
| 31 - 40        | Oligocene    | Salt Fm. (local fan) | sandstone             | HD 93       | 3372779, 5330065        | 22                          | 218 (2435)                 | 25 (277)               | 0                     | 4 (1338)          | 0.30  | 250 $\pm$ 27                 |

Tab. 4 Zircon FT data

Coordinates (x, y) of Gauss Krüger DHDN Zone 3, Number of grains counted (n).  $\rho_s$ ,  $\rho_i$  and  $\rho_d$  are spontaneous, induced and dosimeter track densities in  $10^5$  tracks/cm<sup>2</sup>. N are number of tracks counted shown in brackets. Analyses by external detector method using 0.5 for the  $4\pi/2\pi$  geometry correction factor. Disp., Dispersion, according to Galbraith and Laslett (1993). Ages calculated as central ages according to Galbraith and Laslett (1993) using dosimeter glass CN1 for zircon with  $\zeta_{CN1} = 145 \pm 6.88$  (H. Dresmann).  $P(\chi^2)$  is the probability of obtaining  $\chi^2$  value for  $\nu$  degrees of freedom where  $\nu =$  number of crystals-1.



The zircon FT analyses by TRACKEY (Dunkl 2002) yield a few samples, which pass the chi-square test, suggesting containing only one age population. For these samples only a FT central age was calculated. However, these results were strongly influenced by the low number of analysed grains of these samples.

| deposition age<br>Ma | stratigraphy | lithology            | sample code           | no. of crystals counted<br>(n) | P 1                     | P 2                | P 3                | P 4                 | P 5                  | P 6                  |                      |
|----------------------|--------------|----------------------|-----------------------|--------------------------------|-------------------------|--------------------|--------------------|---------------------|----------------------|----------------------|----------------------|
|                      |              |                      |                       |                                | Ma $\pm 1\sigma$<br>(n) |                    |                    |                     |                      |                      |                      |
| < 2                  | Pleistocene  | Pleistocene gravel   | sandstone             | HD 31, 32                      | 28                      |                    | 48 $\pm 4$<br>(8)  | 68 $\pm 4$<br>(16)  | 98 $\pm 9$<br>(4)    |                      |                      |
| 11 - 14              | Miocene      | Bois de Raube        | sand                  | HD 114                         | 20                      |                    | 58 $\pm 5$<br>(8)  |                     | 119 $\pm 7$<br>(11)  |                      | 312 $\pm 61$<br>(1)  |
| 11 - 14              | Miocene      | Juranagelfluh        | conglomerate          | HD 38, 39                      | 40                      |                    |                    | 78 $\pm 4$<br>(30)  | 128 $\pm 9$<br>(10)  |                      |                      |
| 13 - 17              | Miocene      | karst pocket         | sand                  | HD 118                         | 18                      |                    | 54 $\pm 4$<br>(13) |                     | 125 $\pm 12$<br>(5)  |                      |                      |
| 26.5 - 28.5          | Oligocene    | Grey Marl Fm.        | sandstone             | HD 40                          | 19                      |                    | 52 $\pm 6$<br>(13) |                     | 98 $\pm 14$<br>(6)   |                      |                      |
| 26.5 - 28.5          | Oligocene    | Grey Marl Fm.        | sandstone             | HD 35                          | 23                      | 24 $\pm 4$<br>(6)  | 54 $\pm 5$<br>(17) |                     |                      |                      |                      |
| 26.5 - 28.5          | Oligocene    | Grey Marl Fm.        | sandstone             | HD 43                          | 20                      | 26 $\pm 3$<br>(9)  |                    | 70 $\pm 7$<br>(11)  |                      |                      |                      |
| 26.5 - 28.5          | Oligocene    | Grey Marl Fm.        | sandstone             | HD 44                          | 39                      |                    | 38 $\pm 2$<br>(26) | 72 $\pm 13$<br>(13) |                      |                      |                      |
| 29.5 - 31            | Oligocene    | Grey Marl Fm.        | sandstone             | HD 14                          | 46                      |                    | 50 $\pm 4$<br>(15) | 71 $\pm 5$<br>(27)  | 111 $\pm 4$<br>(31)  |                      |                      |
| 26.5 - 31            | Oligocene    | Grey Marl Fm.        |                       | HD 14, 35, 40, 43, 44          | 147                     | 25 $\pm 3$<br>(16) | 45 $\pm 3$<br>(56) | 70 $\pm 4$<br>(63)  | 100 $\pm 20$<br>(12) |                      |                      |
| 32 - 34              | Oligocene    | Salt Fm. (basin)     | sandstone             | HD 88-1                        | 24                      |                    |                    | 77 $\pm 6$<br>(13)  | 115 $\pm 6$<br>(10)  | 167 $\pm 49$<br>(1)  |                      |
| 32 - 34              | Oligocene    | Salt Fm. (basin)     | sandstone             | HD 88-2                        | 18                      |                    |                    | 91 $\pm 33$<br>(3)  |                      | 205 $\pm 14$<br>(12) | 464 $\pm 77$<br>(4)  |
| 32 - 34              | Oligocene    | Salt Fm. (basin)     |                       | HD 88-1+2                      | 42                      |                    |                    | 78 $\pm 6$<br>(16)  | 119 $\pm 6$<br>(15)  |                      | 260 $\pm 18$<br>(11) |
| 31 - 40              | Oligocene    | Salt Fm. (local fan) | sandstone             | HD 93                          | 11                      |                    |                    |                     |                      | 155 $\pm 23$<br>(5)  | 326 $\pm 50$<br>(6)  |
| 31 - 40              | Oligocene    | Salt Fm. (local fan) | sandstone             | HD 119                         | 25                      |                    |                    | 79 $\pm 6$<br>(14)  | 119 $\pm 10$<br>(9)  | 198 $\pm 20$<br>(3)  |                      |
| 31 - 40              | Oligocene    | Salt Fm. (local fan) | conglomerate          | HD 3                           | 36                      |                    | 44 $\pm 5$<br>(17) | 68 $\pm 6$<br>(19)  |                      |                      |                      |
| 31 - 40              | Oligocene    | Salt Fm. (local fan) |                       | HD 3, 93, 119                  | 72                      |                    | 42 $\pm 5$<br>(15) | 72 $\pm 5$<br>(32)  | 120 $\pm 9$<br>(15)  | 226 $\pm 26$<br>(9)  |                      |
| 31 - 40              | Oligocene    | Salt Fm. (local fan) | conglomerate (gneiss) | HD 85                          | 39                      |                    |                    | 84 $\pm 5$<br>(12)  | 126 $\pm 10$<br>(8)  |                      |                      |

Tab. 5

Apatite FT peak ages (P1-P6),

Samples that have failed the chi-square test ( $P\chi < 5\%$ ) the BinomFit® software (e.g. Brandon et al. 1992, Brandon 2005) applying the binominal "peak-fitting" method (Galbright & Green 1990, Galbright & Laslett 1993) has been used for peak age calculation. Shaded fields are calculations of composite data sets

| deposition age | stratigraphy |                      | lithology            | sample code                    | no. of crystals counted (n) | P 1                           | P 2             | P 3             | P 4               | P 5               | P 6               | P 7               |
|----------------|--------------|----------------------|----------------------|--------------------------------|-----------------------------|-------------------------------|-----------------|-----------------|-------------------|-------------------|-------------------|-------------------|
| Ma             |              |                      |                      |                                |                             | Ma $\pm 1\sigma$ (n)          |                 |                 |                   |                   |                   |                   |
| < 2            | Pleistocene  | Pleistocene gravel   | gravels              | HD 30                          | 16                          |                               | 15 $\pm$ 3 (2)  |                 |                   | 159 $\pm$ 15 (14) |                   |                   |
| < 2            | Pleistocene  | Pleistocene gravel   | gravels              | HD 31-2                        | 10                          |                               |                 |                 | 141 $\pm$ 53 (1)  |                   |                   | 295 $\pm$ 32 (9)  |
| < 2            | Pleistocene  | Pleistocene gravel   | gravels              | HD 32                          | 15                          |                               |                 |                 | 104 $\pm$ 20 (4)  |                   |                   | 271 $\pm$ 31 (11) |
| < 2            | Pleistocene  | Pleistocene gravel   | gravels              | HD 41                          | 37                          |                               |                 |                 |                   | 158 $\pm$ 25 (6)  |                   | 259 $\pm$ 23 (28) |
| < 2            | Pleistocene  | Pleistocene gravel   |                      | HD 30, 32, 31-2, 41            | 78                          |                               | 15 $\pm$ 3 (2)  |                 | 136 $\pm$ 15 (19) |                   |                   | 456 $\pm$ 164 (4) |
| 2.9 - 4.2      | Pliocene     | Sundgau gravel       | gravels              | HD 87                          | 19                          | 13 $\pm$ 1 (2)                |                 |                 |                   |                   |                   | 268 $\pm$ 20 (17) |
| 2.9 - 4.2      | Pliocene     | Sundgau gravel       | gravels              | HD 96                          | 56                          | 11 $\pm$ 1 (22)               | 23 $\pm$ 2 (13) |                 | 146 $\pm$ 10 (21) |                   |                   |                   |
| 2.9 - 4.2      | Pliocene     | Sundgau gravel       | gravels              | HD 98                          | 40                          |                               | 23 $\pm$ 2 (33) |                 |                   | 174 $\pm$ 18 (7)  |                   |                   |
| 2.9 - 4.2      | Pliocene     | Sundgau gravel       |                      | HD 87, 96, 98                  | 115                         | 11 $\pm$ 1 (24)               | 23 $\pm$ 2 (44) |                 | 105 $\pm$ 8 (17)  |                   |                   | 265 $\pm$ 18 (30) |
| 11 - 14        | Miocene      | Bois de Raube        | sand                 | HD 114                         | 8                           |                               |                 |                 |                   | 154 $\pm$ 16 (8)  |                   |                   |
| 11 - 14        | Miocene      | Bois de Raube        | sand                 | HD 115                         | 20                          |                               | 23 $\pm$ 6 (1)  |                 |                   |                   | 236 $\pm$ 21 (19) |                   |
| 11 - 14        | Miocene      | Bois de Raube        |                      | HD 114, 115                    | 28                          |                               |                 |                 | 128 $\pm$ 11 (8)  |                   | 223 $\pm$ 16 (20) |                   |
| 11 - 14        | Miocene      | Juranagelflüh        | sand                 | HD 59-1                        | 20                          |                               |                 | 75 $\pm$ 21 (1) |                   | 165 $\pm$ 20 (11) |                   | 261 $\pm$ 44 (8)  |
| 11 - 14        | Miocene      | Juranagelflüh        | sand                 | HD 59-2                        | 7                           |                               |                 |                 | 149 $\pm$ 15 (5)  |                   |                   | 571 $\pm$ 262 (2) |
| 11 - 12 ?      | Miocene      | Juranagelflüh        | boulder (L.Triassic) | HD58                           | 27                          |                               |                 |                 |                   | 161 $\pm$ 21 (11) | 235 $\pm$ 20 (16) |                   |
| 11 - 14        | Miocene      | Juranagelflüh        | Boulder (gneiss)     | HD 38                          | 10                          |                               |                 |                 | 130 $\pm$ 28 (2)  |                   |                   | 265 $\pm$ 34 (8)  |
| 11 - 14        | Miocene      | Juranagelflüh        | gravels              | HD 39                          | 10                          |                               |                 |                 | 103 $\pm$ 35 (2)  |                   | 204 $\pm$ 30 (8)  |                   |
| 11 - 14        | Miocene      | Juranagelflüh        |                      | HD 38, 39, 58, 59-1-2          | 74                          |                               |                 |                 | 147 $\pm$ 13 (32) |                   | 240 $\pm$ 19 (42) |                   |
| 13-17          | Miocene-     | karst pocket         | sand                 | HD 118                         | 11                          |                               |                 | 63 $\pm$ 25 (1) | 142 $\pm$ 15 (10) |                   |                   |                   |
| 26.5 - 28.5    | Oligocene    | Grey Marl Fm.        | sandstone            | HD 40                          | 20                          |                               |                 |                 | 113 $\pm$ 21 (8)  |                   | 218 $\pm$ 39 (12) |                   |
| 26.5 - 28.5    | Oligocene    | Grey Marl Fm.        | sandstone            | HD 43                          | 16                          |                               |                 | 80 $\pm$ 17 (3) |                   |                   | 200 $\pm$ 20 (13) |                   |
| 26.5 - 28.5    | Oligocene    | Grey Marl Fm.        | sandstone            | HD 44                          | 32                          |                               |                 | 52 $\pm$ 10 (1) |                   | 169 $\pm$ 24 (21) |                   | 306 $\pm$ 72 (10) |
| 29.5 - 31      | Oligocene    | Grey Marl Fm.        | sandstone            | HD 8-1                         | 12                          |                               |                 | 76 $\pm$ 9 (10) |                   |                   | 195 $\pm$ 123 (2) |                   |
| 29.5 - 31      | Oligocene    | Grey Marl Fm.        | sandstone            | HD 8-2                         | 17                          |                               |                 | 38 $\pm$ 3 (8)  | 121 $\pm$ 13 (9)  |                   |                   |                   |
| 29.5 - 31      | Oligocene    | Grey Marl Fm.        | sandstone            | HD 161                         | 28                          |                               |                 |                 |                   |                   | 247 $\pm$ 19 (28) |                   |
| 26.5 - 31      | Oligocene    | Grey Marl Fm.        |                      | HD 40, 43, 8-1-2, 44, 161      | 97                          |                               | 27 $\pm$ 5 (3)  | 45 $\pm$ 4 (10) | 127 $\pm$ 10 (50) |                   |                   | 254 $\pm$ 25 (35) |
| 32 - 34        | Oligocene    | Salt Fm. (basin)     | sandstone            | HD 88                          | 19                          |                               |                 | 40 $\pm$ 9 (1)  | 119 $\pm$ 12 (9)  |                   |                   | 293 $\pm$ 29 (9)  |
| 31 - 40        | Oligocene    | Salt Fm. (local fan) | sandstone            | HD 119                         | 26                          |                               |                 | 67 $\pm$ 8 (5)  |                   |                   | 213 $\pm$ 16 (21) |                   |
| 31 - 40        | Oligocene    | Salt Fm. (local fan) | conglomerate         | HD 138                         | 18                          |                               |                 |                 |                   |                   |                   | 301 $\pm$ 33      |
| 31 - 40        | Oligocene    | Salt Fm. (local fan) | sandstone            | HD 18                          | 7                           |                               |                 |                 |                   |                   |                   | 259 $\pm$ 33      |
| 31 - 40        | Oligocene    | Salt Fm. (local fan) | sandstone            | HD 19                          | 7                           |                               |                 |                 |                   |                   | 203 $\pm$ 34      |                   |
| 31 - 40        | Oligocene    | Salt Fm. (local fan) | conglomerate         | HD 25                          | 10                          |                               |                 |                 | 127 $\pm$ 31 (2)  |                   |                   | 295 $\pm$ 54 (8)  |
| 31 - 40        | Oligocene    | Salt Fm. (local fan) | conglomerate         | HD 4                           | 10                          |                               |                 | 54 $\pm$ 10 (4) |                   |                   | 200 $\pm$ 29 (6)  |                   |
| 31 - 40        | Oligocene    | Salt Fm. (local fan) | sandstone            | HD 93                          | 22                          |                               |                 |                 |                   |                   | 213 $\pm$ 27 (16) | 438 $\pm$ 167 (6) |
| 31 - 40        | Oligocene    | Salt Fm. (local fan) |                      | HD 4, 18, 19, 25, 93, 119, 138 | 100                         |                               |                 | 64 $\pm$ 7 (8)  |                   |                   | 193 $\pm$ 23 (50) | 314 $\pm$ 48 (42) |
| 31 - 40        | Oligocene    | Salt Fm. (local fan) |                      | HD 4, 93, 119                  | 58                          | western margin (vosges)       |                 | 63 $\pm$ 6 (8)  |                   |                   | 196 $\pm$ 15 (39) | 422 $\pm$ 74 (11) |
| 31 - 40        | Oligocene    | Salt Fm. (local fan) |                      | HD 18, 19, 25, 138             | 42                          | eastern margin (Black Forest) |                 |                 | 139 $\pm$ 50 (4)  |                   |                   | 277 $\pm$ 26 (38) |

Tab. 6

Zircon FT peak ages (P1-P7),

Samples that have failed the chi-square test ( $P_{\chi} < 5\%$ ) the BinomFit® software (e.g. Brandon et al. 1992, Brandon 2005) applying the binominal "peak-fitting" method (Galbright & Green 1990, Galbright & Laslett 1993) has been used for peak age calculation. Shaded fields are calculations of composite data sets

Generally, the zircon grain age distributions related to distinct peak ages were clearly separated of each other. Within 7 age peaks (P1-7) some subordinate peaks can be recognized. Some of the peak ages are restricted to one or two or three stratigraphic units, other like the Upper Jurassic and the Palaeozoic peak ages are well represented in nearly all deposits. Note that by calculating of the peak ages of the composite data sets the Lower Jurassic age peak vanished.

The most pronounced age peak is an old one with Palaeozoic ages (P7), which was found nearly in all analysed units. Especially, in the Pliocene and Pleistocene units a mainly Triassic peak age (P6) between  $247 \pm 19$  Ma and  $193 \pm 23$  Ma is missing, while it was well represented in the older units. A Jurassic peak age (P5) between  $174 \pm 18$  Ma and  $154 \pm 16$  Ma is separated from a mainly Cretaceous one between  $149 \pm 15$  Ma and  $103 \pm 35$  Ma (P4), a Late Cretaceous to Eocene peak age (P3) between  $80 \pm 17$  Ma and  $38 \pm 3$  Ma are relatively broad but clear separated from younger peak ages (P1-2). Peak age P2 based on only a low number of analyses yield different sub-peaks in the different stratigraphic units. In Oligocene samples the peak age (P2) was calculated at about  $27 \pm 5$  Ma, in Miocene to Pliocene samples the peak age 2 (P2) date at  $23 \pm 2$  Ma and in Pleistocene samples a less constrained Miocene peak age at  $15 \pm 3$  Ma was found. The youngest peak age (P1) lays between  $11 \pm 1$  Ma and  $13 \pm 1$  Ma estimated in Pliocene samples.

## **7. Discussion and interpretation**

### ***Post-depositional heating***

Palaeo-temperature indicators like vitrinite reflectance values of Cenozoic units from the Tabular - and Folded Jura, as well as from the southern URG (Todorov et al. 1993) yield temperature estimations, which are not high enough to influence the pre-depositional apatite FT age pattern of the syn-rift samples that have been analysed in this study. On the other hand, vitrinite reflectance data determined for the Mesozoic units of the area suggests palaeo-geothermal gradients of up to  $100$  °C/km (e.g. area of Muttenez/Basel) during Oligocene and Early Miocene times (Todorov et al. 1993).

Additionally, Roll (1979) proposed thickness values of about 750 m to 1250 m of Late Oligocene to Middle Miocene deposits that are missing from the current stratigraphy of the southern URG.

The estimations of Roll (1979) and the temperature calculations of Todorov et al. (1993), who supposed convective thermal systems along fault zones, reflect heterogeneous and geographically fast changing geothermal conditions for today outcropping syn-rift sediments of Oligocene units at the southern end of the URG. Combining the overburden estimated by Roll (1979) with the proposed palaeo-geothermal gradients of Todorov et al. (1993), in the today outcropping Oligocene sediments palaeo-temperatures of about 75 °C to 125 °C can be expected for Early Miocene times.

On the other hand, measured temperatures in boreholes suggest that temperatures higher than 60°C are not or only hardly reached in the southern URG area today. Only in the area of the Dannemarie basin, West and North-West of a line Altkirch/France to Mulhouse/France, 60°C and higher were reached within deep (>1500m) buried layers (Munch et al. 1979).

Although, a recent thermal overprint at the sampled localities is not expected considering the borehole data. The above estimated palaeo-temperatures (75 °C to 125 °C) would affect the apatite FT system in Oligocene units and led to a post-depositional apatite FT age signature.

Beside these independent data sources, it is important to focus the apatite and zircon FT ages itself for understanding the thermal syn-rift evolution and the possibility of a rifting related post-depositional heating of the analysed units.

Due to the pre-depositional apatite FT ages in nearly all analysed samples (Tab.: 3, 5; Fig.: 6a) a post-depositional reheating to temperatures, which are able to affect the apatite FT system during significant durations seems to be unlikely. Furthermore, due to a thermal sensitivity of higher temperatures compared to the apatite FT system the zircon FT system should not be influenced post-depositional. Nevertheless, the interpretations of Todorov et al. (1993) suggest accelerated thermal conditions at least along fault structures during Oligocene and Early Miocene times.

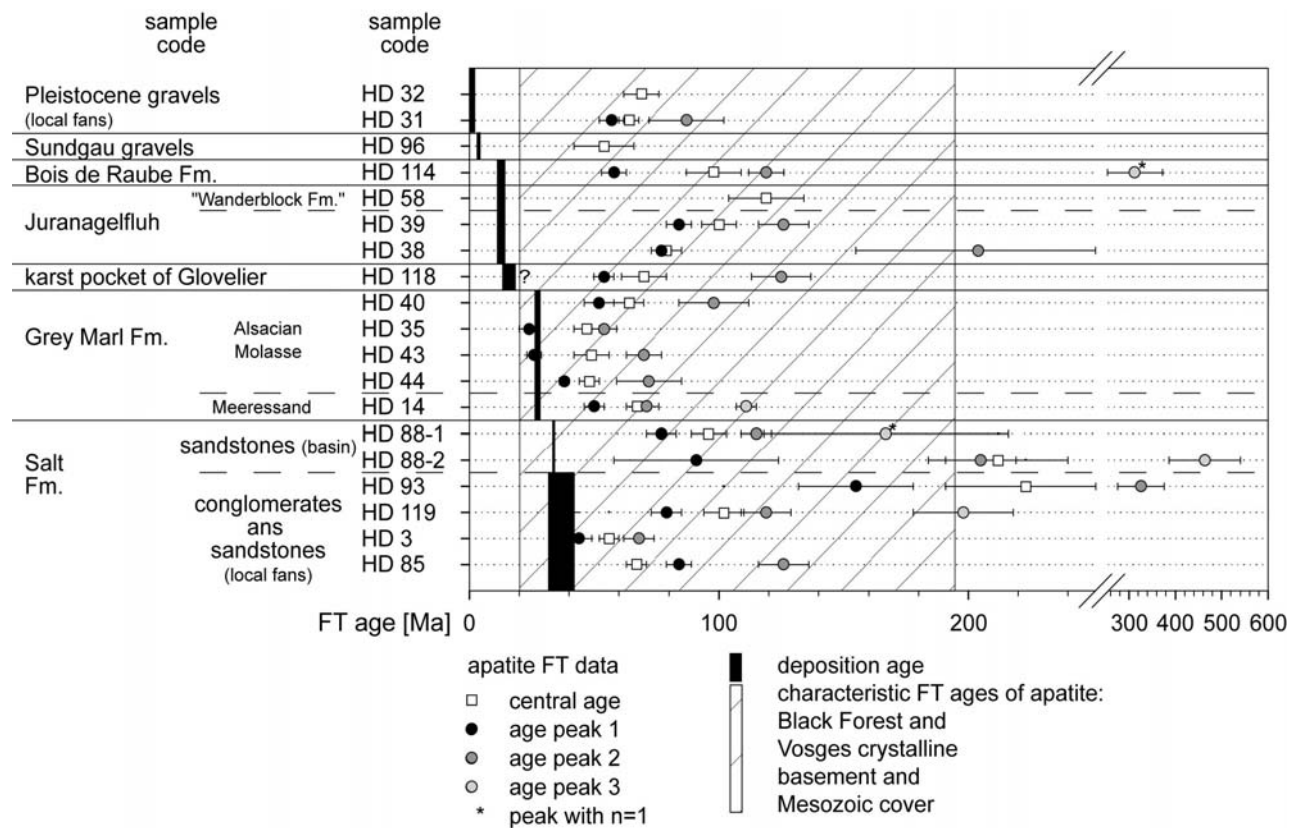


Fig. 6a  
Apatite FT central and peak ages  
Error bars are  $1\sigma$

Most of the FT samples were collected along the graben margins, where the today observable step-like structural architecture argues against a former burial in the range as estimated for the graben interior by Roll (1979). Additionally, hydrothermal activity along faults or fault zones could be responsible for a perturbation of the regional thermal background. Therefore, samples from highly fractured zones as the escarpments could mask the "normal" temperature conditions, these samples should not be interpreted in the same way, as samples from the inner graben.

Some samples were taken from units showing lithologies in basin facies, but the best candidate to discuss the regional geologic/thermal evolution in more detail is only sample (HD88). This sample from the Salt Formation was taken at the village Altkirch/France, where Roll (1979) proposed a thickness of about 1250 m today missing Oligocene to Miocene deposits. Due to the pre-depositional apatite FT ages of the Altkirch sample (HD88) a post-depositional reheating up to temperatures of ca. 60°C is excluded.

Considering a burial of about 1250 m combined with a constant surface temperature of 0 °C (conservative estimation) a maximum palaeo-geothermal gradient of 48 °C/km is allowed to reach the 60 °C isotherm but do not exceed them in the proposed sample depth. Otherwise, if such and higher gradients persist long enough, they would have led to temperatures of 60°C and higher, which should have caused annealing of FTs in apatite and therefore younging of FT ages. The last is not observable in the FT samples here. Therefore, palaeo-geothermal gradients below 48 °C/km were expected right before the overburden of the proposed 1250 m of Oligocene sediments were eroded and during the proposed doming of the southern URG area in Early Miocene times. This value is only comparable to the lower values as estimated by Todorov et al. (1993), who calculated palaeo-geothermal gradients of about 100 °C/km for the southern most URG and about 40 to 50 °C/km for the southern part of the northern Jura for Oligocene to Miocene times. They related their high values to convective thermal systems and a “constructive interference” of the URG rifting with the Alpine forebulge, which suggests a combination of thermal and tectonically induced uplift of the southern Black Forest, Vosges and URG area in the Early Miocene.

Considering the calculated palaeo-geothermal gradients of about 100 °C/km (Todorov et al. 1993) and the inner graben position of sample HD88 at Altkirch, where an overburden of 1250m (Roll 1979) is proposed, higher gradients as the calculated value of about 48 °C/km should be expected during a thermal doming event. Additionally, no apatite FT age of this study shows a relationship to a Miocene thermal event. Therefore, the theory of uplift of the Black Forest – Vosges dome by thermal doming seems to be unlikely during Miocene times. Otherwise, the proposed burial of the Altkirch area (Roll 1979) is overestimated. These findings argue for the Early Miocene uplift of the Black Forest – Vosges dome by lithospheric folding as proposed by Ziegler & Dezes (2007) and Bourgeois et al. (2007). Such a scenario would have led to uplift coinciding with decreasing geothermal gradients and cooling of the uppermost sediment bed.

## Discussion of possible source areas

Concluding, that no post-depositional thermal overprint affected the FT samples, it is possible to discuss in more detail the source areas where the material comes from.

## Salt Formation

The Salt Formation represented by 7 samples was taken from local fans, which are developed along the graben flanks and one sample (HD88) from distal sandstone in a basin interior related facies. The petrography of crystalline pebbles from local fan material indicates incision of rivers down to the Palaeozoic crystalline basement in the area of the Vosges, whereas at the margins along the Black Forest only Mesozoic components could be found (Düringer 1988 and own observations).

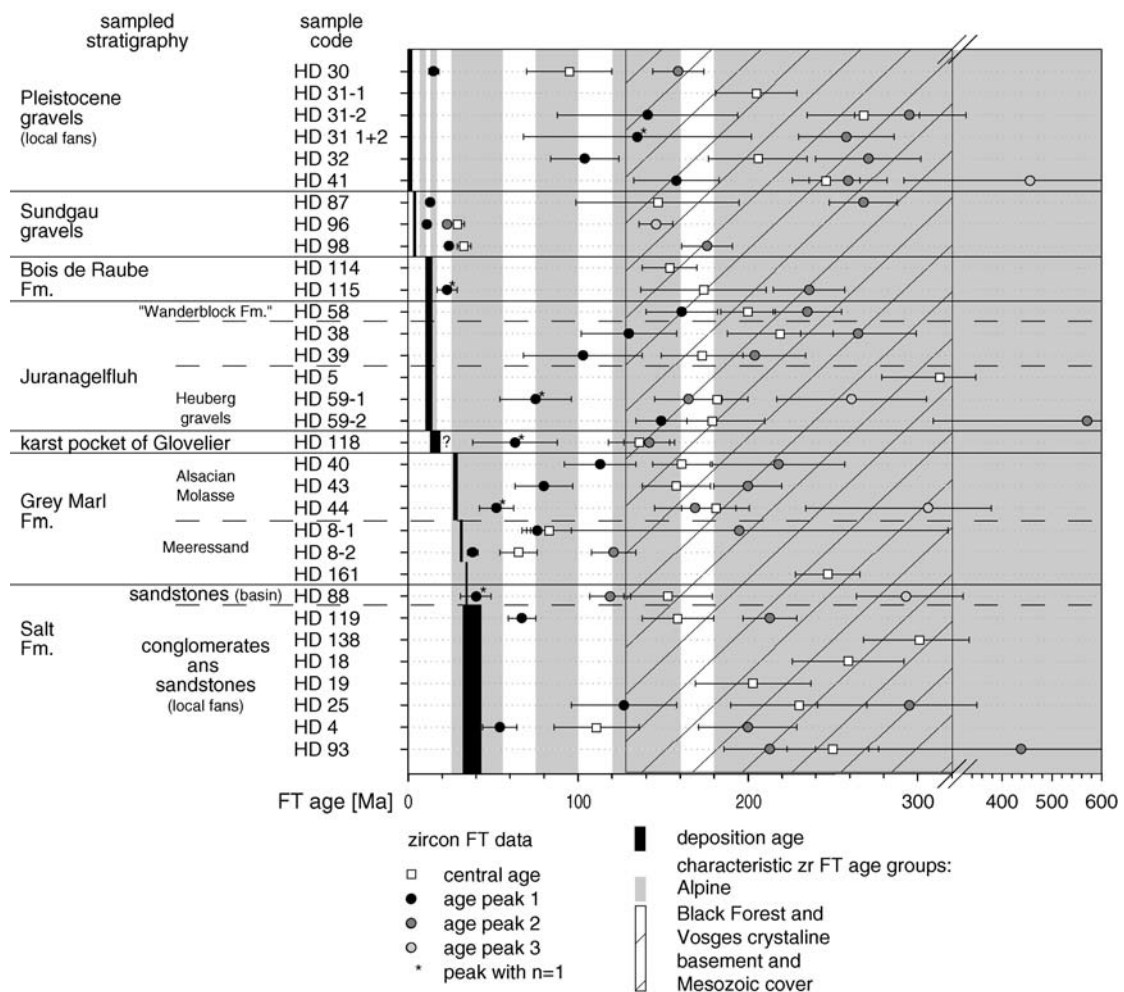


Fig. 7  
Zircon FT central and peak ages, error bars are 1  $\sigma$

The sampled marginal fans display FT peak ages in the compiled dataset for zircon at  $314 \pm 48$  Ma,  $193 \pm 23$  Ma and  $64 \pm 7$  Ma and for apatite at  $226 \pm 26$  Ma,  $120 \pm 9$  Ma,  $72 \pm 5$  Ma and  $42 \pm 5$  Ma, which are in general comparable to ages found by former studies of the crystalline basement of the Black Forest and Vosges (Michalski 1988, Wyss 2001, Timar-Geng et al. 2006a, Spiegel et al. 2007) as well as of their Mesozoic cover (Dresmann et al. 2009, Dresmann 2009). Therefore, the source area of the sampled local fan material along the escarpments has to be located at the graben flanks.

The graben interior basin facies were represented only by sample HD88 from a quarry at Altkirch, it shows apatite FT ages as well as zircon FT ages comparable to the age peaks estimated in the samples along the margins. A characteristic zircon age peak at about 80 Ma determined for Alpine material (Spiegel et al. 2007) cannot be found. Therefore, it is suggested that only the graben flanks deliver material into the southern URG at the transition between Eocene to Oligocene.

A comparison of the zircon FT results from the eastern (Black Forest) and western (Vosges) graben margin shows no clear differences. At both margins dominate the single grain ages corresponding to the Early Triassic and Palaeozoic (86-90%). Younger ages found only in 10-14% of the analysed grains.

Obviously, the youngest zircon FT peak age at  $64 \pm 7$  Ma from the western marginal fan deposits does not match the known zircon FT age pattern documented within the source areas in general and of the Vosges in particular. The samples (HD119, HD4) containing these young zircon FT age signatures were taken near Eguisheim southwest of Colmar (Fig. 1). These findings in a relative close sampled area suggest the occurrence of a thermal anomaly in the source area of this local alluvial fan. Best candidate known from this area seems to be Cenozoic volcanism (Keller et al. 2002) in the nearby Vosges, which is dated at  $60.9 \pm 0.6$  Ma. However, the responsible anomaly was likely related to the initial rifting of the URG during the Early Cenozoic. Anomalies with comparable zircon FT ages are recognized at the south-eastern Main Border Fault (Dresmann et al. 2009, Dresmann 2009).

Due to the large error of the young peak age at  $139 \pm 50$  Ma from the composite file of the eastern margin this age is relatively uncertain.



Nevertheless, this upper Jurassic age match the proposed, last high thermal event, which affected the zircon FT system within Mesozoic deposits of the southern URG area (Dresmann 2009).

### ***Grey Marl Formation***

The Grey Marl Formation was deposited under marine conditions, which developed to a more brackish fluvio-deltaic facies at the end of its deposition. In the Early Rupelian at about 31 Ma the North Sea connected the URG via the Hessian depression (Fig. 4; Doebli 1967, Berger et al. 2005). This marine transgression is documented across the entire graben by the deposition of the Foraminifera marls (NP 23).

A link to the northern alpine Molasse Sea is also proposed (Doebli 1967). In the Meletta beds (Grey Marl Fm.) at Mulhouse zircon FT age signatures were found, which are characteristic for material delivered from the alpine realm (Spiegel et al. 2007). Therefore, a connection between the Alpine Molasse basin and the URG is suggested via the area of the later Jura Mountains at least during the deposition of the Meletta beds (Spiegel et al. 2007). Several studies proposed a gateway along the southern prolongation of the URG, through the so-called “Rauracien depression” (e.g. Fischer 1965) or to the southwest into the Bresse Graben (Brianza et al. 1983). Brianza et al (1983) obtained a heavy mineral signature of the proximal facies of the Lower Grey Marl Fm., the “Meeressand”, which was interpreted by material transported from the Massif Central to the East. However, the exact location of such a marine gateway is still unknown.

The zircon FT analyses of the samples HD8-1 and HD8-2 of the “Meeressand” at Dornach (south of Basel) shows one weak documented age peaks at  $195 \pm 123$  Ma and three age peaks at  $121 \pm 13$  Ma,  $76 \pm 9$  Ma and  $38 \pm 3$  Ma, which reflect a strong similarity to the characteristically Alpine age peaks at about 42 Ma and the more indicative peak at about 76 Ma (Spiegel et al. 2007). Considering the three zircon FT age peaks known from the Massif Central at 181 Ma, 103 Ma and 24 Ma (Tab. 2; Barbarand et al. 2001, Bernet et al. 2004) an influence of this area was not very likely to the “Meeressand” samples at Dornach. This analysis suggests a connection to the northern Alpine Molasse Sea via the adjacent area of the later Jura at

about 31 Ma at the same age as the North-Sea linked the northern URG. Considering a tectonic activity along the eastern URG Main Border Fault a gateway along their southern prolongation through the area of Laufen into the Molasse Basin seem possible, which represent about the eastern margin of the Rauracien depression. Alternatively, the zircon grains causing the young “Alpine” FT peak ages could also be delivered by thermal anomalies from the eastern URG main border fault (Dresmann et al. 2009, Dresmann 2009) by south directed currents along the coast according to Brianza et al (1983). But, considering transport along the coast, the relation of quantities should shift to older ages, due to the erosion of mainly Jurassic and Triassic units in the area of the Dinkelberg (south of the Black Forest), which yield higher values of grains with old FT ages (Dresmann 2009). Therefore, a local source region situated in the area of the Black Forest seems to be highly unlikely.

At the transition from Early to Late Oligocene, the deposition environment changed from marine to brackish and fluvio-deltaic, which was expressed by the increasing dominance of a proximal facies the so-called “Alsacian Molasse” (Upper Grey Marl Fm.).

Its heavy mineral content proves an Alpine origin in addition to an influence of local material (e.g. Liniger & Hofmann 1965, Hagedorn 2004). As well, the zircon FT peak age signature of the upper part of the Grey Marl Fm., the Alsacien Molasse, shows the typical Alpine zircon FT age signature reflecting the proposed influence by a source area within the Alps.

Their relation of quantities of FT grain ages in comparison to the “Meeressande” is shifted to older FT ages may indicating a decreasing influence by alpine material to favours of local sources. This seems to be a signal showing the change from marine (Early Gray Marl Fm. as the Meeressande) to brackish (Alsacien Molasse) to lacustrine environments as recognised within the layers of the Late Oligocene (Tüllingen-Delsberg Limestones; Fig.:2)

### ***Bois de Raube Formation***

The FT analyses of the samples from the Bois de Raube Formation show zircon and apatite FT age peaks comparable to the proposed source area in the Vosges (Liniger 1967, Kählin 1997). Only one single zircon grain shows a

young age at about 23 Ma, which is not compatible with the known zircon FT age pattern of the Vosges (Timar-Geng et al. 2004). Reworking of today eroded alpine material, which was included in the Grey Marl formation, may explain such an outlier in the dataset.

### ***Juranagelfluh***

The lower part of the Juranagelfluh lends the formation its name (Kemna & Becker-Haumann 2003). The samples are collected in the area of Schloss Rötteln near Lörrach (Fig.1). While the zircon FT analyses yield the common age spectrum known from the crystalline basement and the Mesozoic units of the southern URG area (Timar-Geng et al. 2004, 2006a, Dresmann et al. 2009, Dresmann 2009), the apatite FT ages tend to the old part (119 ±15 Ma to 79 ±6 Ma) of the known apatite FT age range of the URG area (Timar-Geng et al. 2006a, Dresmann 2009). Today, the Black Forest, the proposed source area of the Juranagelfluh (Kälin 1990) delivers “older” apatite FT ages (>80 Ma) more often in the southernmost part today than in the central part of the southern Black Forest (Michalski 1987, Wyss 2001, Timar-Geng et al. 2006a&b). Supposing a comparable setting at the Late Miocene most likely a locally more restricted source area of the Juranagelfluh can be indicated in contrast to a broad network of rivers delivering the material to the south. Considering this the source area was probably located south of the Badenweiler-Lenzkirch zone (Fig.1).

*“Wanderblock Formation”*: In the area of Breitenbach a single boulder (HD58) of the “Wanderblock Formation” was taken and analysed by the zircon FT method. The Jurassic to Triassic FT ages shown in the results (Tab. 6) are characteristic for the Lower Triassic sandstones analysed in the area of the southern URG (Dresmann 2009). Therefore, the suggested source area in the Black Forest (Kemna & Becker-Baumann 2003) is also confirmed by the FT method.

*Heuberg gravels*: The Heuberg gravels consist of components derived of the crystalline basement of the Black Forest as well as of Middle to Lower Triassic sandstones. Therefore, the expected zircon FT age pattern as known from the BF and the Mesozoic units of the area (Timar-Geng et al. 2004, 2006a,

Dresmann et al. 2009 Dresmann 2009) are recognized in the strongly weathered Heuberg gravels.

### ***Karst pocket of Glovelier***

Hug et al. (1997) described the material as delivered from the Alpine Molasse basin. The FT analyses of the sandy material allows no clear decision between an Alpine source or a source area north of the Jura like the Bois de Raube Fm. or the Juranagelfluh. But it should be noted that the typical young Alpine zircon FT age peaks at 42 Ma and 76 Ma are nearly completely missing from the determined zircon FT age pattern within the analysed sample from the karst pocket.

### ***Sundgau gravels***

While the FT analyses of apatite yielded results of only 5 grains, the statistics within the zircon FT analyses is quite better with 115 dated grains. The pebble petrography clearly supports a large value of Alpine material (ca. 70 %) within the Sundgau gravels, which also contain pebbles of Vosges and Black Forest basement rocks (Liniger 1967). These, source areas are also reflected in the results of the zircon FT analyses, which display a narrow young and a broad old grain cluster shown in the radial plot (Fig. 8). Four peak ages can be calculated by the peak-fitting method showing two young peaks at  $23 \pm 2$  Ma and  $11 \pm 1$  Ma and to old peaks at  $265 \pm 18$  Ma and  $105 \pm 8$  Ma. Especially, the both young peaks are very typical for an Alpine source. But significant differences between these samples ask for discussion in more detail.

Sample HD87 from the northern most part of the Sundgau gravels at Altkirch yield grains with an old age group at ca.  $268 \pm 20$  Ma and a subordinate peak (n=2) at  $13 \pm 1$  Ma. The old peak age seems to be dominated by a provenance region localised in the Vosges and/or Black Forest, which indicate a stronger influence by local material along the northern margin of the Sundgau gravels.

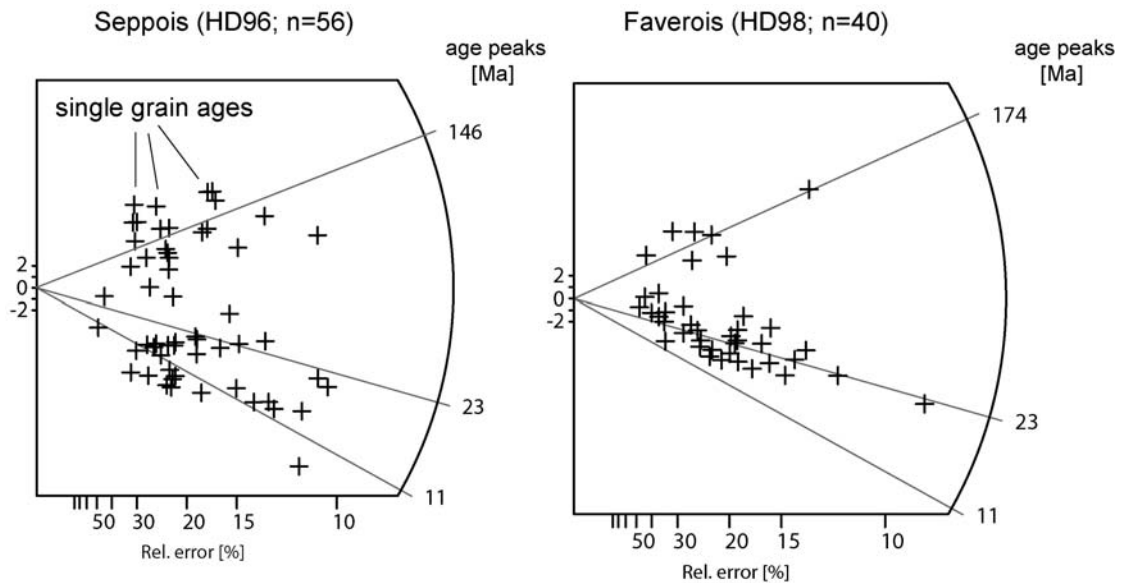


Fig. 8  
Zircon FT data;  
Radial plots (Galbraith 1988, 1990) of the samples from Faverois (HD98) and Seppois (HD96)

The both other samples from Faverois (HD98; n=40) and Seppois (HD96; n=56) within the Ajoie are from the central part of the Sundgau gravels. The old peak age ( $268 \pm 20$  Ma) found in sample HD87 are not represented in these samples, which imply no or only a subordinate influence of material from the neighbouring areas in the north.

Additionally, also they display a clear difference within the young FT ages. While the Seppois sample contains (HD96) 22 grains of the  $11 \pm 1$  Ma age peak and only 13 grains of the second peak at  $23 \pm 2$  Ma, the Faverois sample (HD98) yield no grain within the youngest age group at about 11 Ma and 33 grains in the  $23 \pm 2$  Ma age group (Fig. 8, Tab. 6).

It has to be noted, that the sample from Seppois (HD96) originates from sand in contrast to the Faverois sample (HD98), which originates from gravels. Therefore, a kind of sorting by different transport and/or deposition characteristics of the material within a fluvial environment cannot ruled out.

On the other hand, even changes of the shape of the drainage area could explain the different age spectra of both samples. By the loss of drainage areas a loss of parts of the characteristic FT age signatures of the sediment seems to be possible. Such a change in the upper palaeo-Aare system, which drained parts of the Alps enclosing various FT age patterns, would be responsible for a narrowing of the spectrum of the FT ages of palaeo-Aare

sediments. Otherwise, it could be possible that an increasing drainage area and/or deeper incision of the upper reaches are responsible for an access to regions or depths with additional FT age signatures, which could support a spreading of the FT age spectrum. Such a spreading of the FT age spectrum should occur quickly by getting new reaches, which delivers new FT age patterns. Reworking of remnants, which are deposited along the whole Aare river, argues against a substantial and quick change within the FT age spectrum due to the loss of parts of the drainage area.

The statistic significance of only two samples with different FT age signatures is not very high. Additionally, the outcrops of Seppois and Faverois are indistinguishable in matters of their relative or absolute deposition ages.

Nevertheless, a widening of the FT age spectrum, as recognized within the Faverois sample (HD98), related to an increasing and/or deeper incision of the river system seems to be more probable, than a decreasing drainage area of the Aare river. Such an argumentation suggests a younger deposition age of the Faverois sample compared to the Seppois sample.

### ***Pleistocene gravel***

The samples from the local fan deposits along the eastern graben margin of Pleistocene age yield the same apatite and zircon FT age pattern as known from the Black Forest crystalline basement and the Mesozoic units of the URG area (Michalski 1987, Wyss 2001, Timar-Geng et al. 2004 & 2006a, Spiegel et al. 2007, Dresmann et al. 2009, Dresmann 2009). An unusual outlier represented by the subordinate zircon FT age peak at ca.  $15 \pm 3$  Ma (n=2) within the sample HD30 was found at Bollschweil. These young zircon FT ages are so far not known from the Black Forest. Considering the elevated position in respect to the altitude of Pleistocene graben sediments containing Alpine material a contamination by them can be excluded. The sampled outcrop at Bollschweil is located about 15 km away of the about 14 to 19 Ma old Kaiserstuhl volcano complex (Keller et al. 2002, Wimmenauer 2003). Additionally, around Bollschweil further Cenozoic volcanoes are known. Therefore, volcanic sources could be responsible for the 15 Ma zircon FT age peak.

## 8. Conclusions

A comprehensive characterisation of the apatite and zircon FT age signatures of the Cenozoic sediments from the URG area has been performed. These analyses show that the Cenozoic units of the southern URG were not significantly reheated after their deposition. As well as the analyses on zircon grains, that showed no young thermal overprint, in general, the FT system in apatite were also not effected. Nevertheless, strong heterogeneities of the thermal pattern due to convective thermal anomalies along fault zones or deep burial (e.g. Dannemarie basin), in small parts of the area a thermal overprint of the FT system in apatite can not ruled out.

However, especially FT analyses of zircons encompass a high potential for analysing their provenance areas. Therefore, by comparing the known FT signatures of potential provenance areas of these deposits from the URG area with the new FT data for the Cenozoic deposits, changes in the drainage system becomes clearer.

During the initial rifting of the URG solely the transport of material delivered from the graben flanks can be recognised. This fluvial to lacustrine environment changed abruptly after a marine transgression during the Early Oligocene. A first connection between the URG and the Northern Alpine Molasse Basin has been indicated by the characteristically Alpine zircon FT age signature obtained from the lower, most proximal facies, of the Grey Marl formation (“Meeressand”) near Dornach. The locality at the south-eastern Border of the URG suggests a connection to the Alpine Molasse basin via the southern prolongation of the URG the so-called “Rauracien depression”. The upper Grey Marl formation shows clearly the sedimentation of Alpine-derived material in its zircon FT age signature as well.

After a hiatus in the depositional record of the southern URG area in the Miocene, sedimentation started again and was dominated by material derived from local source areas in the Vosges and the Black Forest. This observation has been confirmed by the known zircon FT signature of the Vosges and the Black Forest, which have been found in the Bois de Raube Formation as well as in the Juranagelfluh and their equivalents.

The Pliocene Sundgau gravels, which are basically composed of Alpine material, may hint on a widening of the drainage area between the deposition of the samples of Seppois and Faverois.

Since the Pleistocene the river Rhine has dominated the fluvial systems and the content of the young deposits of the URG interior. Additionally, along the margins of the URG many fans developed leading to a growing influence of local material while the flanks were uplifted and denuded.

## **Appendix**

### *Analytical procedure*

Apatite and zircon grains were separated from each sample (2 to 8 kg rock material) following standard mineral separation procedure including crushing, magnetic and heavy liquid separation. The zircon samples were mounted in Teflon PFA<sup>®</sup>, while the apatite samples were embedded in epoxy resin. After polishing, the apatites were etched for 40 s in 6.5 % HNO<sub>3</sub> at ~18 °C and the zircons for 5 to 14 h in an eutectic-melt of KOH-NaOH (220 °C). Muscovite was used as an external detector (Naeser 1976, Gleadow 1981) and CN-5 (apatite) and CN-1 (zircon) standards as dosimeter glasses. Irradiation with thermal neutrons was carried out at the Australian Nuclear Science and Technology Organisation facility (ANSTO).

Muscovite detectors were etched in 40 % HF for 40 min at ~18 °C. Tracks were counted with a 1600x magnification (dry) for apatite and zircon samples on a Zeiss (Axioplan2) optical microscope with a computer-controlled motorised scanning stage, run by the "FT-STAGE 3.11" software (Dumitru, 1993). The FT age determination followed the zeta calibration method (Hurford & Green 1983) with a zeta value of  $380.67 \pm 10.58$  (Durango, CN-5) for apatite and  $145 \pm 6.88$  (Fish Canyon Tuff, CN-1) for zircon.



## **Acknowledgments**

This work is a contribution of the EUCOR-URGENT Project (Upper Rhine Graben, Evolution and NeoTectonics). It has been supported by the Swiss National Science Foundation (Project Nos. 21-57038.99 and 20-64567.01). We thank Philippe Durringer for a fruitful meeting in the field and providing information about the Equisheim area. Alexander Kounov, Elmar Wosnitza, Nynke Keulen, Fred Gaidis and Tjerk Heijboer gratefully thanked for discussions and proof readings.

#### **IV. Key conclusions of the thesis**

Cenozoic and Mesozoic FT ages within the Permian and Mesozoic sediments of the URG area prove a post-depositional thermal overprint in a regional scale of the apatite and partly the zircon FT system.

At the end of a period of widespread hydrothermal activity during the Triassic and Jurassic a last intense regional hydrothermal pulse appears. Probably between 150 Ma and 140 Ma temperatures of at least 180 °C in the uppermost crystalline basement and the Permian to Triassic sediments were reached. After this Jurassic to Early Cretaceous event the thermal regime of the upper crust cools rapidly to temperatures below 120 °C, before, during the Late Eocene to Early Oligocene temperatures of up to 120 °C were reached and effected the apatite FT system in the uppermost crystalline basement and the Permian to Mesozoic sediment cover, followed once more by a cooling regime.

Accompanying, the initial phase of the Cenozoic URG rifting several localised thermal anomalies developed along the main border faults of the southern URG leading occasionally to temperatures in excess of 180 °C. Such partly short-lived thermal anomalies caused by hydrothermal fluid migration and convection are probably related to tectonic and volcanic activity.

FT analyses on Cenozoic to Quaternary sediments in the area of the URG confirm generally the knowledge of the syn-rift drainage system history.

During the Cenozoic and Quaternary fluvial systems dominates the southern URG. At an age of about 31 Ma south of Basel a connection developed to the Northern Alpine Molasse Sea and persisted during about 5 Ma interrupting the dominance of fluvial environments. This is evidenced by the characteristically Alpine zircon FT age signature found in the deposits of the lower and upper units of the Grey Marl Formation.

## V. References (Bibliography)

- Allen PA, Allen JR (1990) Basin Analysis, Blackwell Sci Publ Oxford, p 451
- Allia V (1996) Sedimentologie und Ablagerungsgeschichte des opalinustons in der Nordschweiz. PhD thesis, Basel University, Nr 10, p 185
- Barbarand J, Lucazeau F, Pagel M, Seranne M (2001) Burial and exhumation history of the south-eastern Massif Central (France) constrained by apatite fission-track thermochronology. *Tectonophysics*. 335(3-4):275-290
- Berger JP, Reichenbacher B, Becker D, Grimm M, Grimm K, Picot L, Storni A, Pirkenseer C, Derer C, Schäfer A (2005a) Paleogeography of the Upper Rhine Graben (URG) and the Swiss Molasse Basin (SMB) from Eocene to Pliocene. *Int J Earth Sci* 94:697-710
- Berger JP, Reichenbacher B, Becker D, Grimm M, Grimm K, Picot L, Storni A, Pirkenseer C, Schäfer A (2005b) Eocene-Pliocene time scale and stratigraphy of the Upper Rhine Graben (URG) and the Swiss Molasse Basin (SMB). *Int J Earth Sci* 94:711–731
- Bernet M (2002) Exhuming the Alps through time: clues from detrital zircon fission-track ages. PhD thesis, Yale University
- Bernet M, Brandon M, Garver J, Molitor B (2004) Downstream changes of Alpine zircon fission track ages in the Rhone and Rhine rivers. *J Sedim Res* 74(1):82–94
- Bernet M, Garver JI (2005) Fission-Track Analysis of detrital zircon. In: Reiners PW, Ehlers TA (eds) *Low-temperature thermochronology: techniques, interpretations, and applications*. *Rev Mineral Geochem, Mineral Soc Am* 58
- Bitterli-Brunner P (1987): *Geologischer Führer der Region Basel*. Birkhäuser, Basel.
- Boigk H, Schöneich H (1970) Die Tiefenlage der Permbasis im nördlichen Teil des Oberrheingrabens. In: J.H. Illies, St. Müller (eds) *Graben Problems*. Schweizerbart'sche Verlagsbuchhandlung Stuttgart. *Int Upper Mantle Project, Sci. Rept.* 27, 48-55
- Borel G. (1995) Préalpes médianes: courbes de subsidence et implications géodynamiques. *Bulletin de la Société Vaudoise des Sciences naturelles* 83(4):293-315
- Boullier AM, Fujimoto K, Ito H, Ohtani T, Keulen N, Fabbri O, Amitrano D, Dubois M, Pezard P. (2004) Structural evolution of the Nojima Fault (Awaji Island, Japan) revisited from the GSJ drillhole at Hirabayashi. *Earth Planets Space* 56:1233–1240
- Brandon MT, Vance JA (1992) Zircon fission-track ages for the Olympic subduction complex and adjacent Eocene basins, western Washington State. *Open-File Report - Washington (State)*. Division of Geology and Earth Resources
- Brandon MT (1996) Probability density plots for fission-track grain age distributions. *Radiat Meas* 26:663-676
- Brandon MT, Roden-Tice MK, Garver JI (1998) Late Cenozoic exhumation of the Cascadia accretionary wedge in the Olympic Mountains, northwest Washington State. *Geol Soc Am Bull* 110:985-1009
- Brandon MT (2005) BINOMFIT: a Windows® program for estimating fission-track ages for concordant and mixed grain age distributions. In: Reiners

- PW, Ehlers TA (eds) Low-temperature thermochronology: techniques, interpretations, and applications. *Rev Mineral Geochem, Mineral Soc Am* 58:600-602
- Brianza M, Hauber L, Hottinger L, Maurer H (1983) Die geologischen Resultate der Thermalwasserbohrung von Leymen (Haut-Rhin, Frankreich) suedlich von Basel, unter besonderer Beruecksichtigung der Schwerminerale. *Eclogae Geologicae Helvetiae*. 76(1):253-279
- Brockamp O, Clauer N, Zuther M (2003) Authigenic sericite record of a fossil geothermal system; the Offenburg Trough, central Black Forest, Germany. *Int J Earth Sci* 92(6):843-851
- Brügel A Dunkl I, Frisch W, Kuhlemann J, Balogh K (2003) Geochemistry and Geochronology of Gneiss Pebbles from Foreland Molasse Conglomerates: Geodynamic and Paleogeographic Implications for the Oligo-Miocene Evolution of the Eastern Alps. *J Geol* 111(5):543-563
- Bourgeois, O., Ford, M., Diraison, M., Pik, R., Gerbault, M., Le Carlier de Veslud C., Ruby, N. and Bonnet, S. (2007) Separation of rifting and lithospheric folding signatures in the NW alpine foreland. *International Journal of Earth Sciences*, doi:10.1007/s00531-007-0202-2
- Carpéna J (1992) Fission Track Dating of Zircon: Zircons from Mont Blanc Granite (French-Italian Alps). *J Geol* 100:411-421
- Carter A (1999) Present status and future avenues of source region discrimination and characterization using fission track analysis. *Sedim Geol* 124:31-45
- Chantraine J, Autran A, Cavelier C et coll. (1996) Carte géologique de la France à l'échelle du millionième, 6e édition. BRGM, Orléans
- Crank J, Nicolson P (1947) A practical method for numerical evaluation of solutions of partial differential equations of the heat-conduction type. *Proc Cambridge Phil Soc* 43(50):50-67
- Crowley KD, Cameron M, Schaefer RL (1991) Experimental studies of annealing etched fission tracks in fluorapatite. *Geochimica et Cosmochimica Acta* 55:1449-1465
- van Daalen M, Heilbronner R, Kunze K (1999) Orientation analysis of localized shear deformation in quartz fibres at the brittle-ductile transition. *Tectonophysics* 303:1-4
- Diebold, P. (1989): Der Nordschweizer Permokarbon-Trog und die Steinkohlenfrage der Nordschweiz. *Vjschr. natf. Ges. Zürich*, 133/1, 143-174.
- Doehl F. (1967) The Tertiary and Pleistocene sediments of the northern and central Upper Rhinegraben. In: Rothe J, Sauer K (eds) *The Rhinegraben Progress Report 1967*. *Abh Geol Landesamt B-W* 6:48-55
- Dresmann H. (2009) Fission-Track analyses in the area of the southern Upper Rhine Graben. PhD thesis, Basel University (this study)
- Dresmann H., Keulen N., Timar-Geng Z., Fügenschuh B., Wetzel A, & Stünitz H. (2009) The south-western Black Forest and the Upper Rhine Graben Main Border Fault: thermal history and hydrothermal fluid flow. *International Journal Earth Science*. DOI 10.1007/s00531-008-0391-3
- Dumitru TA (1993) A new computer-automated microscope stage system for fission-track analysis. *Nuclear Tracks and Radiation Meas* 21: 575-580
- Dunkl I (2002) Trackkey; a Windows® program for calculation and graphical presentation of fission track data. *Comp Geosci* 28(1):3-12

- Düringer P (1988). Les conglomérates des bordures du rift cénozoïque rhénan. Dynamique sédimentaire et contrôle climatique. PhD thesis, Université Louis Pasteur, Strasbourg
- Edel JB, Fluck P (1989) The upper Rhenish Shield basement (Vosges, Upper Rhinegraben and Schwarzwald): Main structural features deduced from magnetic, gravimetric and geological data. *Tectonophysics* 169:303–316
- Eisbacher GH, Lüschen E, Wickert F (1989) Crustal-Scale Thrusting and Extension in the Hercynian Schwarzwald and Vosges, Central Europe. *Tectonics* 8(1):1-21
- Echtler HP, Chauvet A (1992) Carboniferous convergence and subsequent crustal extension in the southern Schwarzwald (SW Germany). *Geodinamica Acta* 5(1-2):37-49
- Ernst M, Hergesell G, (1997) Geologische Karte von Baden-Württemberg 1:25.000, BL. 8211, Kandern, Landesvermessungsamt, Stuttgart
- Fischer H (1965) Geologie des Gebietes zwischen Blauen und Pfirter Jura. *Beitr Geol Kt Schweiz* 122:1–106
- Fitz Gerald JD, Stünitz H (1993) Deformation of granitoids at low metamorphic grade; I, Reactions and grain size reduction. *Tectonophysics* 221:3-4.
- Fügenschuh B, Seward D, Mancktelow NS (1997) Exhumation in a convergent orogen: the western Tauern window. *Terra Nova* 9:213-217
- Fügenschuh B, Mancktelow NS, Seward D. (2000) Cretaceous to Neogene cooling and exhumation history of the Oetztal-Stubai basement complex, Eastern Alps; a structural and fission track study. *Tectonics* 19(5):905-918
- Fügenschuh B, Schmid SM (2003) Late stages of deformation and exhumation of an orogen constrained by fission-track data: A case study in the Western Alps. *Geol Soc Am Bull* 115:1425-1440
- Funk H (1985) Mesozoische Subsidenzgeschichte im Helvetischen Schelf der Ostschweiz. *Eclogae Geologicae Helvetiae*. 78(2):249-272
- Galbraith RF (1988) Graphical display of estimates having differing standard errors. *Technometrics* 30:271-281
- Galbraith RF, Green PF (1990) Estimating the component ages in a finite mixture. In: Durrani SA, Benton EV (eds) *Proc 6th international fission track dating workshop*. *Nuclear Tracks and Radiation Meas* 17(3):197-206
- Galbraith RF, Laslett GM (1993) Statistical models for mixed fission track ages. *Nuclear Tracks Radiation Meas* 21:459-70
- Garver JI, Soloviev AV, Bullen ME, Brandon MT (2000) Towards a more complete record of magmatism and exhumation in continental arcs, using detrital fission-track thermochronometry. In: Andriessen PAM (ed) *Erosion and tectonic movements; from measurements to physical modelling*. *Phys Chem Earth A: Solid Earth and Geodesy* 25(6-7):565-570
- Garver JI (2006) The significance of radiation damage in zircon for fission track dating. *European Conference on Thermochronology, Bremen, Schriftenreihe der Deutschen Gesellschaft für Geowissenschaften* 49:56-58
- Geyer OF, Gwinner MP (1991) *Geologie von Baden-Württemberg*. Schweizerbart, Stuttgart, pp1-482

- Geyer OF, Gwinner MP (2004) Geologie von Baden-Württemberg. Schweizerbart, Stuttgart, pp1-482
- Giamboni M, Ustaszewski K, Schmid SM, Schumacher ME, Wetzel A (2004) Plio-Pleistocene transpressional reactivation of Paleozoic and Paleogene structures in the Rhine-Bresse transform zone (Northern Switzerland and Eastern France). *Geol Runds* 93:207–233, doi: 10.1007/s00531-00003-00375-00532
- Glasmacher U, Zentilli M, Grist AM (1997): Apatite Fission Track thermochronology of Paleozoic sandstones and the Hill-intrusion at the northern part of the Linksrheinisches Schiefergebirge, Germany. In: Van den Haute, De Corte (1998): *Advances in Fission-Track Geochronology* 151-172
- Gleadow AJW (1981) Fission track dating: what are the real alternatives. *Nucl. Tracks* 5:3-14
- Gleadow AJW, Duddy IR (1981) A natural long-term track annealing experiment for apatite. *Nucl. Tracks* 5:169-174
- Gleadow AJW, Brown RW (2000) Fission-track thermochronology and the long-term denudational response to tectonics. In: Summerfield MA (ed.) *Geomorphology and global tectonics*. pp57-75
- Gonzalez R & Wetzel A (1996) Stratigraphy and paleogeography of the Hauptrogenstein and Klingnau Formations, northern Switzerland. *Eclogae Geologicae Helvetiae* 89(1):695-720
- Green PF, Duddy IR, Gleadow AJW, Lovering JF (1985) Apatite fission-track analysis as a paleotemperature indicator for hydrocarbon exploration. In: Naeser ND, McCulloh TH (eds) *Thermal history of sedimentary basins; methods and case histories*. pp 181-195
- Green PF, Duddy IR, Gleadow AJW, Tingate PR, Laslett GM (1986) Thermal annealing of fission tracks in apatite 1: A qualitative description. *Chem Geol* 59:237-253
- Green PF (1989): Thermal and tectonic history of the East Midlands shelf (onshore UK) and surrounding regions assessed by apatite fission track analysis. *Geol Soc J [London]* 146:755-773
- Groschopf R, Kessler G, Leiber J, Maus H, Ohmert W, Schreiner A, Wimmenauer W (1977) *Erläuterungen zur Geologischen Karte Freiburg i.Br. und Umgebung 1:50.000*, Geologisches Landesamt Baden-Württemberg.
- Gürler B, Hauber L, Schwander M (1987) Die Geologie der Umgebung von Basel. *Beitr Geol Karte der Schweiz* 160:1-33
- Haas IO, Hoffmann CR (1929) Temperature gradient in Pechelbronn oil – bearing region, Lower Alsace: its determination and relation to oil reserves. *Bull Am Assoc Petrol Geol* 13:1257-1273
- Häring MO (2002) Sondierbohrung Otterbach, Basel. Der erste Schritt zur Entwicklung eines geothermischen Heiz-Kraftwerks nach dem Hot-Dry-Rock Verfahren. *Bull angew Geol* 7(1):19-30
- Hagedorn EA (2004) Sedimentpetrographie und Lithofazies der jungtertiären und quartären Sedimente im Oberheingebiet, PhD Thesis, University Cologne
- Hamza VM (2001) Tectonic leakage of fault bounded aquifers subject to non-isothermal recharge: a mechanism generating thermal precursors to seismic events. *Phys Earth Planet Interiors* 126:163–177

- Hanisch J (1984) The Cretaceous opening of the Northeast Atlantic. *Tectonophysics* 101(1-2):1-23
- Hann HP and Sawatzki G (2000) Neue Daten zur Tektonik des Südschwarzwaldes. *Jahresberichte und Mitteilungen des oberrheinischen geologischen Vereins*, 82:363-376
- Heilbronner R, Keulen N (2006) Grain size and grain shape analysis of fault rocks, *Tectonophysics* 427:199-216
- Hejl E, Coyle D, Lal N, van den Haute P, Wagner GA (1997) Fission-track dating of the western border of the Bohemian Massif; thermochronology and tectonic implications. *Geol Runds* 86(1):210-219
- Herrgsell G (1996a) Beiheft zur Geologischen Karte Müllheim 8111, 1:25.000 Baden-Württemberg
- Herrgsell G (1996b) Beiheft zur Geologischen Karte Freiburg im Breisgau-SW 8012, 1:25.000 Baden-Württemberg
- Hill DP, Reasenberga PA, Michael AJ, Arabasz WJ, Beroza GC, Brune JN, Brumbaugh DS, Castro R, Davis SD, dePolo DM, Ellsworth WL, Gomberg JS, Harmsen SC, House L, Jackson SM, Johnston MJ, Jones LM, Keller R, Malone SD, Munguia L, Nava S, Pechmann JC, Sanford AR, Simpson RW, Smith RS, Stark MA, Stickney MC, Vidal A, Walter SR, Wong V, Zollweg JE (1993) Seismicity in the Western United States remotely triggered by the M 7.4 Landers, California, earthquake of June 28, 1992. Open-File Report - US Geol Surv 238-276
- Hinsken S (2003) Geologische Untersuchungen an Syn-Riftsedimenten des südlichen Oberrheingrabens. unpubl MSc thesis, Universität Basel, p 285
- Hinsken S (2003) Geologische Kartierung am südwestlichen Schwarzwaldrand, zwischen Kandern, Sitzenkirch und Scheideckhöhe. unpubl MSc thesis II: 225-267
- Hinsken S, Ustaszewski K, Wetzel A (2007) Graben-width controls synrift sedimentation: The Palaeogene southern Upper Rhine Graben as an example. *Int J Earth Sci.* doi:10.1007/s00531-006-0162-y
- van Hinte (1978) Geohistory analysis; application of micropaleontology in exploration geology. *AAPG Bull* 62(2):201-222
- Huang F, Jian C, Tang Y, Xu G, Deng Z, Chi G (2004) Response changes of some wells in the mainland subsurface fluid monitoring network of China, due to the September 21, 1999, Ms7.6 Chi-Chi Earthquake. *Tectonophysics* 390:217– 234
- Huber M, Huber-Aleffi A (1990) Zur Tektonik des Schwarzwaldes. NAGRA Technischer Bericht 90-03:2-1–3-27
- Hug WA, Berger JP, Clement I, Kälin D, Weidmann M (1997) Sedimentological history of a Miocene fossiliferous palaeokarst near Glovelier (Swiss Jura Mountains). In: Abstracts; 18th IAS regional European meeting of Sedimentology. *Gaea Heidelbergensis* 3:168-169
- Hunziker J., Desmons J. and Hurford A.J. 1992, Thirty-two years of geochronological work in the Central and Western Alps: A review on seven maps. *Memories de Geologie Lausanne* 13, 59 p
- Hurford AJ, Green PF (1983) The zeta age calibration of fission-track dating. *Chem Geol* 41(4):285-317
- Hurford AJ (1990) International Union of Geological Sciences Subcommittee on Geochronology recommendation for the standardization of fission

- track dating calibration and data reporting. *Nuclear Tracks and Radiation Meas* 17(3):233-236
- Illies JH (1967) Development and tectonic pattern of the Rhinegraben. In: *The Rhinegraben Progress Rept, Abh Geol Landesamt B-W, Freiburg* 6: 7-9
- Illies JH (1977) Ancient and recent rifting in the Rhinegraben. *Geologie en Mijnbouw* 56:329–350
- Jelinek AR, Bastos-Neto AC, Lelarge MLV, Soliani Jr E (1999) Apatite fission-track dating of fluorite ore veins from Santa Catarina state, Brasil: a complex hydrothermal evolution. *J South Am Earth Sci* 12:367-377
- Kählin D (1997) Litho- und Biostratigraphie der mittel- bis obermiozänen Bois de Raube-Formation (Nordwestschweiz). *Eclogae Geologicae Helvetiae*, 90(1): 97-114
- Karg H, Carter A, Brix MR, Littke R (2005) Late- and post-Variscan cooling and exhumation history of the northern Rhenish massif and the southern Ruhr Basin: new constraints from fission-track analysis. *Int J Earth Sci* 94(2):180–192
- Kasuya M, Naeser CW (1988) The effect of alpha-damage on fission-track annealing in zircon. *Nuclear Tracks and Radiation Meas* 14(4):477-480
- Kato A, Ohnaka M, Mochizuki H (2003) Constitutive properties for the shear failure of intact granite in seismogenic environments. *J Geophys Res* 108(B1) doi:10.1029/2001JB000791
- Keller J, Kraml M, Henjes-Kunst F (2002)  $^{40}\text{Ar}/^{39}\text{Ar}$  single crystal laser dating of early volcanism in the Upper Rhine Graben and tectonic implications. *Schweiz Mineral Petrogr Mitt* 82(1):121-130
- Kemna HA, Becker-Haumann R (2003) Die Wanderblock-Bildungen im Schweizer Juragebirge südlich von Basel: Neue Daten zu einem alten Problem. *Eclogae Geologicae Helvetiae* 96:71-83
- Keulen N, Heilbronner R, Stünitz H, Boullier AM, Ito H (2007) Grain size distribution of gouge; a comparison between experimentally deformed granitoids and the Nojima Fault Zone. *J Structural Geology*, 29(8):1282-1300 doi: 10.1016/j.jsg.2007.04.003
- Keulen, N., Stünitz, H. and Heilbronner, R. (2008) Healing microstructures of experimental and natural fault gouge. *Journal of Geophysical Research* 113, B06205, doi:10.1029/2007JB005039.
- Köppen A, Carter A (2000) Constraints on provenance of the Central European Triassic using detrital zircon fission track data. *Palaeogeogr Palaeoclimat Palaeoecol* 161:193–204
- Kuhlemann J, Kempf O (2002) Post-Eocene evolution of the North Alpine Foreland Basin and its response to Alpine tectonics. *Sediment Geol* 152:45–78
- Lampe C, Person MA (2002) Advective cooling within sedimentary rift basins—application to the Upper Rhinegraben (Germany). *Marine and Petroleum Geology* 19/3:361-375
- Laubscher H (1987) Die tektonische Entwicklung der Nordschweiz. *Eclogae Geologicae Helvetiae* 80(2):287-303
- Laubscher H (1992) Jura kinematics and the Molasse Basin. *Eclogae Geologicae Helvetiae*, 85:653-675



- Laubscher H (2003) The Miocene dislocations in the northern foreland of the Alps oblique subduction and its consequences (Basel area, Switzerland-Germany) *Jber. Mitt. oberrhein. geol. Ver. N.F.* 85:423-439
- Laubscher, H. & Noack, T. (1997), The deep structure of the Basel Jura. In: PFIFFNER, O. A., LEHNER, P., HEITZMANN, P., MUELLER, ST. & STECK, A. Editors: *Deep structure of the Swiss Alps: results of NFP 20*, 54-58.
- Liniger H, Hofmann F (1965) Das Alter der Sundgauschotter westlich von Basel. *Eclogae Geologicae Helvetiae* 85(1):215-229
- Liniger H (1966) Das Plio-Altpleistozäne Flussnetz der Nordschweiz. *Regio Basiliensis* 7(2):158–177
- Liniger H (1970) Erläuterungen Blatt Bonfol 1:25.000, Geologischer Atlas der Schweiz.
- Liniger H. (1967) Pliozän und Tektonik des Juragebirges. *Eclogae Geologicae Helvetiae* 60(2):407–490
- Lüders V. (1994) Geochemische Untersuchungen an Gangmineralen aus dem Bergbaurevier Freiamt-Sexau und dem Badenweiler-Quarzriff (Schwarzwald). *Abh Geol Landesamt B-W* 14:173-190
- Lin A (1999) S-C cataclasite in granitic rock. *Tectonophysics* 304:257-273
- Magloughin JF (1992) Microstructural and chemical changes associated with cataclasis and frictional melting at shallow crustal levels: the cataclasite-pseudotachylyte connection. *Tectonophysics* 204:243-260
- Madritsch H., Kounov A., Schmid S.M. & Fabbri O. (2009) Multiple fault reactivation within the intra-continental Rhine-Bresse Transfer Zone (La Serre Horst, Eastern France), *Tectonophysics*, doi:10.1016/j.tecto.2009.02.044
- Mazurek M, Hurford AJ, LEU W (2006) Unravelling the multi-stage burial history of the Swiss Molasse Basin: integration of apatite fission track, vitrinite reflectance and biomarker isomerisation analysis. *Basin Research* 18:27–50
- Metz R, Rein G (1957) Geologisch-petrographische Übersichtskarte des Südschwarzwaldes mit Erz- und Mineralgängen, 1:50000, Moritz Schauenburg Verlag, Lahr/Schwarzwald
- Michalski I (1987) Apatit-Spaltspuren-Datierungen des Grundgebirges von Schwarzwald und Vogesen: Die postvariszische Entwicklung. PhD thesis Heidelberg University, p 125
- Milliken KL, Laubach SE (2000) Brittle deformation in sandstone diagenesis as revealed by scanned cathodoluminescence imaging with application to characterization of fractured reservoirs. In: Pagel M, Barbin V, Blanc P, Ohnenstetter D (eds) *Cathodoluminescence in geosciences*. Springer, Berlin, pp 225-243
- Mogi K, Mochizuki H, Kurokawa Y (1989) Temperature changes in an artesian spring at Usami in the Izu Peninsula (Japan) and their relation to earthquakes. *Tectonophysics* 159:95-108
- Montadert L, Roberts DG, De Charpal O, Guennoc P (1979) Rifting and subsidence of the northern continental margin of the Bay of Biscay. *Initial Reports of the Deep Sea Drilling Project*. 48:1025-1060
- Müller WH, Huber M, Isler A, Kleboth P (1984) Erläuterungen zur Geologischen Spezialkarte Nr. 121 der zentralen Nordschweiz 1: 100

- 000 mit angrenzenden Gebieten von Baden-Württemberg. – NAGRA und Schweiz. Geol. Kommission, pp 234
- Munck, F., Sauer, K., Maget, Ph., Neeb, I., Tietze, R., Walgenwitz, F., (1979): Geothermische Synthese des Oberrheingrabens. Strasbourg: BRGM.SGR Alsace und GLA Baden Württemberg, Freiburg i. Br.
- Murakami M, Tagami T (2004) Dating pseudotachylite of the Nojima Fault using the zircon fission-track method. *Geophys Res Lett* 31:L12604
- Naeser CW (1976) Fission-track dating. Open-File Rep – US Geol Surv 76-190
- Odin GS, Barbin V Hurford AJ, Baadsgaard H, Galbrun B, Gillot PY (1991) Multi-method radiometric dating of volcano-sedimentary layers from northern Italy; age and duration of the Priabonian Stage. *Earth Planet Sci Lett* 106(1-4):151-168
- Parry WT (1998) Fault-fluid composition from fluid-inclusion observations and solubilities of fracture-sealing minerals. *Tectonophysics* 290:1-26
- Parry WT, Bunds MP, Bruhn RL, Hall CM, Murphy JM (2001) Mineralogy,  $^{40}\text{Ar}/^{39}\text{Ar}$  dating and apatite fission track dating of rocks along the Castle Mountain fault, Alaska. *Tectonophysics* 337:149-172
- Passchier CW, Trouw RAJ (2005) *Microtectonics*, 2<sup>nd</sup> ed, Springer Heidelberg, p 366
- Paul W (1955) Zur Morphogenese des Schwarzwaldes (I). *Jh geol Landesamt B-W* 1:395–427
- Person M, Garven G (1992) Hydrologic constraints on petroleum generation within continental rift basins; theory and application to the Rhine Graben. *Am Ass Petrol Geol Bull* 76(4):468-488
- Petitt C, Campy M, Chaline J, Bonvalot J (1996) Major palaeohydrographic changes in Alpine foreland during the Pliocene-Pleistocene. *Boreas* 25, 131–143
- Pflug R (1982) *Bau und Entwicklung des Oberrheingrabens*. Wissenschaftliche Buchgesellschaft, Darmstadt, p 145
- Rahn MK, Brandon MT, Batt GE, Garver JI (2004) A zero-damage model for fission-track annealing in zircon. *Am Mineral* 89(4):473-484
- Ramseyer K, Fischer J, Matter A, Eberhardt P, Geiss J (1989) A cathodoluminescence microscope for low intensity luminescence. *J Sedim Petrol* 59:619-622
- Ramseyer K, AlDahan AA, Collini B, Landström O (1992) Petrological modifications in granitic rocks from the Siljan impact structure: evidence from cathodoluminescence. *Tectonophysics* 216:195-204
- Ravenhurst CE, Roden-Tice MK, Miller DS (2003) Thermal annealing of fission tracks in fluorapatite, chlorapatite, manganoapatite, and Durango Apatite; experimental results. *Canadian J Earth Sci* 40(7):995-1007
- Reiners PW, Ehlers TA (2005) Low-temperature thermochronology: techniques, interpretations, and applications. *Rev Mineral Geochem, Mineral Soc Am* 58:1-622
- Rohrman, M., van der Beck, P., Andriessen, P., 1994. Syn-rift thermal structure and post-rift evolution of the Oslo Rift (southeast Norway): New constraints from fission track thermochronology. *Earth Planet Sci Lett* 127:39–54

- Roll A (1979) Versuch einer Volumenbilanz des Oberrheingrabens und seiner Schultern. *Geologisches Jahrbuch. Reihe A* 52:3-82
- Roussé S. (2006) Architecture et dynamique des séries marines et continentales de l'Oligocène Moyen et Supérieur du Sud du Fossé Rhénan. These, L'Université Strasbourg
- Rousset, D., Bayer, R., Guillon, D. & Edel, J.-B. (1993). *Structure of the southern Rhine Graben from gravity and reflection seismic data (ECORS-DEKORP program)*. *Tectonophysics*, 221, 135-153.
- Sammis CG, King G, Biegel RL (1987) The Kinematics of Gouge Deformation. *Pure Applied Geophys* 125:777-812
- Sawatzki G. (1999) Beiheft zur Geologischen Karte Staufen im Breisgau 8112, 1:25.000 Baden-Württemberg
- Sawyer DS, Toksoz MN, Sclater JG, Swift BA, (1982) Thermal evolution of the Baltimore Canyon Trough and Georges Bank basin. In: Watkins JS, Drake CL (eds) *Studies in continental margin geology*. AAPG Mem 34:743-762
- Schaltegger U, Schneider JL, Maurin JC, Corfu F (1996) Precise U-Pb chronometry of 345-340 Ma old magmatism related to syn-convergence extension in the southern Vosges (central Variscan Belt). *Earth Planet Sci Lett* 144(3-4):403-419
- Schaltegger U (2000) U-Pb geochronology of the Southern Black Forest Batholith (Central Variscan Belt): timing of exhumation and granite emplacement. *Int J Earth Sci* 88:814-828
- Schellschmidt R, Clauser C (1996) The thermal regime of the Upper Rhine Graben and the anomaly at Soultz. *Zeitschr Angewandte Geologie*. 42(1):40-44
- Schegg R, Leu W (1998) Analysis of erosion events and palaeogeothermal gradients in the North Alpine Foreland Basin of Switzerland. *Geol Soc Spec Publ* 141: 137-155
- Schmoker JW, Halley RB (1982) Carbonate porosity versus depth; a predictable relation for South Florida. *AAPG Bull* 66(12):2561-2570
- Schnarrenberger K (1985) Erläuterungen zu Blatt 8211 Kandern-Geologische Karte 1:25.000 von Baden-Württemberg, Geologisches Landesamt B-W, Heidelberg/Stuttgart pp1-131
- Scholz CH (1990) *The mechanics of Earthquakes and faulting*. Cambridge University Press, Cambridge, pp 1-439
- Schreiner A, Soell H, Wimmenauer W (1957) Ueber zwei neugefundene tertiäre Tuffschlote bei Feuerbach (Südbaden). *Jh Geol Landesamt B-W* 2:179-192
- Schumacher ME (2002) Upper Rhine Graben: the role of pre-existing structures during rift evolution. *Tectonics* 21, 10.1029/2001TC900022 (6-1-6-17)
- Sclater JG, Christie PAF (1980) Continental stretching; an explanation of the post-Mid-Cretaceous subsidence of the central North Sea basin. *J Geophys Res* 85(B7):3711-3739
- Seward D, Sibson RH (1985) Fission Track age for a pseudotachylite from the Alpine Fault Zone, New Zealand. *New Zealand J Geol Geophys* 28:553-557
- Shao SM, Zou JC (1996) Fractal research of fault gouge. *Acta Seismologica Sinica* 9(3):485-491

- Sibson RH (1990) Faulting and fluid flow. In: Nesbitt BE (eds) Short course on fluids in tectonically active portions of the continental crust. Mineral Assoc Canada, Vancouver, 18:93-129
- Sissingh W (1998) Comparative Tertiary stratigraphy of the Rhine Graben, Bresse Graben and Molasse Basin; correlation of Alpine Foreland events. *Tectonophysics* 300(1-4):249-284
- Spiegel C, Kuhlemann J, Dunkl I, Frisch W, von Eynatten H, Kadosa B (2000) Erosion history of the Central Alps: evidence from zircon fission track data of the foreland basin sediments. *Terra Nova* 12:163-170
- Spiegel C, Kuhlemann J, Dunkl I, Frisch W (2001) Paleogeography and catchment evolution in a mobile orogenic belt: the Central Alps in Oligo-Miocene times. *Tectonophysics* 341(1-4):33-47
- Spiegel C, Kuhlemann J, Frisch W (2007) Tracing sediment pathways by zircon fission track analysis: Oligocene marine connections in Central Europe. *Int J Earth Sci* 96(2):363-374
- Stewart RJ, Brandon MT (2004) Detrital-zircon fission-track ages for the "Hoh Formation"; implications for late Cenozoic evolution of the Cascadia subduction wedge. *Geol Soc Am Bull* 116(1-2):60-75
- Stipp M, Stünitz H, Heilbronner R, Schmid SM (2002a) The eastern Tonale fault zone: a 'natural laboratory' for crystal plastic deformation of quartz over a temperature range from 250-700°C. *J Struct Geol* 24:1861-1884
- Stipp M, H Stünitz, R Heilbronner, SM Schmid (2002b), Dynamic recrystallization of quartz: Correlation between natural and experimental conditions. In: De Meer S, Drury M, Pennock J (eds) *Deformation Mechanisms, Rheology and Tectonics: Current Status and Future Perspectives*, *Geol Soc Spec Publ London* 200:171-190
- Stampfli GM, Marchant RH (1997) Geodynamic evolution of the Tethyan margins of the Western Alps. In: Results of NRP 20; deep structure of the Swiss Alps. Pfiffner OA, Lehner P, Heitzman P, Mueller S, Steck A (eds) pp223-239
- Stewart RJ, Brandon MT (2004) Detrital-zircon fission-track ages for the "Hoh Formation"; implications for late Cenozoic evolution of the Cascadia subduction wedge. *Geol Soc Am Bull* 116(1-2):60-75
- Surma F, Geraud Y, Pourcelot L, Gauthier-Lafaye F, Clavaud JB, Zamora M, Lespinasse M, Cathelineau M (2003) Microstructures d'un gres affecte par une faille normale; anisotropie de connectivite et de permeabilite. *Bull Soc Geol France* 174(3):295-303
- Tagami T, Shimada C (1996) Natural long-term annealing of the zircon fission track system around a granitic pluton. *J Geophys Res* 101(B4):8245-8255
- Tagami T, Galbraith RF, Yamada R, Laslett GM (1998) Revised annealing kinetics of fission tracks in zircon and geological implications. In: P. Van den Haute and F. De Corte (eds.) *Advances in Fission Track Geochronology*, Kluwer Academic Publ, Dordrecht, pp 99-112
- Tagami T, O'Sullivan PB (2005) Fundamentals of Fission-Track Thermochronology. in Reiners PW, Ehlers TA (2005) *Low-temperature thermochronology: techniques, interpretations, and applications*. *Rev Mineral Geochem* 58:19-47
- Tagami T (2005) Zircon Fission-Track Thermochronology and Applications to Fault Studies. In: Reiners PW, Ehlers TA (2005) *Low-temperature*

- thermochronology: techniques, interpretations, and applications. *Rev Mineral Geochem, Mineral Soc Am* 58:95-122
- Teichmueller M (1979) Die Diagenese der kohligen Substanzen in den Gesteinen des Tertiärs und Mesozoikums des mittleren Oberrhein-Grabens In: Reiche E Hilden HD (eds) *Inkohlung und Geothermik; Beziehungen zwischen Inkohlung, Illit-Diagenese, Kohlenwasserstoff Fuehrung und Geothermik. Fortschritte in der Geologie von Rheinland und Westfalen. Geologisches Landesamt Nordrhein-Westfalen, Krefeld* 27:19-49
- Thomson SN, Zeh A (2000) Fission-track thermochronology of the Ruhla crystalline complex: new constraints on the post- Variscan thermal evolution of the NW Saxo-Bohemian Massif. *Tectonophysics* 324:17–35
- Thury M, Gautchi A, Mazurek M, Müller WH, Naef H, Pearson FJ, Vomvoris S, Wilson W (1994) Geology and hydrology of the crystalline basement of northern Switzerland. *NAGRA Technischer Bericht* 93-01:3-1-11
- Timar-Geng Z, Fügenschuh B, Schaltegger U, Wetzel A (2004) The impact of the Jurassic hydrothermal activity on zircon fission track data from the southern Upper Rhine Graben area. *Schweiz Mineral Petrogr Mitt* 84:257–269
- Timar-Geng Z, Fügenschuh B, Wetzel A, Dresmann H (2006) Low-temperature thermochronology of the flanks of the southern Upper Rhine Graben. *Int J Earth Sci* 95(4): 685-702
- Timar-Geng Z, Fügenschuh B, Wetzel A, Dresmann H (2006) The low-temperature thermal history of northern Switzerland as revealed by fission track analysis and inverse thermal modelling. *Eclogae Geologicae Helveticae* 99:255-270
- Todorov I., Schegg R. and Wildi W., 1993. Thermal maturity and modelling of Mesozoic and Cenozoic sediments in the south of the Rhine Graben and the eastern Jura (Switzerland). *Eclogae Geologicae Helveticae*, 86(3):667-692
- Todt W (1976) Zirkon-U/Pb-Alter des Marlsburg-Granites vom Süd-Schwarzwald. *N Jb Miner, H12*:532-544
- Tokunaga T (1999) Modeling of earthquake-induced hydrological changes and possible permeability enhancement due to the 17 January 1995 Kobe Earthquake, Japan *J Hydrol* 223:221–229
- Tournier B, Liewig N, Edel JB, Montigny R (1999) Concordance d'ages K-Ar sur illite avec des ages de reaimantations; exemple des gres triasiques d'Alsace. *Comptes Rendus de l'Academie des Sciences, Serie II. Sciences de la Terre et des Planetes* 329(1):7-13
- Trepmann CA, Stöckhert B (2003). Quartz microstructures developed during non-steady state plastic flow at rapidly decaying stress and strain rate. *Journal of Structural Geology*, 25(12):2035-2051
- Truesdell AH, (1984) Chemical geothermometers for geothermal exploration. In: Henley RW, Truesdell AH, Barton PB (Jr.) (eds) *Fluid-mineral equilibria in hydrothermal systems. Reviews in economic geology. Soc econom geologists, Chelsea MI, pp31-43*
- Tullis J, Yund RA (1977) Experimental deformation of dry Westerly Granite. *J Geophys Res*, 82(36):5705-5718

- Ustaszewski K, Schumacher ME, Schmid SM (2005) Simultaneous normal faulting and extensional flexuring during rifting; an example from the southernmost Upper Rhine Graben. *Int J Earth Sci* 94(4):680-696
- Van Hinte (1978) Geohistory analysis; application of micropaleontology in exploration geology. *AAPG Bull* 62(2):201-222
- Villinger E (1998) Zur Flussgeschichte von Rhein und Donau in Südwestdeutschland  
*Jb Mitt Oberrhein. Geol. Ver.* 80:361-398
- Vonderschmitt L (1942) Die geologischen Ergebnisse der Bohrungen von Hirtzbach bei Altkirch (Ober-Elsass). *Eclogae Geologicae Helvetiae* 35(1):67-99
- Wagner, G.A., Michalski, I. And Zaun, P. (1989): Apatite fission track dating of the Central European basement. Postvariscan thermo-tectonic evolution. In: Emmermann, R. and Wohlenberg, J. (eds) *The German Continental Deep Drilling Program (KTB). Site-selection studies in the Oberpfalz and Schwarzwald.* Springer-Verlag, Berlin, pp 481-500
- Wagner GA, van den Haute P (1992) Fission-Track Dating. *Kluwer Academic Publ, Dordrecht*, pp 1-285
- Werner D, Doehl F (1974) Eine Geothermische Karte des Rheingrabenuntergrundes. In: Illies JH, Fuchs K (eds) *Approaches Taphrogenesis*, Stuttgart, pp182-191
- Werner W, Franzke HJ (1994) Zur Tektonik und Mineralisation der Hydrothermalgänge am Schwarzwaldrand im Bergbaurevier Freiamt-Sexau (Mittlerer Schwarzwald). *Abh Geol Landesamt B-W* 14:27-98
- Werner W, Franzke HJ (2001) Postvariszische bis neogene Bruchtektonik und Mineralisation im südlichen Zentralschwarzwald. *Z Dt Geol Ges* 152:405-437
- Wetzel A, Allia V (2003) Der Opalinuston in der Nordschweiz: Lithologie und Ablagerungsgeschichte. *Eclogae geologicae Helvetiae* 96(3):451-469
- Wetzel A, Allenbach R, Allia V (2003) Reactivated basement structures affecting the sedimentary facies in a tectonically "quiescent" epicontinental basin; an example from NW Switzerland. *Sedim Geol* 157(1-2):153-172
- Wildi W, Funk H, Loup B, Amato E, Huggenberger P (1989) Mesozoic subsidence history of the European marginal shelves of the Alpine Tethys (Helvetic realm, Swiss Plateau and Jura). *Eclogae Geologicae Helvetiae.* 82(3):817-840
- Wilser JL (1914) Die Rheintallexur nördöstlich von Basel zwischen Lörrach und Kandern und ihr Hinterland. *Mitt. Bad. Geol. L.-Anst.* 7(2):485-640
- Wimmenauer W, Schreiner A (1990) Erläuterungen zu Blatt 8114, Feldberg. *Geol Karte Baden-Württemberg 1:25 000*, Stuttgart, p 134
- Wimmenauer W. (2003), Erläuterungen zu Blatt Kaiserstuhl, *Geol Karte Baden-Württemberg, Landesamt für Geologie, Rohstoffe und Bergbau Baden-Württemberg, Freiburg i. Br.*
- Wittmann O (1988) Erläuterungen zu Blatt Lörrach 8311, *Geol Karte Baden-Württemberg 1:25.000*, Geologisches Landesamt Baden-Württemberg, p 153
- Wirth G (1984) Kleintektonische Untersuchungen im Grund- und Deckgebirge des Südostschwarzwaldes (Baden-Württemberg). *Arb. Inst. Geol. Paläont. Univ. Stuttgart*, NF 78, pp 85-136

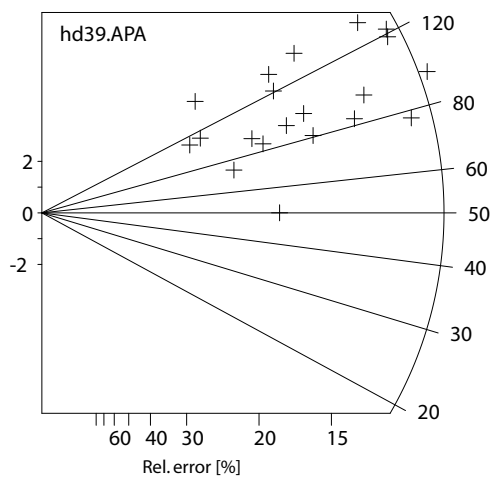
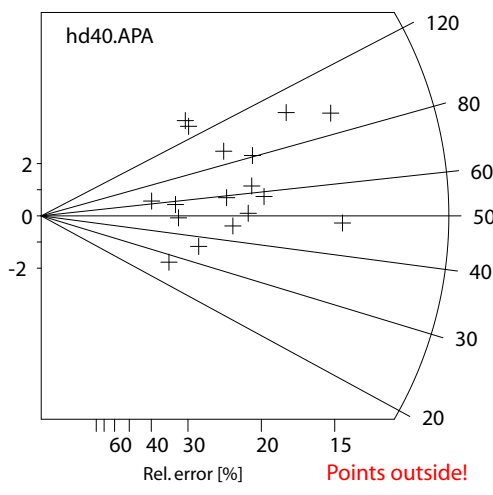
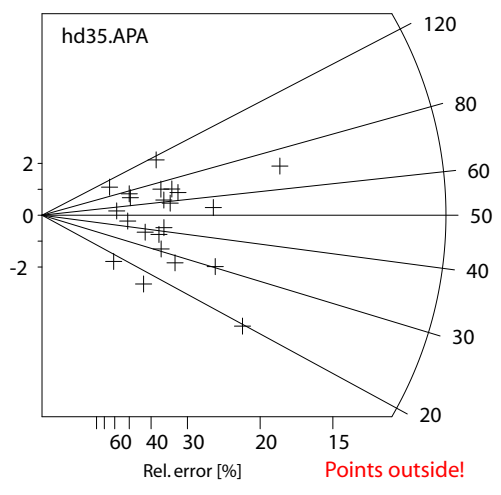
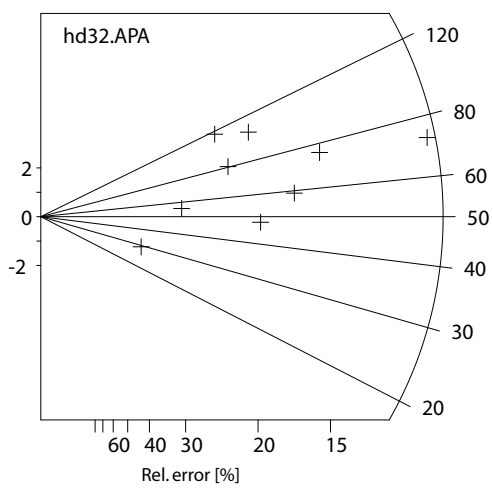
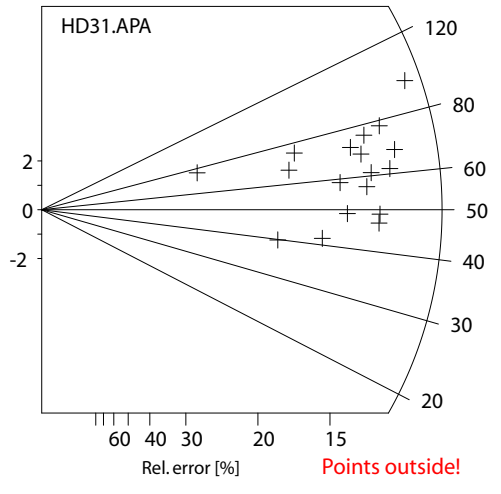
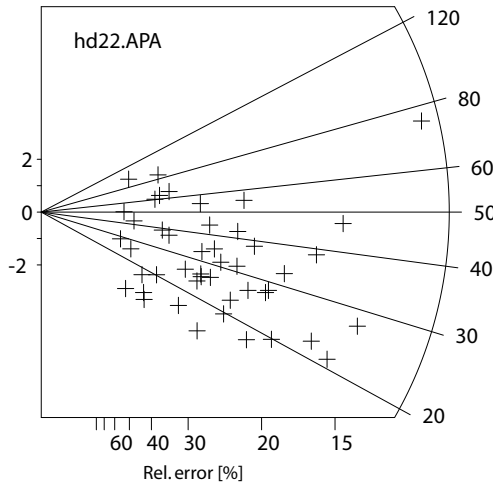
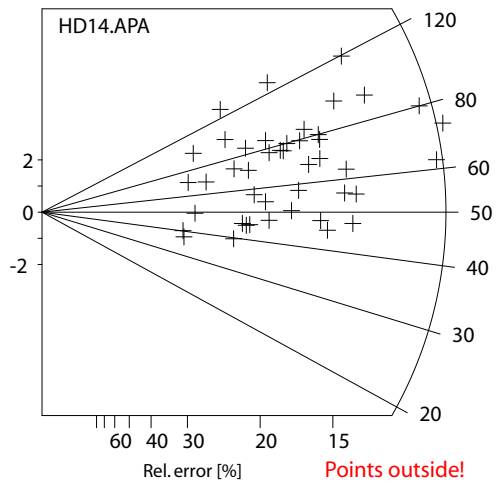
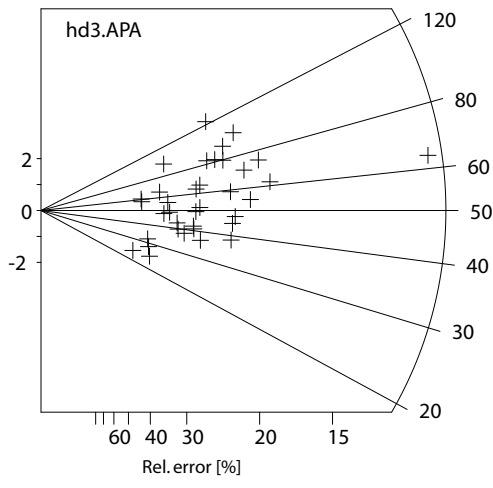
- Wohnlich S (1996) The spa of Baden-Baden. Germany. *Environm Geol* 27:108-109
- Wyss A (2001) Apatit Spaltspur Untersuchungen in der Vorwaldscholle (SW-Deutschland). Unpubl MSc thesis, Basel University, p 69
- Yamada R, Tagami T, Nishimura S, Ito H (1995) Annealing kinetics of fission tracks in zircon: an experimental study. *Chem Geol* 122:249-258
- Ziegler PA (1990) Geological atlas of Western and Central Europe. Shell Internationale Petroleum Maatschappij, Geol Soc Publ House, London, p 239
- Ziegler PA (1994) Cenozoic rift system of western and central Europe: an overview, *Geologie en Mijnbouw* 73:99-127
- Ziegler PA, Schumacher ME, Dèzes P, van Wees JD, Cloetingh S (2004) Post-Variscan evolution of the lithosphere in the Rhine Graben area: constraints from subsidence modelling. In: Wilson M, Neumann, ER, Davies GR, Timmerman MJ, Heeremans M, Larsen BT (eds) *Permo-Carboniferous Magmatism and Rifting in Europe*. Geol Soc London Spec Publ 223:289-317
- Ziegler PA, Dezes P, (2005) Evolution of the lithosphere in the area of the Rhine rift system. *Int J Earth Sci* 94(4):594-614
- Ziegler PA, Dezes P (2007) Neogene uplift of Variscan Massifs in the Alpine foreland: Timing and controlling mechanisms. *Global Planet. Change* (in press)
- Zienert A (1986) Grundzüge der Grossformenentwicklung Süddeutschlands zwischen Oberrheinebene und Alpenvorland. Selbstverlag, Heidelberg, pp1-160
- Zollinger G. (1982) Geomorphologische Studien am Norsinger Grund bei Ehrenkirchen/Breisgau. *Berichte der Natforsch. Ges. Freiburg*. 71/72

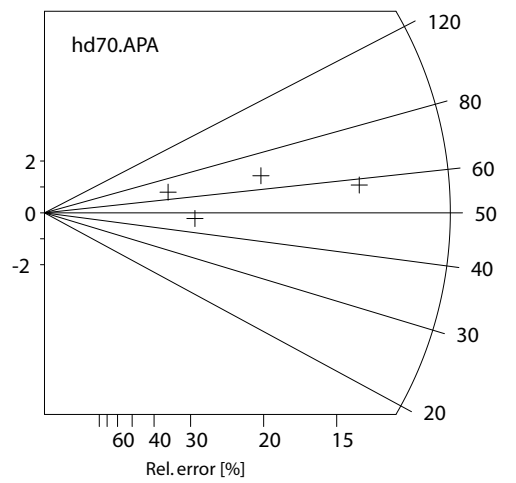
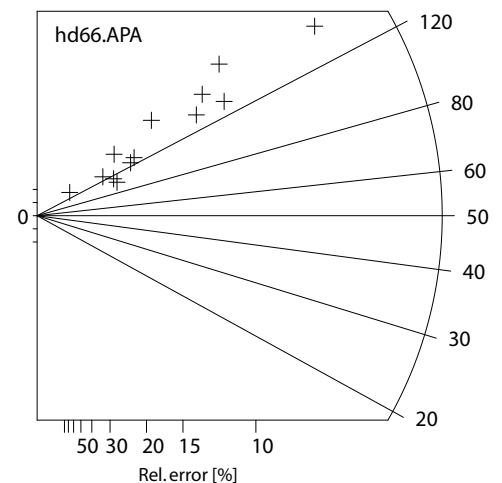
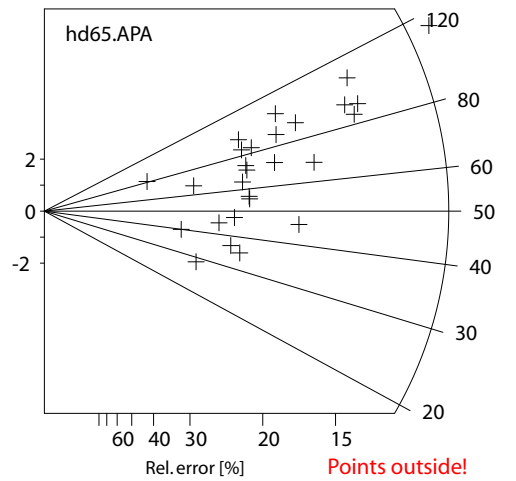
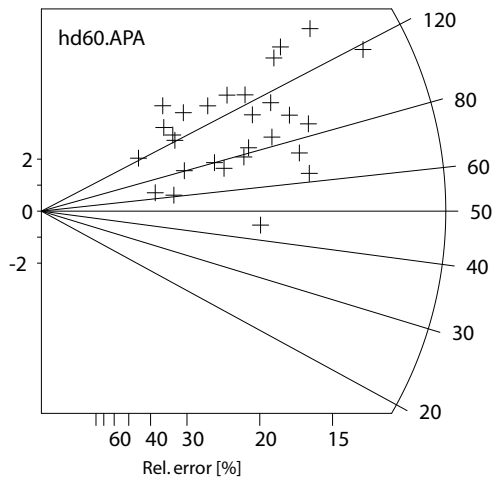
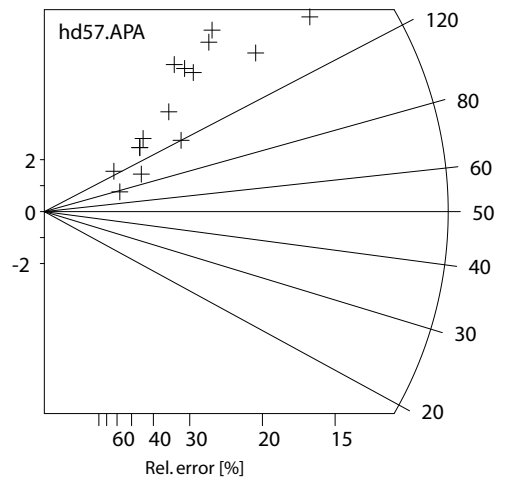
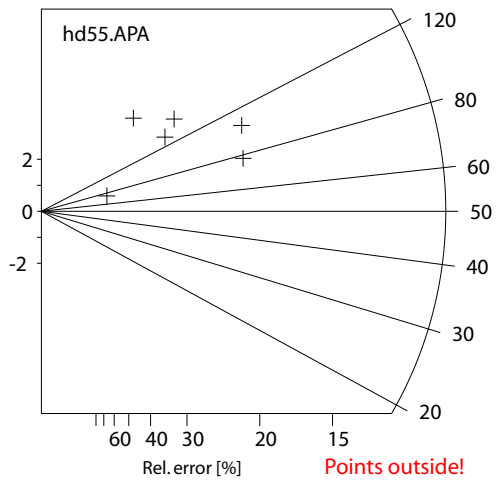
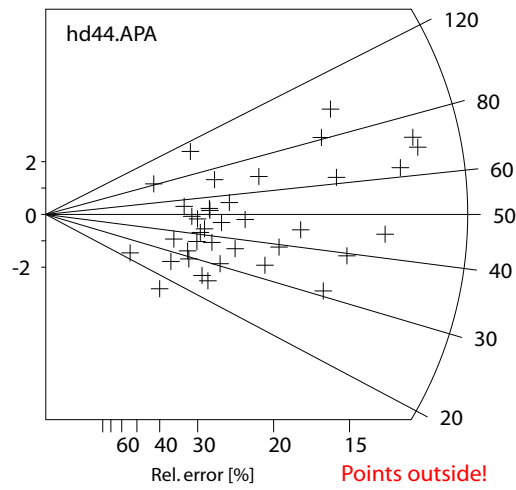
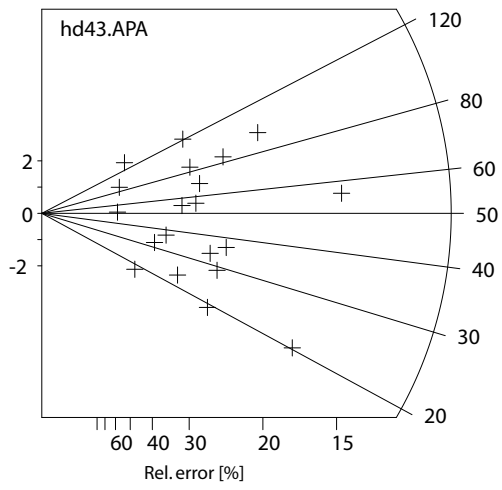
## **VI. Appendix**

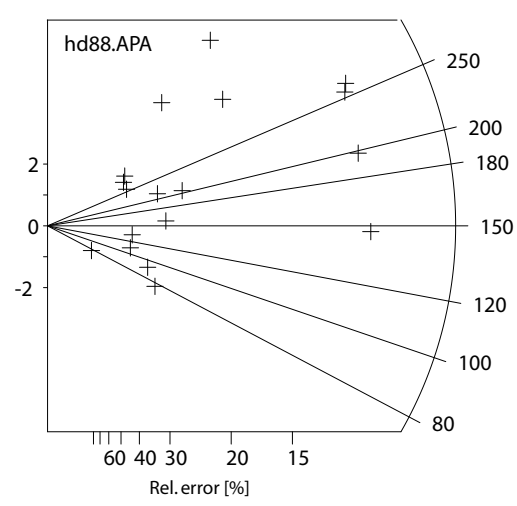
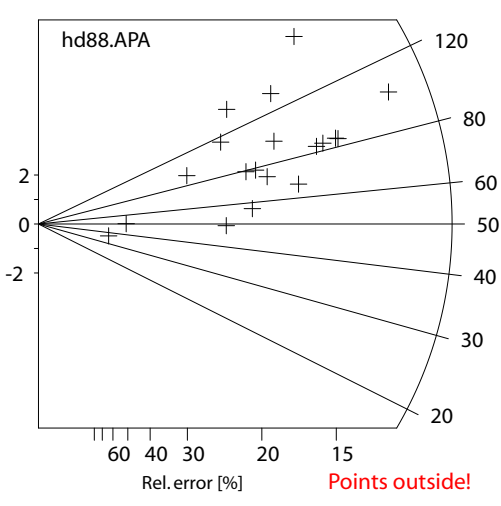
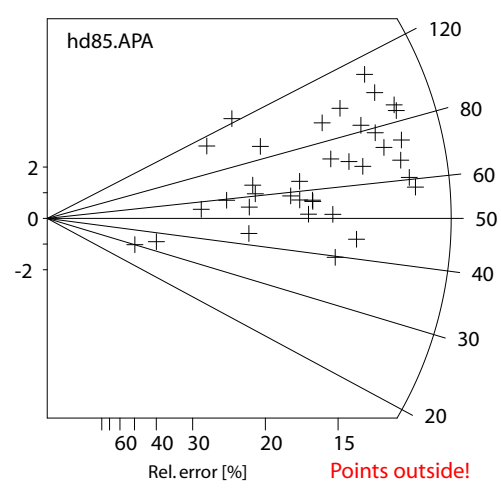
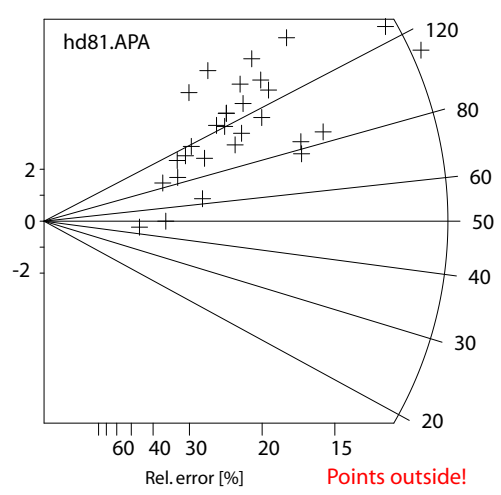
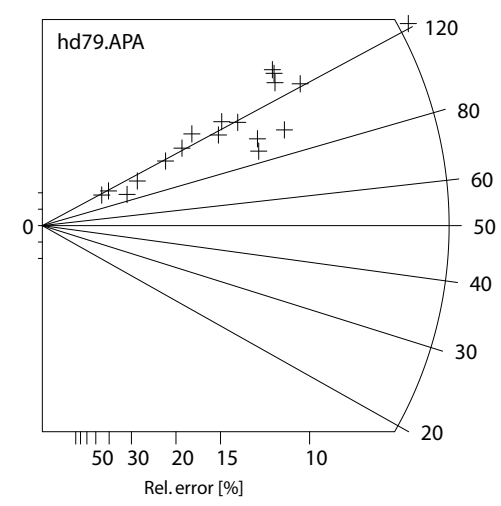
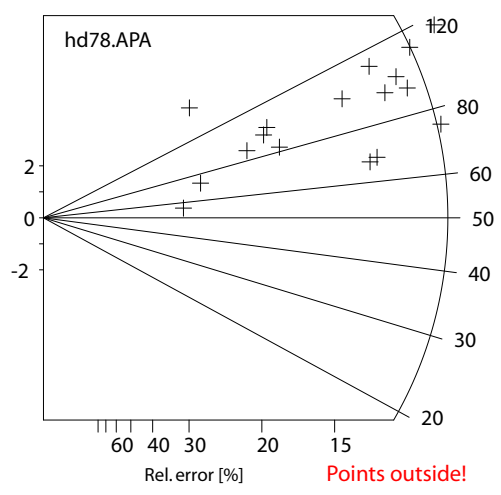
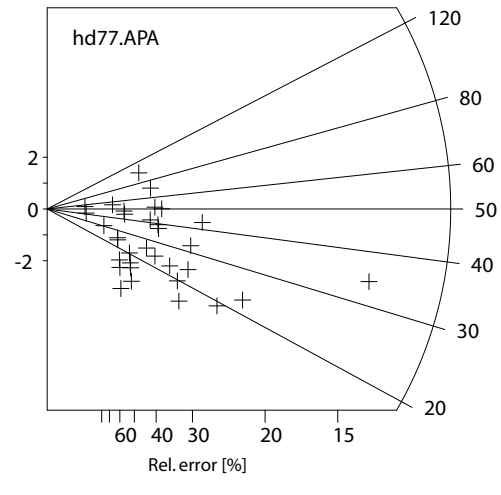
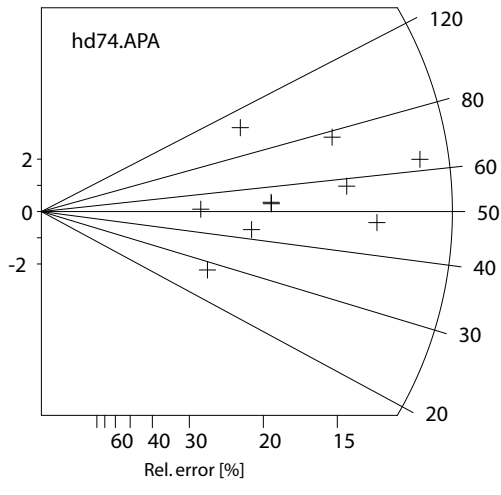
### Fission Track data

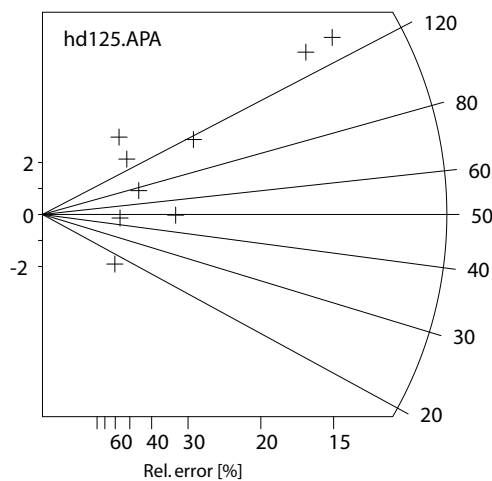
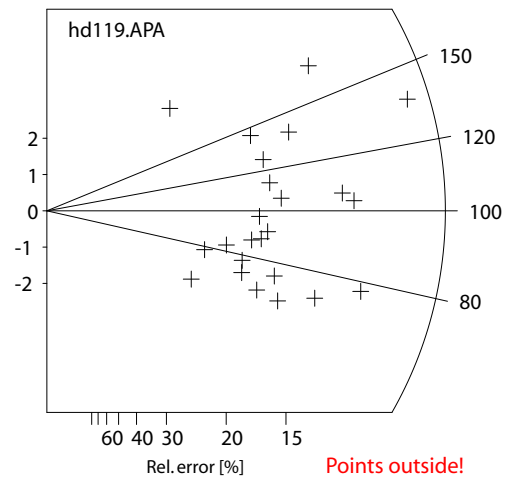
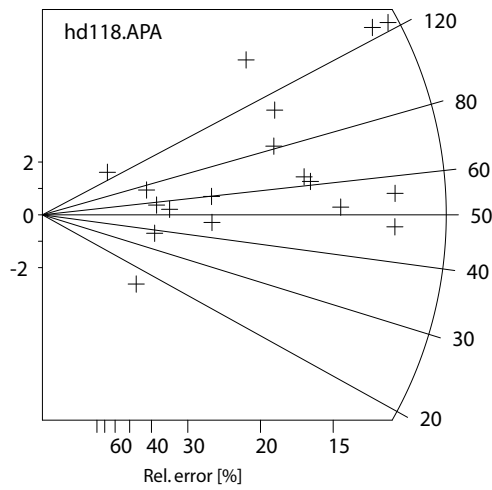
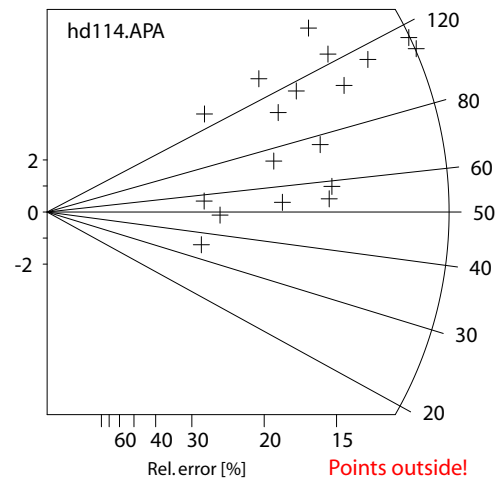
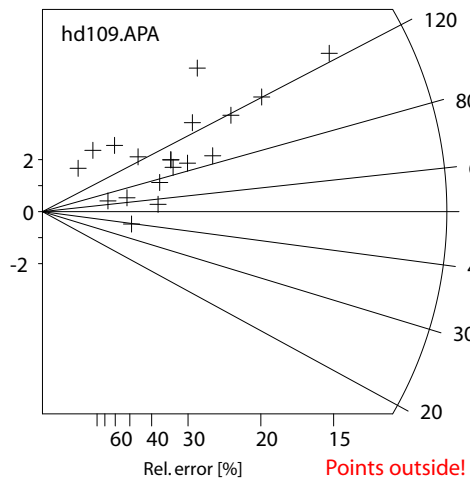
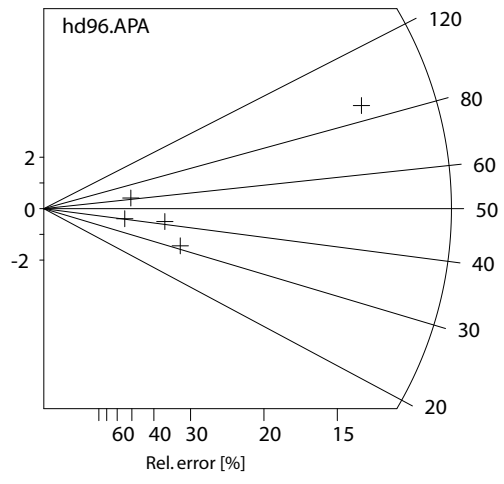
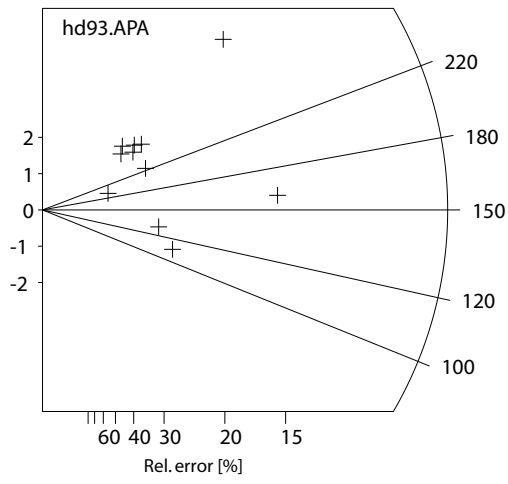
Radial plots, which in the manuscript are not shown; containing single grain data of apatite and zircon FT analyses. The radial plots (Galbraith 1988, 1990) were calculated using the software Trackkey (Dunkl 2002)

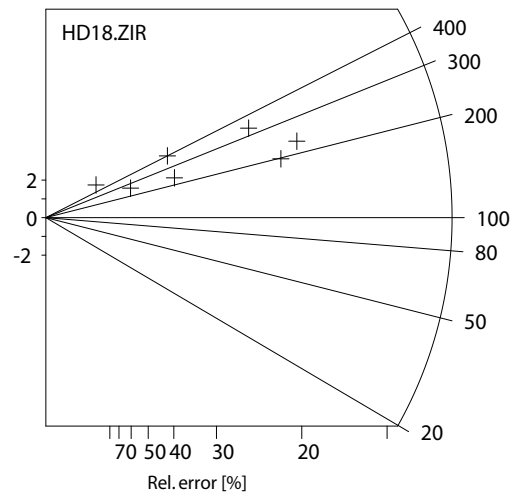
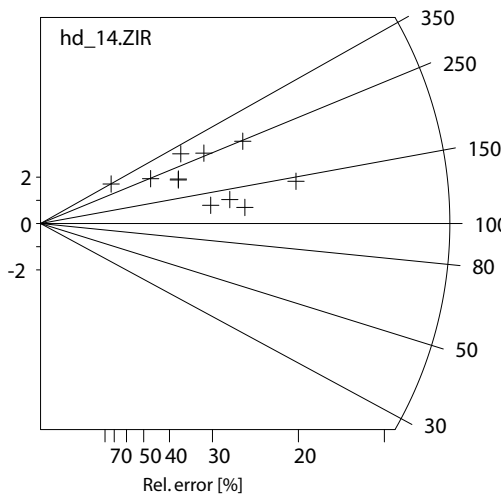
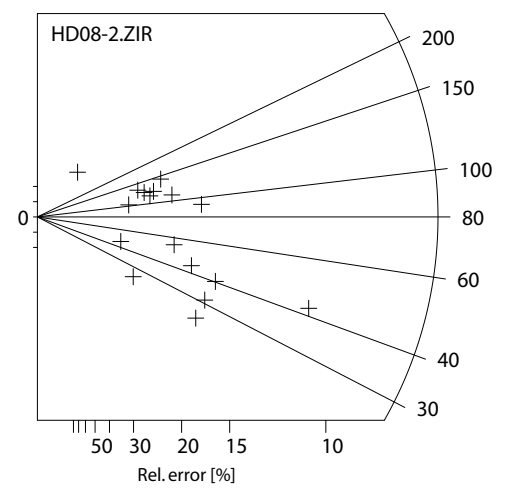
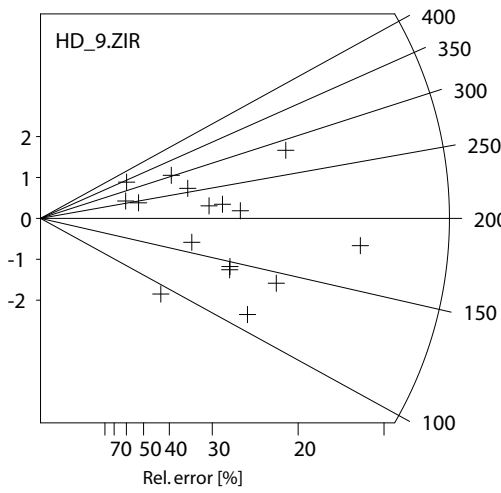
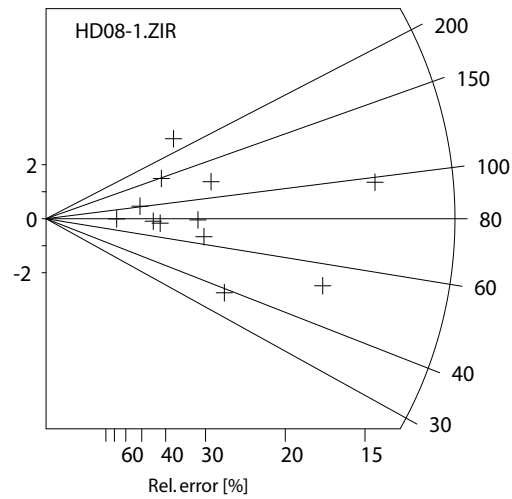
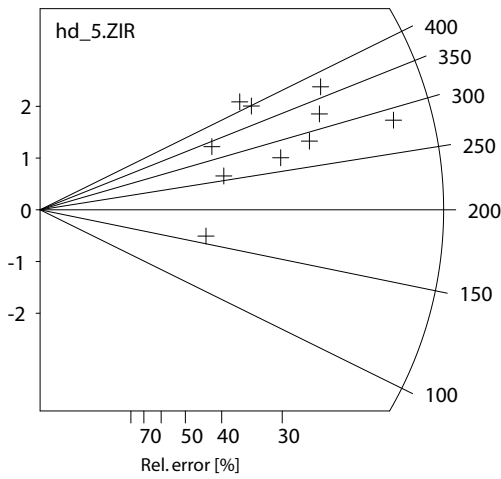
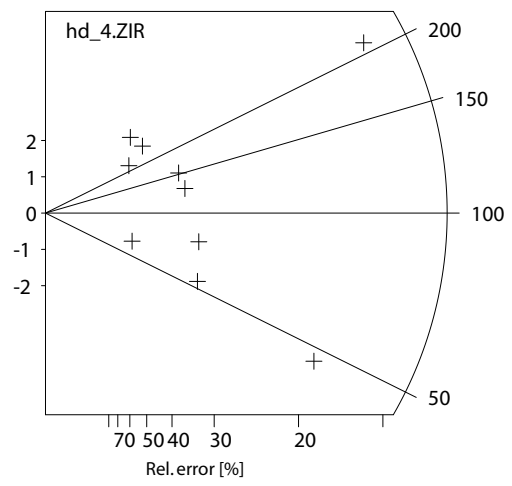
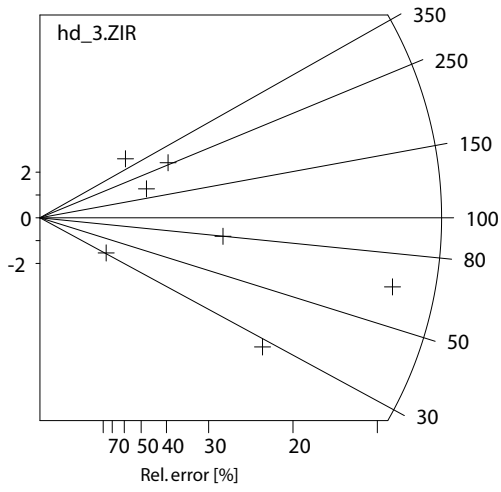


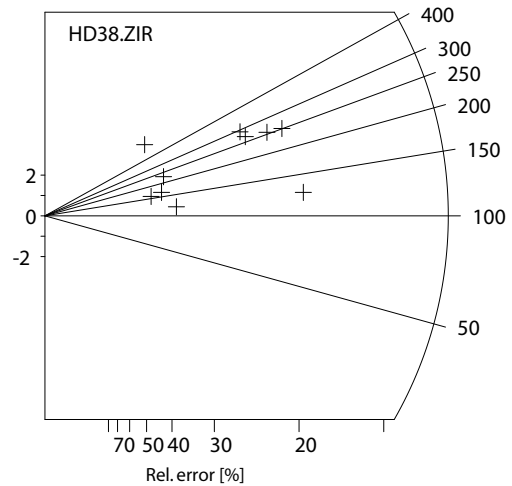
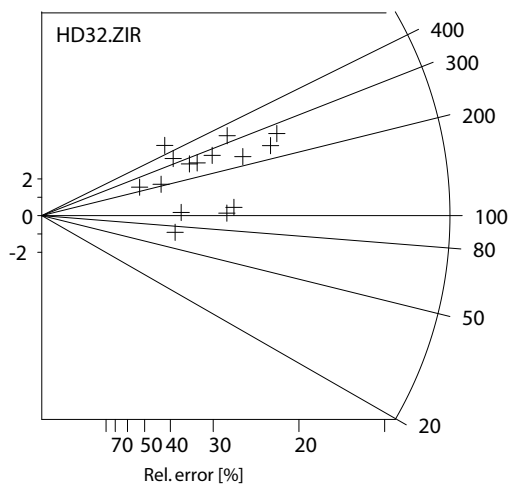
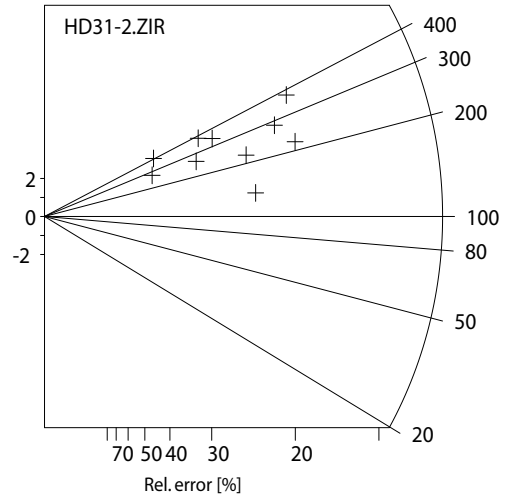
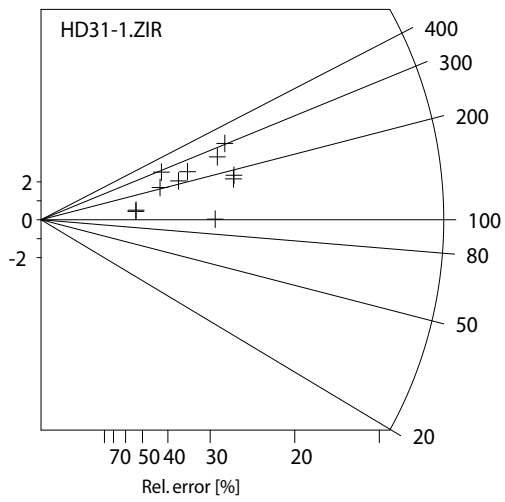
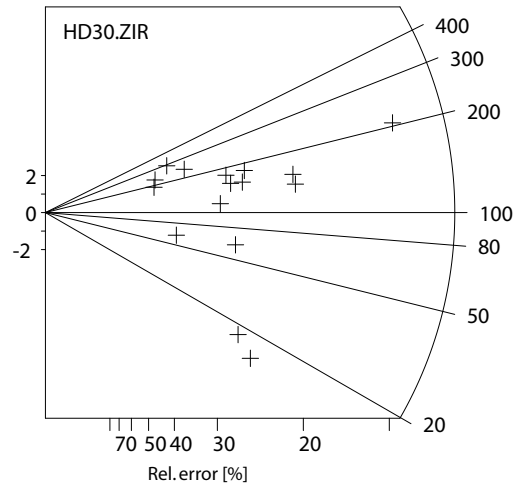
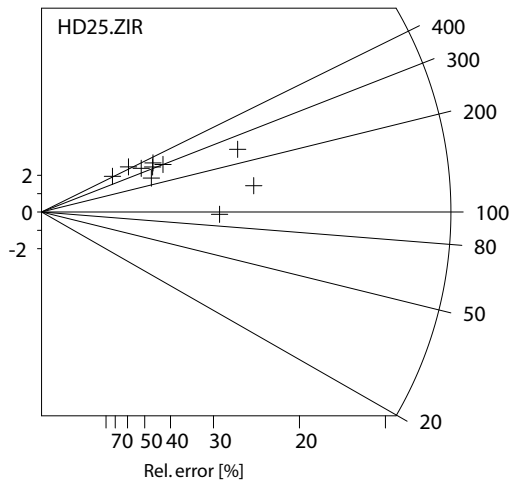
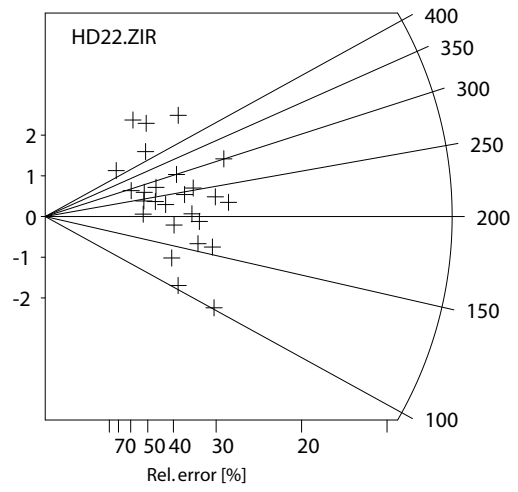
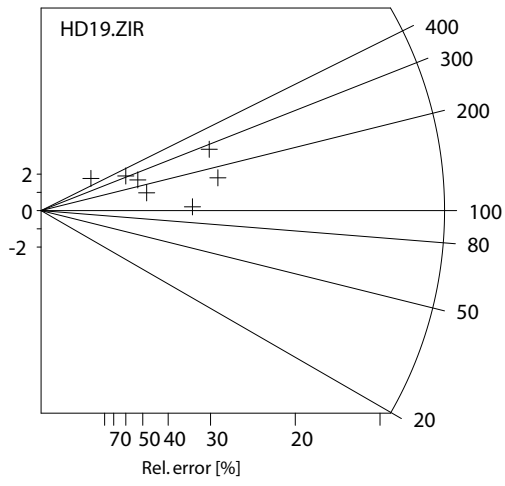


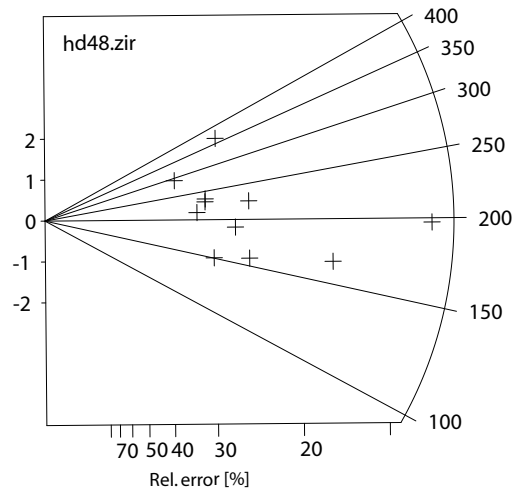
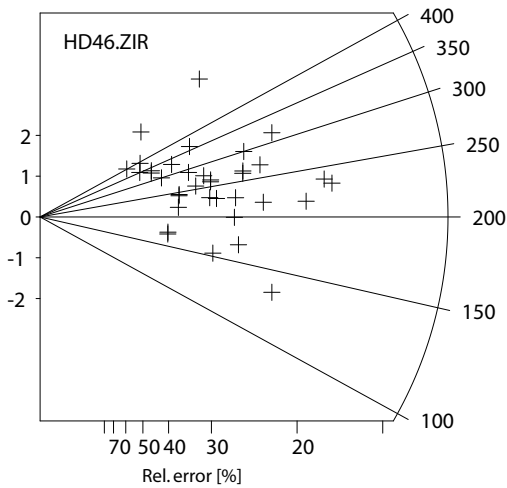
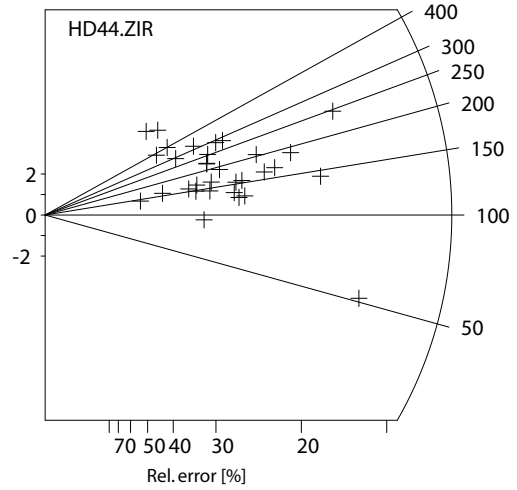
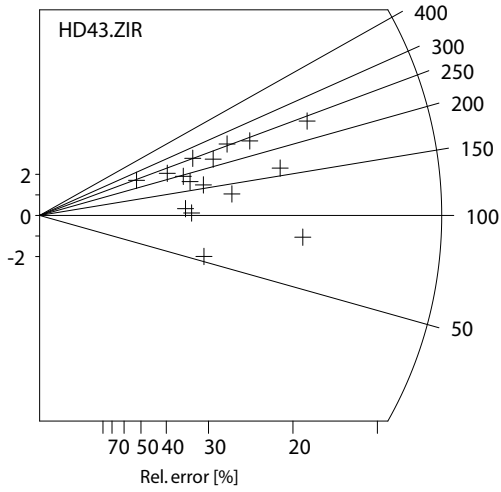
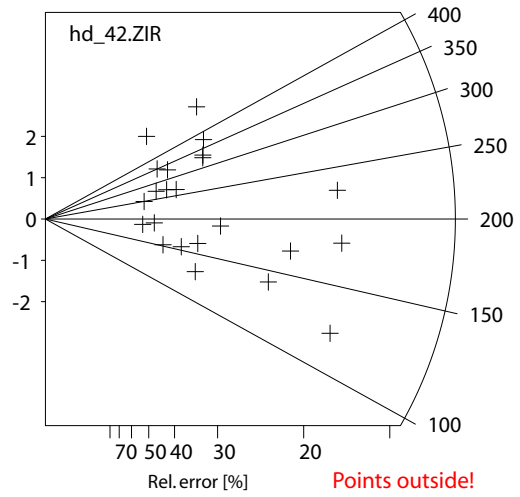
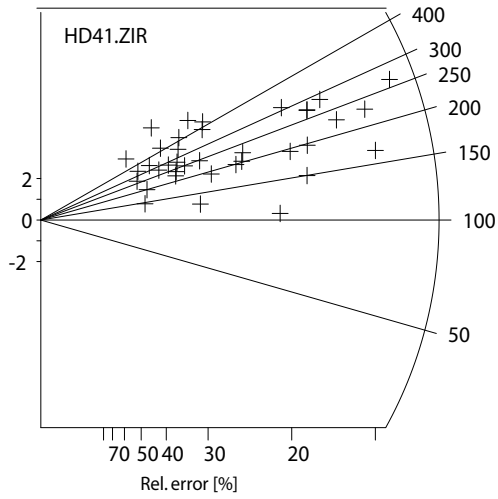
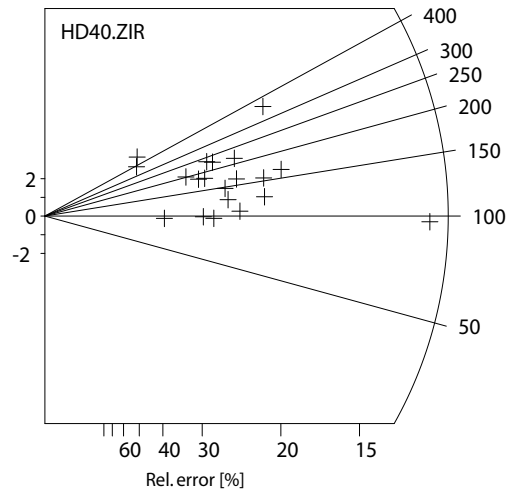
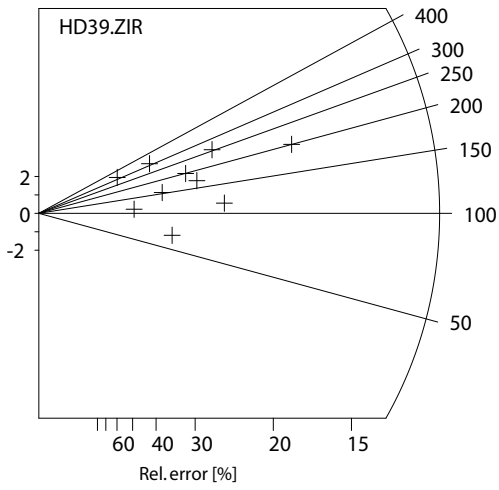


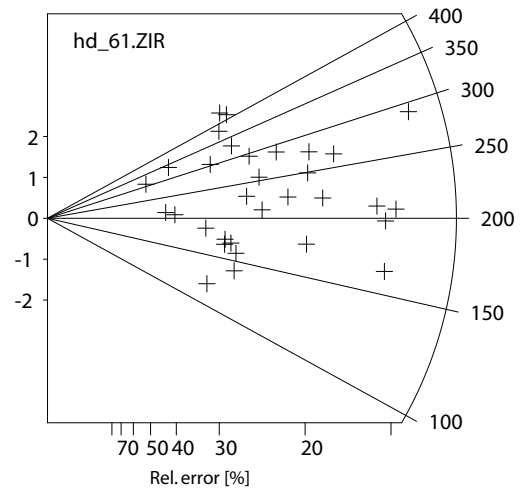
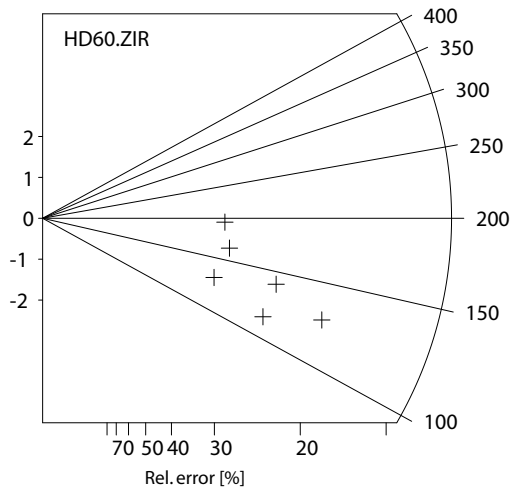
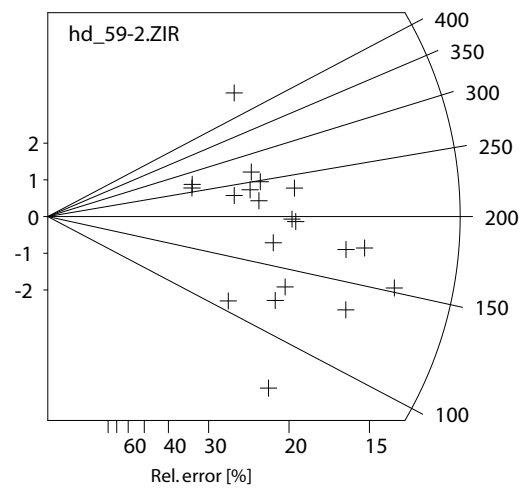
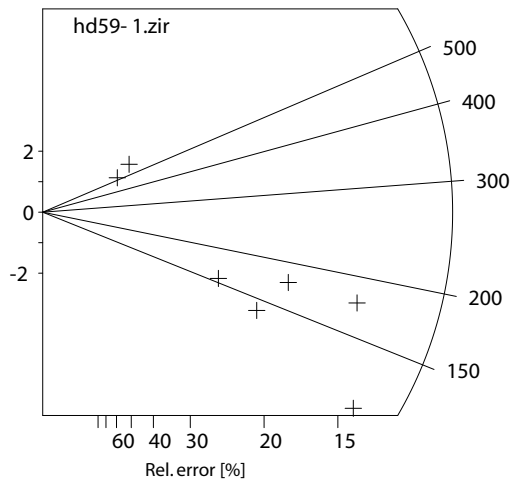
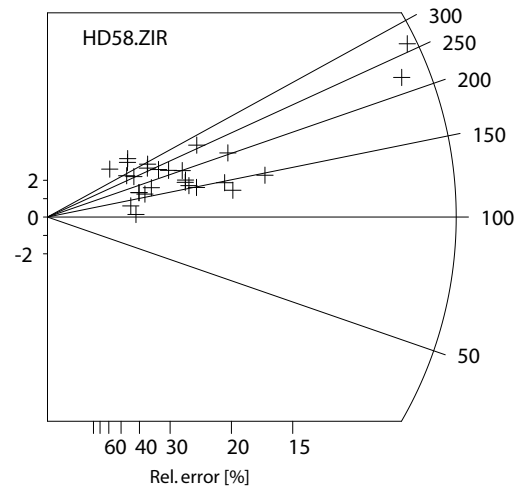
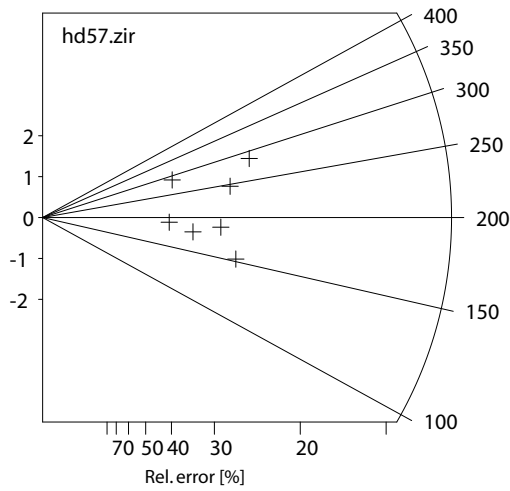
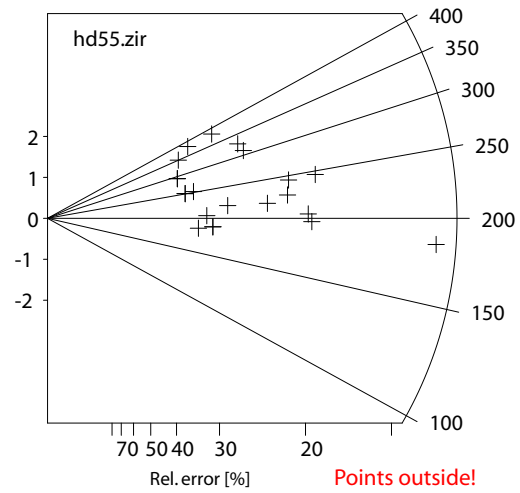
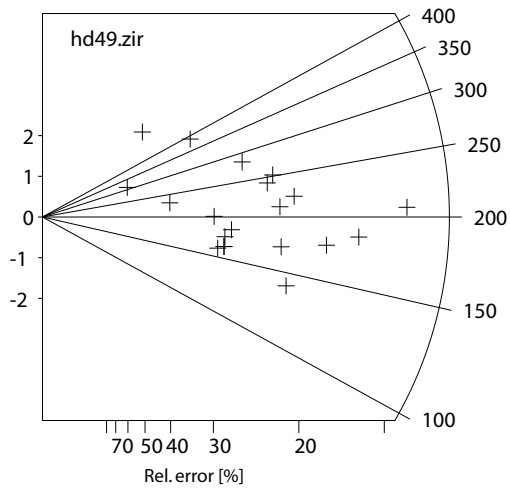




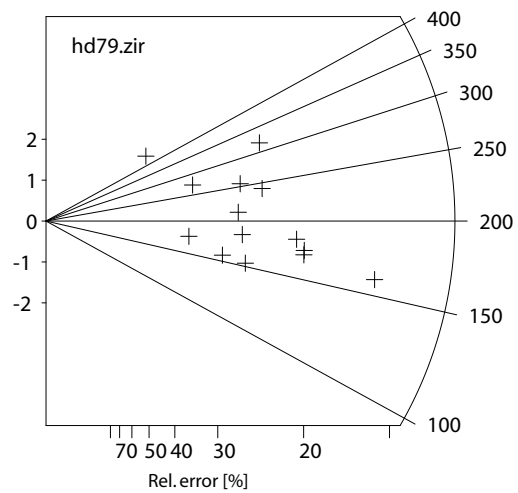
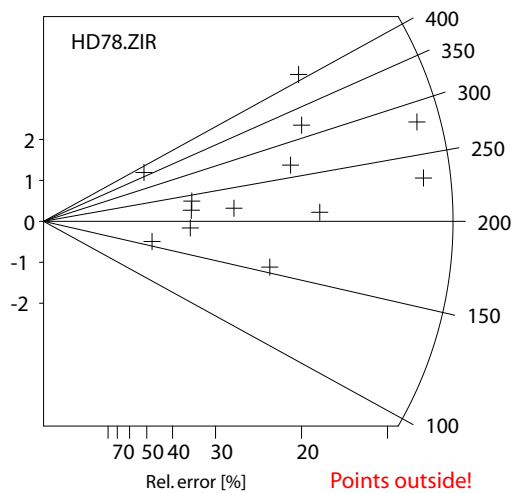
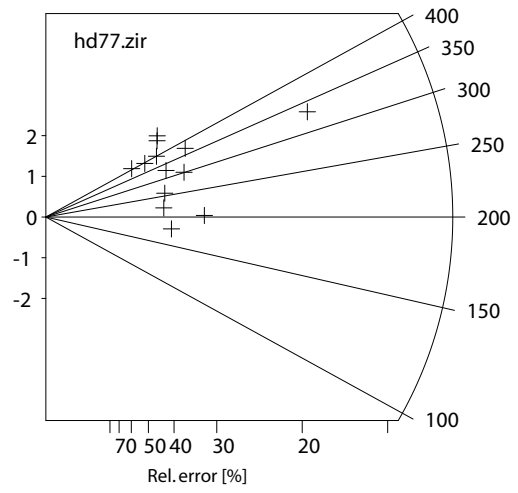
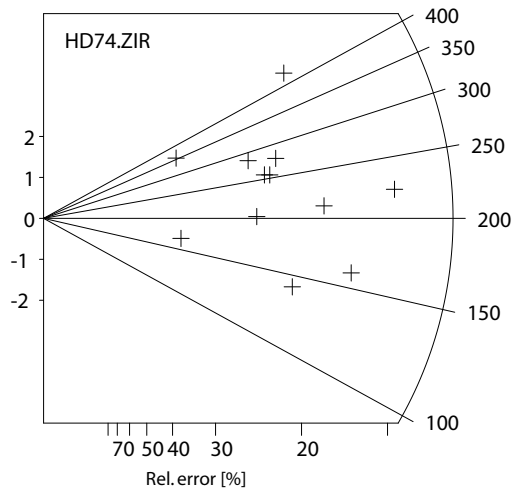
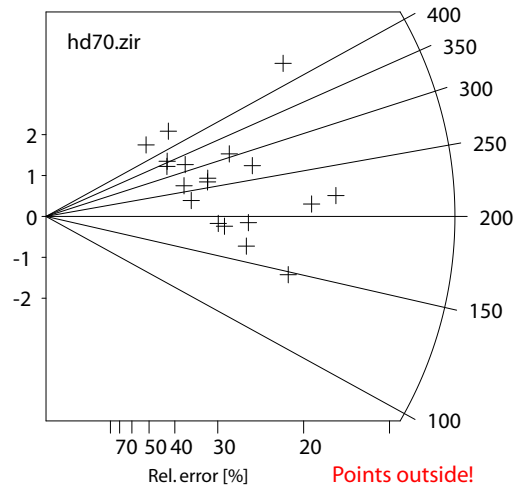
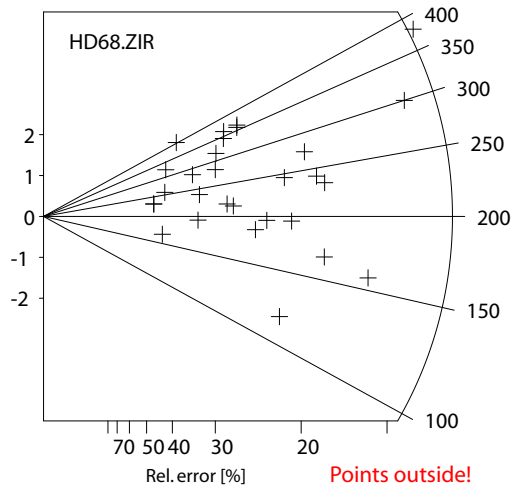
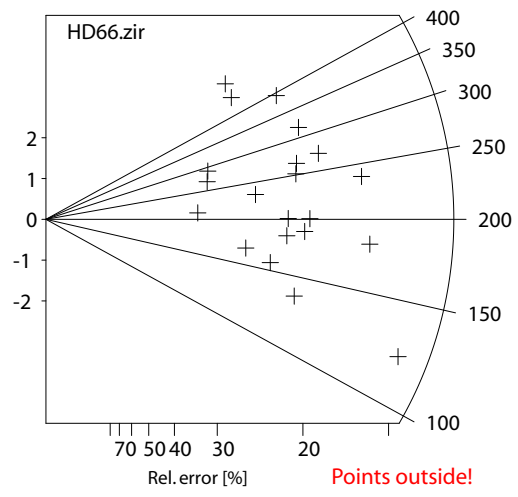
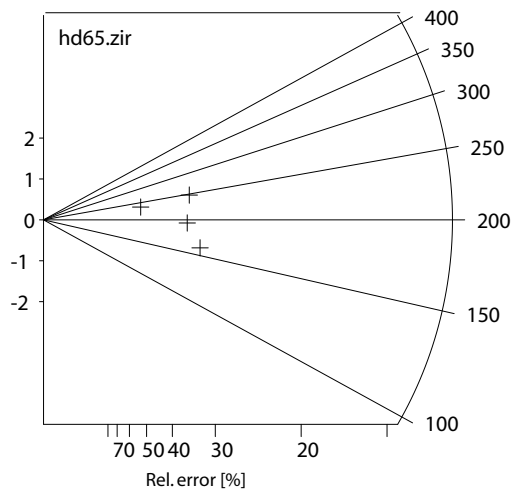


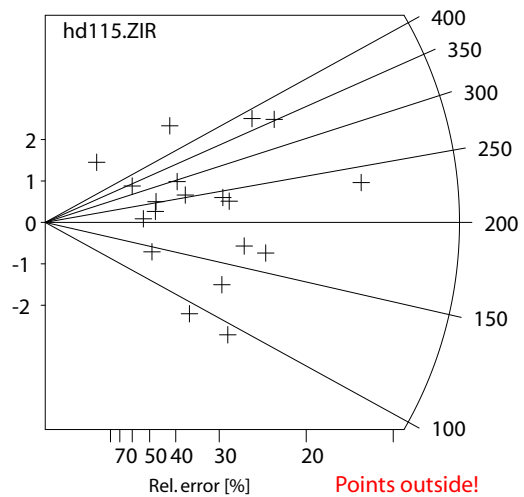
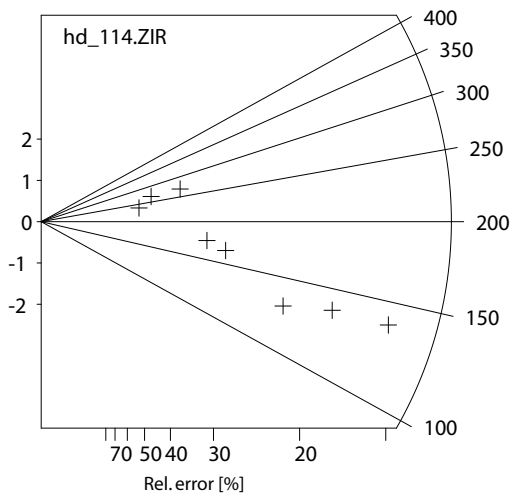
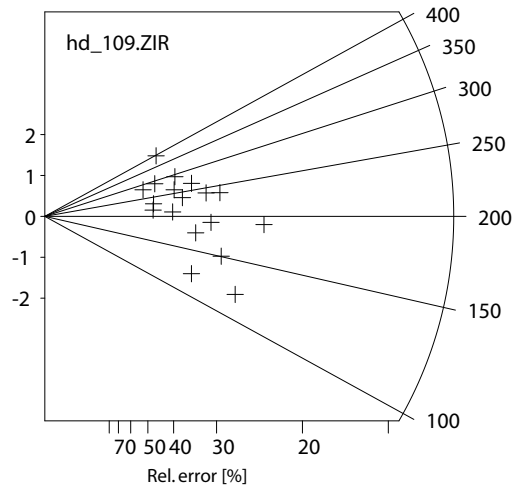
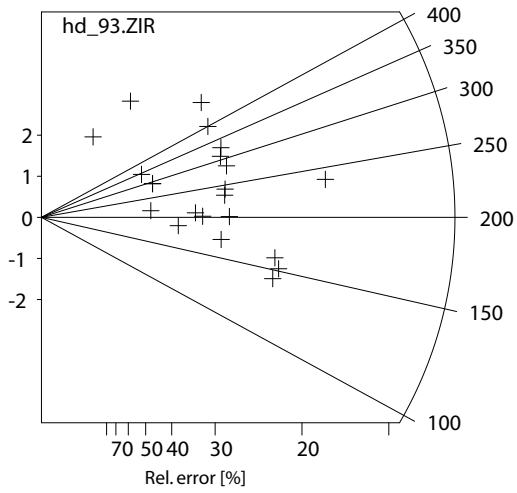
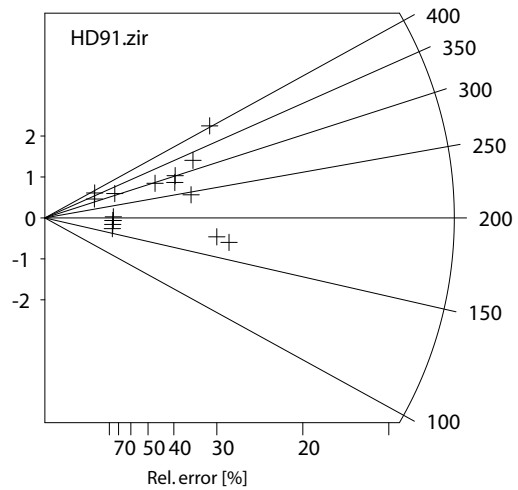
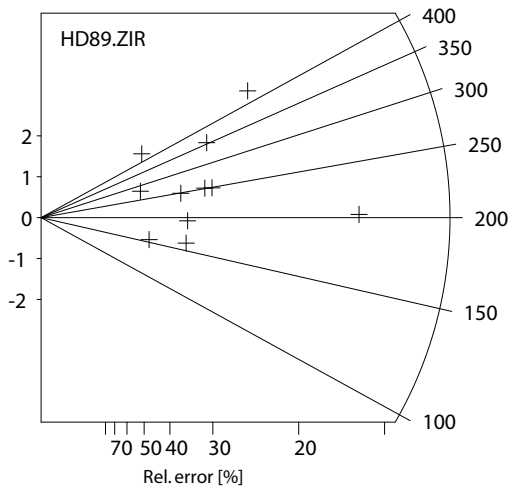
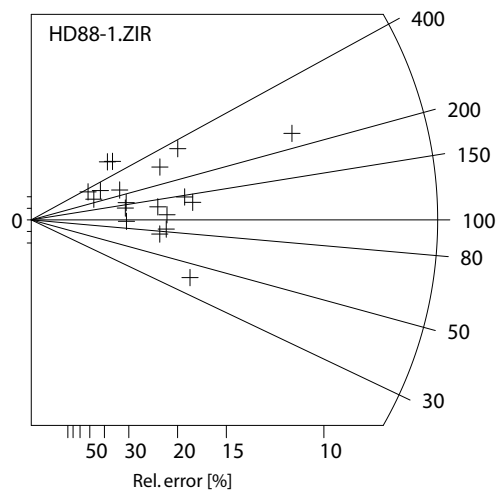
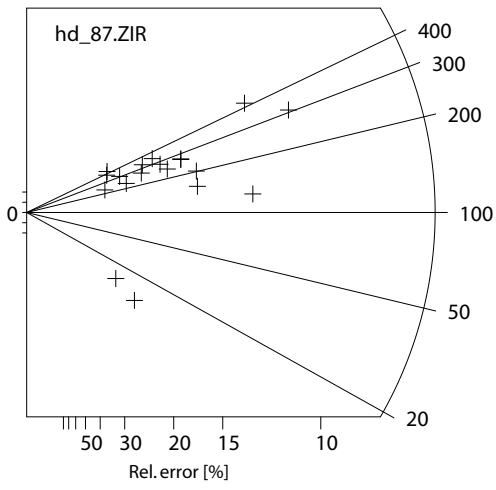


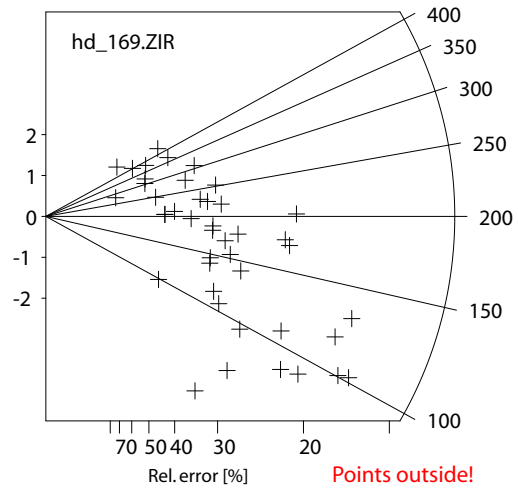
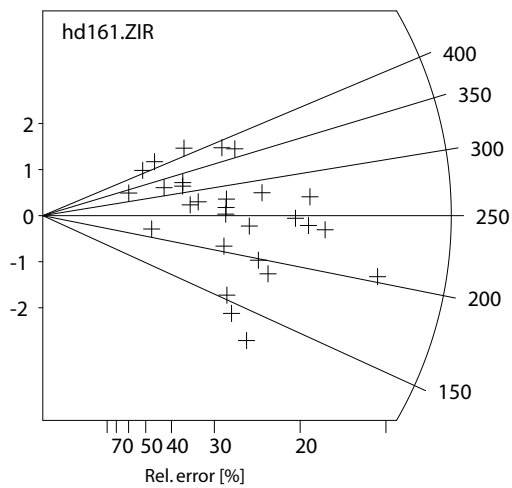
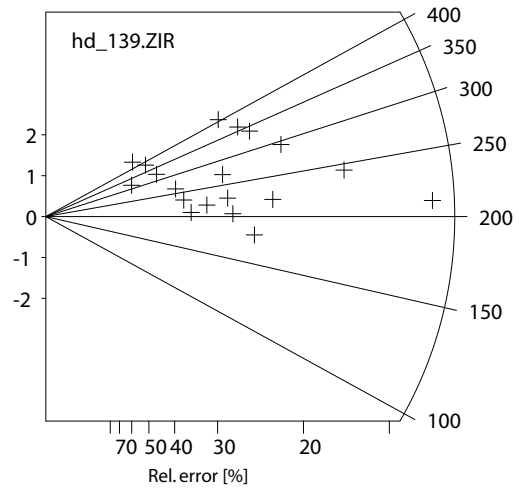
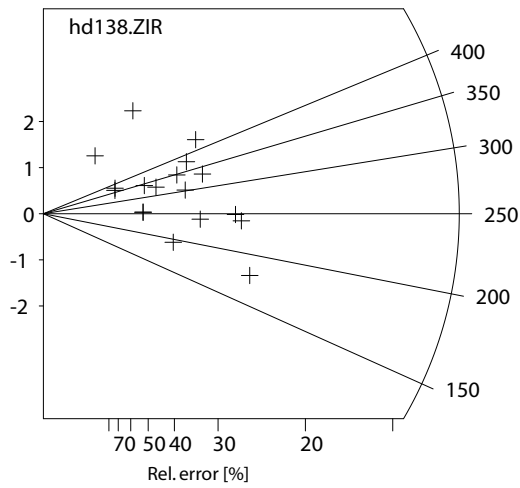
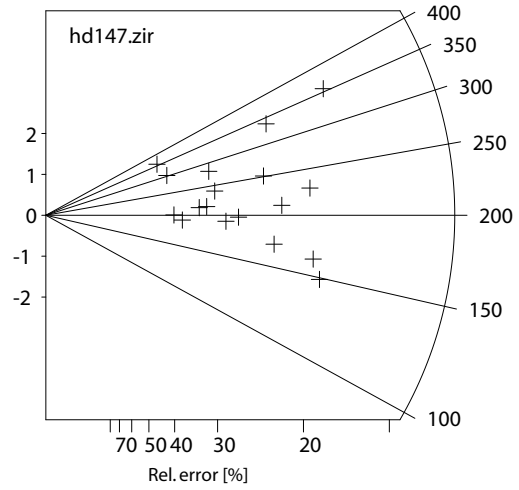
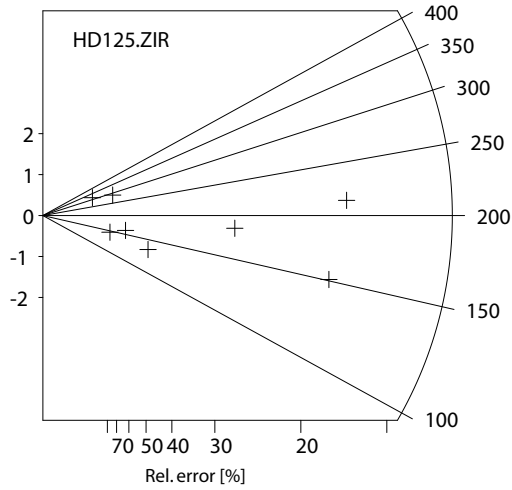
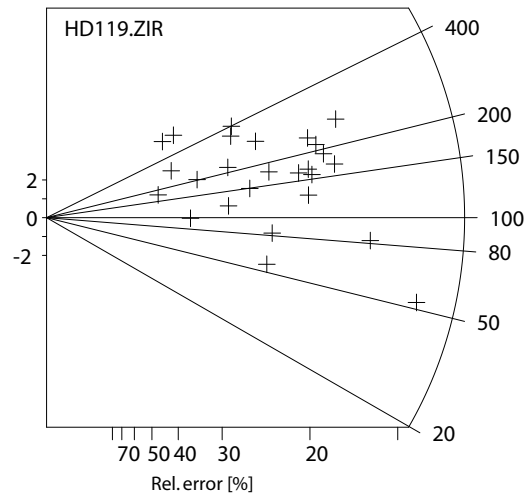
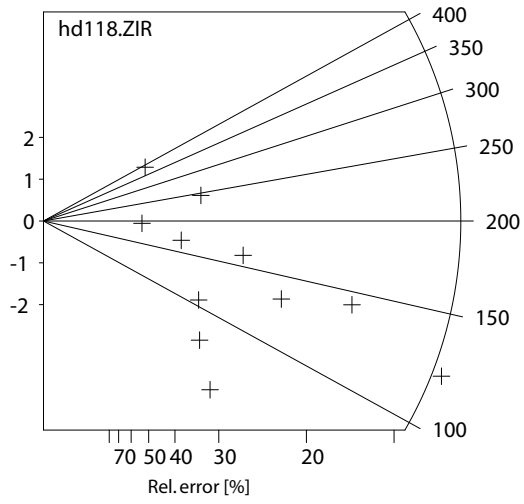


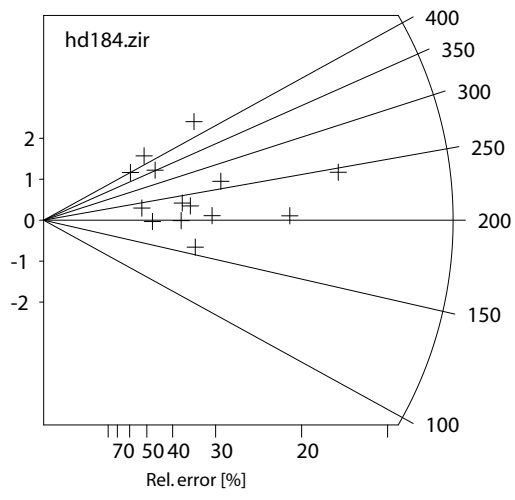












## VII. Curriculum Vitae of Horst Dresmann

Date of Birth: 20.08.1968  
Place of Birth: Freiburg in Breisgau, Germany  
Nationality: German

### Education and Professional Experience

**2007- present:** Scientist at the Applied and Environmental Geology, Department of Environmental Sciences at the University of Basel (Switzerland).

**2001-2007:** Ph.D. at the Institute of Geology and Paleontology, Department of Environmental Sciences at the University of Basel (Switzerland).

Title: *“Fission-Track analyses in the area of the southern Upper Rhine Graben”*

Supervisor: Prof. Dr. Andreas Wetzel and Prof. Dr. Bernhard Fügenschuh

**2000-2001:** Tutor at the Institute of Geology at the Albert Ludwig-University Freiburg.

**1997-2000:** Study at the Institute of Geology at the Albert Ludwig-University Freiburg (Germany). Diploma-thesis: *“Bilanzierung zweier geologischer Profile zwischen Tegernsee (Deutschland) und Schwaz (Österreich)”* and Diploma-mapping: *“Die Nördlichen Kalkalpen zwischen Hochunnutz und Thierseemulde (Achensee, Tirol 1:10.000)”*

**1994-1997:** Study at the Institute of Geology and Palaeontology at the Ruprecht-Karls-University Heidelberg

Basel, 7. April 2007